UCRL 9203

UNIVERSITY OF
CALIFORNIA

Ernest O. Lawrence

Radiation Laboratory

AN ANALYSIS OF THE ABSORPTION SPECTRA OF TmIV AND AmIV

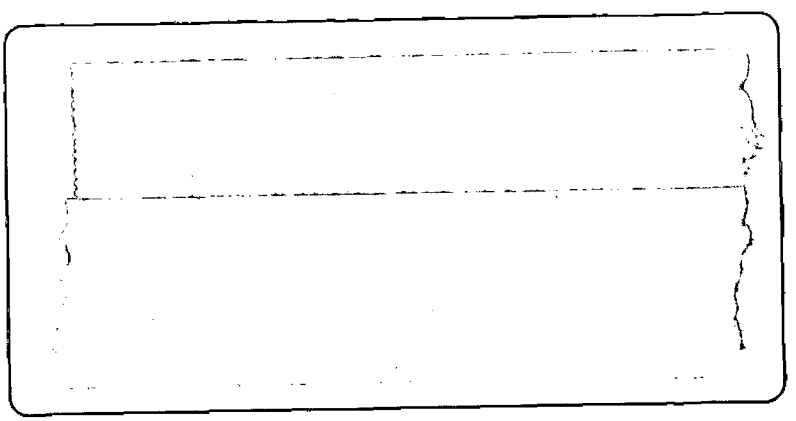

DISCLAIMER

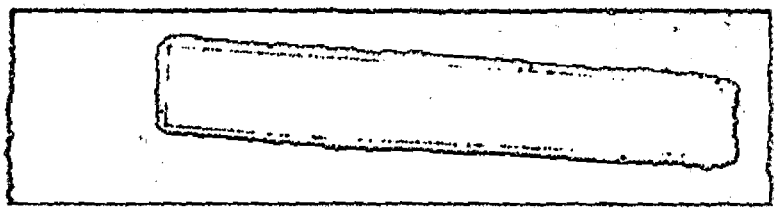

UCRL-9203
UC-4 Chemistry-General
TID-4500 (16th Ed.)

UNIVERSITY OF CALIFORNIA
Lawrence Radiation Laboratory
Berkeley, California

Contract No. W-7405-eng-48

AN ANALYSIS OF THE ABSORPTION SPECTRA OF TmIV AND AmIV

John Balsbaugh Gruber

(Thesis)

January 1961

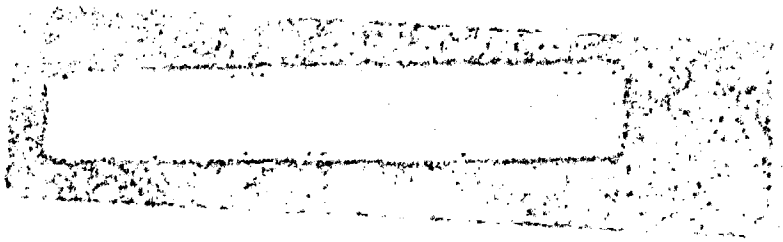

Printed in USA. Price $2.75. Available from the
Office of Technical Services
U. S. Department of Commerce
Washington 25, D.C.

AN ANALYSIS OF THE ABSORPTION SPECTRA OF TmIV AND AmIV

Contents

AN ANALYSIS OF THE ABSORPTION SPECTRA OF TmIV AND AmIV

John Balsbaugh Gruber

(Thesis)

Department of Chemistry and Lawrence Radiation Laboratory
University of California
Berkeley, California

January 1961

ABSTRACT

An analysis of the absorption spectra of $Tm(C_2H_5SO_4)_3 \cdot 9H_2O$ and AmIV in $LaCl_3$ is presented here. For TmIV, all levels corresponding to $\underline{4f} \rightarrow \underline{4f}$ transitions except transitions from $^3H_6$ to $^1S_0$ have been observed and fitted to a theoretical model which gives $\zeta_{\underline{4f}} = 1350\,cm^{-1}$, and $F_2(\underline{4f}) = 450\,cm^{-1}$.

The 119 electronic energy levels for the $\underline{nf}^6$ configuration have been calculated for three different sets of Slater F_k ratios: $\underline{4f}^6$ hydrogenic--$F_4/F_2 = 0.1381$, $F_6/F_2 = 0.01511$; $\underline{5f}^6$ hydrogenic--$F_4/F_2 = 0.1422$, $F_6/F_2 = 0.0161$; and $\underline{5f}^6$ based on a Hartree-Fock calculation--$F_4/F_2 = 0.159$, $F_6/F_2 = 0.0204$. A tentative theoretical analysis of the absorption spectra of Eu IV can be made by using $\zeta = 1360\,cm^{-1}$ and $F_2(\underline{4f}) = 370\,cm^{-1}$.

It has been possible to carry out a crystal-field splitting analysis of all the infrared electronic energy levels of AmIV. Parameters that fit the observed data are $A_2^0\langle r^2\rangle = 206\,cm^{-1}$, $A_4^0\langle r^4\rangle = -94.1\,cm^{-1}$, $A_6^0\langle r^6\rangle = -93.8\,cm^{-1}$, and $A_6^6\langle r^6\rangle = 1100\,cm^{-1}$.

I. INTRODUCTION

In recent years there has been an increased activity in the study of the fluorescence and the absorption spectra of the complicated $\underline{f}$ electron systems of rare earth and actinide ions. Part of the increase in interest may be ascribed to the widening application of the rather sophisticated theory enunciated by Giulio Racah.[1-4] Since the appearance of Racah's papers, several persons have reported direct application of his work to the $\underline{f}$ electron systems. The spin-orbit matrices for $\underline{f}^3$ have been evaluated by Judd and Loudon,[5] and the electrostatic energy matrices have been reported by Reilly, by Elliott, Judd, and Runciman, and by Wybourne.[6-8] Actual electrostatic energy levels for $4\underline{f}$ configurations, based on $4\underline{f}$ hydrogenic Slater ratios, have been presented by Elliott, Judd, and Runciman,[7] and a recent tabulation of the $5\underline{f}^6$ configuration, based on hydrogenic as well as Hartree-Fock Slater ratios, has been reported.[9]

Since experimental studies of the ions are necessarily restricted to condensed systems, it has proved useful to calculate the crystal-field splitting of a given electronic energy level. The wide-spread application of the crystal-field theory has been made possible by the pioneer work of Bethe and Kramers.[10] Stevens, Elliott, and Judd have presented a theoretical approach which has proved successful in the analysis of the crystal-field splitting of rare earth ions.[11-13]

In succeeding sections of this thesis, the application of the theories mentioned above to the analysis of the absorption spectra of TmIV and AmIV will be presented in detail.

II. THEORETICAL CALCULATIONS

A. The General Hamiltonian

The general problem in quantum mechanics is to solve the equation,

$$H\psi = E\psi \,, \tag{1}$$

where H is the Hamiltonian in operator form, ψ is a particular wave function, and E is the corresponding eigenvalue or energy value in this case. In solving this expression for the energy levels of the hydrogen atom in free space, we are able to obtain exact values of E because the exact wave functions are known. In the case of a complex atom, however, only approximate wave functions are known, and only an approximate Hamiltonian is available. In the approximate Hamiltonian we assume that (a) the nucleus and electrons are point charges, (b) the nucleus has an infinite mass, and (c) relativistic effects are negligible. We may write the approximate Hamiltonian of the free ion as

$$H = \sum_{i}^{n} \left[\frac{\vec{p}_i^{\,2}}{2m_i} - Z\frac{e^2}{r_i} + \xi(r_i)\,\vec{s}_i \cdot \vec{\ell}_i \right] + \sum_{i>j=1}^{n} \frac{e^2}{r_{ij}} \,. \tag{2}$$

Here $\vec{p}_i$ is the linear momentum vector of the ith electron, r_i is the radius vector extending from the nucleus to the ith electron, m_i is the electronic mass, and $-Ze^2/r_i$ is the electrostatic attraction between the ith electron and the nucleus. Additional interactions include the coulombic repulsions between the electrons. We may express these repulsions as $\sum_{i>j=1}^{n} e^2/r_{ij}$, where r_{ij} is the distance between the ith and jth electron. Also the magnetic moment of the electron spin may couple with the orbital angular momentum of the electron. If we confine our considerations to Russell-Saunders coupling, the spin-orbit interaction may be written as a constant

multiplied by $\vec{s} \cdot \vec{l}$, or $\xi(r_i)\,\vec{s}_i \cdot \vec{l}_i$, where

$$\xi(r_i) = \frac{\hbar^2}{2m^2c^2r_i}\left[\frac{\partial U(r_i)}{\partial r_i}\right]. \qquad (3)$$

Here $U(r_i)$ is the spherically symmetric potential of the atom.

If the free ion is located in a crystal lattice, the presence of near-by neighbors will tend to reduce the degeneracy of the energy levels of the ion. Thus an additional term must be added to the field-free Hamiltonian. In our case, the crystal-field interaction is largely electrostatic and has been found to be smaller than the spin-orbit term. We may then add an expression, $\sum_{i,j} q_j e^2/r_{ij}$, to the Hamiltonian given in Eq. (2).

Additional perturbations such as spin-other orbit, and spin-spin interaction have been discussed recently.[14] Similarly, if the nucleus has a spin I and a quadrupole moment Q, the various energy levels will be split still further.

Thus one can add to the original approximate Hamiltonian many smaller interactions and effects, but the three most important to our study of TmIV and AmIV are (a) the electrostatic interactions H_E, (b) the spin-orbit effect $H_{S\text{-}O}$, and (c) the crystal or ligand field perturbation H_C. The Hamiltonian may then be written as,

$$H = H_E + H_{S\text{-}O} + H_C \qquad (4)$$

Let us now discuss each portion of the Hamiltonian in some detail.

B. Evaluation of L-S Term Energies For TmIV, $4f^{12}$

1. Factorization by Angular Momentum for TmIV, $4f^{12}$

The vectors $\vec{L}$ and $\vec{S}$, and therefore $\vec{J} = \vec{L} + \vec{S}$, commute with the Hamiltonian so long as we continue to exclude the spin-orbit coupling. Thus H_E is invariant under a rotation of spatial coordinates $(\vec{L})$, spin coordinates $(\vec{S})$, or both, $(\vec{J})$. Applying the matrix-element theorem for scalar (invariant) operators, we can state that there can be no matrix elements of H_E between states with different L, S, or J or different M_L, M_S, or M_J, since these quantum numbers label the irreducible representations and their rows. Thus we can factor the secular equation by choosing determinants that are angular-momentum eigenfunctions.

However, we are limited in the extent we can go in this direction, because all angular momenta that commute with H do not commute with each other. We can simultaneously diagonalize four operators. The most useful sets have the good quantum numbers $L\ S\ M_L\ M_S$ and $L\ S\ J\ M$.

It is easiest to start with $L\ S\ M_L\ M_S$ sets, since we are using one-electron functions characterized by m_ℓ and m_s. Thus we automatically give "sharp" values to $M_L = \sum m_\ell$ and $M_S = \sum m_s$. Then if we collect states by their M_L and M_S values, we will already have achieved a great amount of factorization.

Let us now consider the TmIV, $4f^{12} \equiv 4f^2$, example of two equivalent "electron holes." We may classify all the 91 determinants consistent with the exclusion principle in the following manner.

M_L	M_S	
	1	0
6		(3^+3^-)
5	(3^+2^+)	$(3^+2^-)(3^-2^+)$
4	(3^+1^+)	$(3^+1^-)(3^-1^+)(2^+2^-)$
3	$(2^+1^+)(3^+0^+)$	$(3^+0^-)(3^-0^+)(2^+1^-)(2^-1^+)$
2	$(3^+-1^+)(2^+0^+)$	$(3^+-1^-)(3^-=1^+)(2^-0^+)(2^+0^-)(1^+1^-)$
1	$(3^+-2^+)(2^+-1^+)(1^+0^+)$	$(3^+-2^-)(3^--2^+)(2^+-1^-)(1^+0^-)(1^-0^+)(2^--1^-)$
0	$(3^+-3^+)(2^+-2^+)(1^+-1^+)$	$(3^+-3^-)(3^-3^+)(2^+-2^-)(1^+-1^-)(0^+0^-)(1^--1^+)(2^--2^+)$

This is only the upper left quadrant of the complete table. The other portions can be obtained by suitable systematic sign changes. Since there are no matrix elements between states of different M_L or M_S, we have succeeded in factoring our 91 by 91 secular equation down to ten 1 by 1's, ten 2 by 2's, eight 3 by 3's, two 4 by 4's, two 5 by 5's, two 6 by 6's and one 7 by 7, by $M_L M_S$ factorization alone.

To proceed further, we must inquire after the L and S values as well. For example, the state (3^+3^-) must have $L \geq 6$ because $M_L = 6$. But the vector model only allows L = 0, 1, 2, 3, 4, 5, and 6; therefore it must be an I state (L = 6). Since only one state with

$M_L = 6$ exists, it must be part of a ^1I term. In the case of ^3I we would have to have two other states with $M_S = \pm 1$. These are forbidden by the exclusion principle, however, because they would have double occupancies like (3^+3^+). Since a ^1I term is present, we must have the other twelve "partners" in the 13-dimensional representation. This accounts for one state out of each row of the $M_S = 0$ column. The remaining 78 states are those required for a $^3H(M_L = \pm 5, 0; M_S = \pm 1, 0)$, $^1G(M_L = \pm 4; M_S = 0)$, $^3F(M_L = \pm 3; M_S = \pm 1, 0)$, $^1D(M_L = \pm 2, 0; M_S = 0)$, $^3P(M_L = \pm 1, 0; M_S = \pm 1, 0)$, and a $^1S(M_L = M_S = 0)$ term. In this way we obtain the result that the terms allowed by the Pauli principle in the $4f^{12}$ configuration are $^1I, ^3H, ^1G, ^3F, ^1D, ^3P$, and ^1S.[15]

2. TmIV, $4f^{12}$, Slater Sum-Rule Method

The Slater method is based on the fact that the energy of an L-S term is independent of M_L and M_S.[16] Thus we have only seven distinct eigenvalues to find from our 91 by 91 matrix problem, namely, the energies of the $^1I, ^3H, ^1G, ^3F, ^1D, ^3P$, and ^1S terms. Since we can calculate these energies for whatever M_L and M_S is most convenient, we choose M_L and M_S so that there is only one determinant in the box, assuring us that we are dealing with an eigenfunction of L and S, i.e., a pure term. Thus we have

$$W(^1I) = (3^+3^- | H_E | 3^+3^-) = (3^+3^-),$$

$$W(^3H) = (3^+2^+ | H_E | 3^+2^+) = (3^+2^+),$$

$$W(^1G) = \text{Tr. (3 by 3)} - W(^1I) - W(^3H),$$

$$W(^3F) = \text{Tr. (2 by 2)} - W(^3H),$$

$$W(^1D) = \text{Tr. (5 by 5)} - W(^1I) - W(^3H) - W(^1G) - W(^3F),$$

$$W(^3P) = \text{Tr. (3 by 3)} - W(^3H) - W(^3F),$$

and

$$W(^1S) = \text{Tr. (7 by 7)} - W(^1I) - W(^3H) - W(^1G) - W(^3F) - W(^1D) - W(^3P) ,$$

where Tr. (3 by 3) means the trace of a 3 by 3 matrix. The trace is the sum of the diagonal elements in a matrix.

We are able to calculate $W(^1G)$ because we already know the other two roots, $W(^1I)$ and $W(^3H)$, and by the invariance of traces under unitary transformations, we know that the sum of the three roots is just the sum of the three diagonal values. Thus we can express our unknown energy as

$$W(^1G) = \text{Tr. (3 by 3)} - W(^1D) - W(^3P)$$

$$= (3^+1^-) + (3^-1^+) + (2^+2^-) - (3^+3^-) - (3^+2^+) ,$$

where we have abbreviated the notation for diagonal matrix elements still further. Having found $W(^1G)$, we can go on to evaluate other electrostatic terms. But before going into detail, let us consider the general properties of these matrix elements.[15,16]

3. Examination of Matrix Elements, TmIV, $4f^{12}$

The diagonal matrix elements to which we have reduced our TmIV, $4f^{12}$, problem are the matrix elements of

$$H = \sum_1^2 \left[\vec{p}_i^{\,2}/2m - Z e^2/r_i \right] + \sum_{i>j} e^2/r_{12} . \qquad (5)$$

The one-electron terms will contribute equally to all diagonal elements since all come from the same configuration. Thus they shift only the zero of energy for the configuration and have no effect on the splitting apart of the terms. The term structure is determined wholly by $H_E = Q = \sum_{i>j} e^2/r_{ij}$.

Since only the diagonal elements are needed when using the Slater method, we write following the method outlined by Condon and Shortley,[17]

$$(A \mid Q \mid A) = \sum_{a>b} [J(a,b) - K(a,b)] \equiv \sum_{a>b} [(ab \mid q \mid ab) - (ab \mid q \mid ba)] \ . \tag{6}$$

Because of the symmetry, we can condense the notation and reduce the general expression to

$$J(a,b) = \sum_{k=0}^{\infty} a^k (\ell^a m_\ell^a , \ell^b m_\ell^b) \ F^k (n^a \ell^a, n^b \ell^b), \tag{7}$$

and

$$K(a,b) = \delta(m_s^a \ m_s^b) \sum_{k=0}^{\infty} b^k (\ell^a m_\ell^a , \ell^b m_\ell^b) \, G^k (n^a \ell^a, n^b \ell^b), \tag{8}$$

where new notations introduced are

$$a^k(\ell^a m_\ell^a , \ell^b m_\ell^b) = C^k (\ell^a m_\ell^a , \ell^a m_\ell^a) \, C^k (\ell^b m_\ell^b, \ell^b m_\ell^b) ,$$

$$b^k (\ell^a m_\ell^a , \ell^b m_\ell^b = \left[C^k (\ell^a m_\ell^a , \ell^b m_\ell^b) \right]^2 ,$$

$$F^k (n^a \ell^a, n^b \ell^b) = R^k (n^a \ell^a n^b \ell^b, n^a \ell^a n^b \ell^b) ,$$

$$G^k (n^a \ell^a, n^b \ell^b) = R^k (n^a \ell^a n^b \ell^b, n^b \ell^b n^a \ell^a) ,$$

$$C^k (\ell^a m_\ell^a , \ell^a m_\ell^a) = (-1)^{m_\ell - m_\ell'} \left(\frac{2}{2k+1} \right)^{1/2} \int_0^{\pi} \Theta (k, m_\ell - m_\ell') \, \Theta (\ell, m_\ell) \, \Theta (\ell', m_\ell') \sin \theta d\theta ,$$

$$R^k (n\ell (a,b)) = e^2 \int_0^{\infty} \int \frac{r_<^k}{r_>^{k+1}} \, R_1 (n^a \ell^a) \, R_2 (n^b \ell^b) \, R_1 (n^a \ell^a) \, R_2 (n^b \ell^b) \, dr_1 dr_2 .$$

The coefficients a^k and b^k have been tabulated by Condon and Shortley.[17] Also F^k equals G^k if the electrons are equivalent. The R^k's are the radial distribution functions.

For

$$W(^1I) = (3^+3^- \mid H_E \mid 3^+3^-) = (3^+3^-)$$

we have

$$(3^+3^-) = J(3^+3^-) - K(3^+3^-)$$

$$= \sum_k a^k F^k - 0 .$$

From Condon and Shortley, we find

$$W(^1I) = (3^+3^-) = F_0 + 25\,F_2 + 9F_4 + F_6 ,$$

where we have absorbed the common factors 1/225, 1/1089, and 1/7361.64 by dropping the superscript to a subscript. Thus we have

$$W(^3H) = (3^+2^+ \mid H_E \mid 3^+2^+) = (3^+2^+)$$

$$(3^+2^+) = J(3^+2^+) - K(3^+2^+)$$

$$W(^3H) = F_0 - 25\,F_2 - 51\,F_4 - 13F_6 .$$

The rest of the pure electrostatic energy levels may be written as:

$$W(^1G) = (3^+1^-) + (3^-1^+) + (2^+2^-) - (3^+3^-) - (3^+2^+)$$

$$W(^1G) = F_0 - 30\,F_2 + 97\,F_4 + 78\,F_6$$

$$W(^3F) = (2^+1^+) + (3^+0^+) - (3^+2^+)$$

$$W(^3F) = F_0 - 10F_2 - 33F_4 - 286F_6$$

$$W(^1D) = (3^+-1^-) + (3^+-1^-) + (2^+0^-) + (2^-0^+) + (1^+1^-) - (3^+3^-)$$

$$- (3^+2^+) - (2^+1^+) - (3^+0^+) + (3^+2^+) - (3^+1^-) - (3^-1^+)$$

$$- (2^+2^-) + (3^+3^-) + (3^+2^+)$$

$$W(^1D) = F_0 + 19F_2 - 99F_4 + 715F_6$$

$$W(^3P) = (3^+-2^+) + (2^+-1^+) + (1^+0^+) - (3^+2^+) - (2^+1^+) - (3^+0^+) + (3^+2^+)$$

$$W(^3P) = F_0 + 45F_2 + 33F_4 - 1287F_6 ,$$

$$W(^1S) = (3^+-3^-) + (3^--3^+) + (2^+-2^-) + (1^+-1^-) + (0^+0^-)$$

$$+ (1^--1^+) + (2^--2^+) - (3^+3^-) - (3^+2^+) - (3^+1^-)$$

$$- (3^-1^+) - (2^+2^-) + (3^+3^-) + (3^+2^+) - (2^+1^+)$$

$$- (3^+0^+) + (3^+2^+) - (3^+-2^+) - (2^+-1^+) - (1^+0^+)$$

$$+ (3^+2^+) + (2^+1^+) + (3^+0^+) - (3^+2^+) - (3^+-1^-)$$

$$- (3^+-1^-) - (2^+0^-) - (2^-0^+) - (1^+1^-) + (3^+3^-)$$

$$+ (3^+2^+) + (2^+1^+) + (3^+0^+) - (3^+2^+) + (3^+1^-)$$

$$+ (3^-1^+) + (2^+2^-) - (3^+3^-) - (3^+2^+)$$

$$W(^1S) = F_0 + 60F_2 + 198F_4 + 1716F_6 .$$

4. Evaluation of F_k Integrals For, TmIV, $4f^{12}$

In order to obtain numerical values for the pure electrostatic energy levels, it is necessary to consider what radial-wave equations, R^k, should be put into the Slater integrals F_k. The simplest approximation is to assume hydrogenic functions. These differ from the atomic hydrogen eigenfunctions only by the replacement of the nuclear charge by $(Z - \sigma)$, where σ is the screening charge of the inner electrons.[18] A more systematic approach is to choose a simple form for the radial function and the best values for parameters entering the function by the variational method of minimizing the total energy. This method was introduced by Morse, Young, and Haurwitz,[19] extended by Duncanson and Coulson,[20] and recently carried further by machine computation by Tubis.[21]

The Hartree-Fock method, using the variational method again, leads to a set of coupled integro-differential equations for the single-electron functions. This method offers the greatest possibility to date of giving the best eigenfunctions for heavy-metal atoms. The reason is to be found in the method of iteration, which is carried out as follows. First we guess a set of functions $u_1 \cdots u_n$. Then by averaging the potential produced by the other electrons $(j \neq i)$ and the nucleus, we calculate the spherically averaged u_i seen by each electron

$$U_i(r_i) = -\frac{Ze^2}{r_i} + \left[\sum_{j \neq i} e^2/r_{ij}\right]_{\text{average}} . \tag{9}$$

Using these potentials, we solve the Schrödinger equation,

$$\left[\vec{p}_i^{\,2}/2m_i + U_i(r_i)\right] u_i = E_i u_i , \tag{10}$$

by numerical integration. The resulting set of u_i values will not in general agree with the assumed value. On the basis of this new set, another guess is made, and the calculation is repeated over and over until self-consistency is reached.

For TmIV, $4f^{12}$, Gruber and Conway found that the ratios of F_k integrals are reasonably insensitive to the choice of actual radial distribution functions.[22] Thus, we can evaluate the ratios of F_4/F_2 and F_6/F_2, assuming a simpler variational function than that reached by the Hartree-Fock method. Although there is no reason to expect that the simplified radial functions will describe satisfactorally the f electrons in TmIV, the ratios obtained by the use of simplified eigenfunctions are in close agreement with those obtained experimentally.

Ridley recently published the Hartree-Fock calculations for TmIV.[23] Accordingly, we wish to present the simple methods used in evaluating the F_k ratios and discuss Ridley's work on TmIV.

5. Calculation of F_k Ratios by Using a "Rectangular" Radial Distribution Function for $4f^2 \equiv 4f^{12}$, TmIV.[24]

Consider the radial distribution function

$$F_k = e^2/D^k \int R^2_{4f(1)}\, R^2_{4f(2)}\, (r_<^k / r_>^{k+1})\, r_1^2 \cdot r_2^2\, dr_1\, dr_2 \qquad (11)$$

Now, let us consider the rectangular radial function

$$R^2 = \frac{1}{\ell - 1}\,, \qquad (12a)$$

for $1 \leqslant r \leqslant \ell$, and elsewhere

$$R^2 = 0\,. \qquad (12b)$$

The ℓ is a variable integral parameter which is a constant $\ell = 3$ for the rare earth, 4f series. The orbital angular momentum for an f electron is $\ell = 3$. Thus for $k \neq 0$ we have

$$F_k = \frac{e^2}{D^k} \frac{1}{(\ell-1)^2} \int_1^{\ell} \left[\int_1^{r_2} (r_1^k / r_2^{k+1})\, dr_1 + \int_{r_2}^{\ell} (r_2^k / r_1^{k+1})\, dr_1 \right] dr_2 \qquad (13)$$

and

$$F_k = \left[e^2/D^k (\ell-1)^2 \right] \left[\frac{2\ell}{k+1} - \frac{2}{k} + \frac{2}{\ell^k \cdot k(k+1)} \right] . \quad (14)$$

For $k = 0$ we have

$$F_0 = \frac{2\, e^2}{D^k (\ell-1)^2} \quad (\ell - 1 - \ln \ell). \quad (15)$$

Even though the integrals do not diverge for $k > 2$, as in the case of hydrogen-like wavefunctions, values of $4\underline{f}$, $\ell = 3$ seem to exhibit ratios of F_4 / F_2 such as those actually observed. For $k = 2$, $D^k = 225$; $k = 4$, $D^k = 1089$; and $k = 6$, $D^k = 7361.64$, we have[17]

$$F_2 = \frac{e^2}{225 \cdot 4} \left(\frac{2 \cdot 3}{3} - \frac{2}{2} + \frac{2}{3^2 \cdot 2 \cdot 3} \right) = \frac{e^2}{225 \cdot 4} \left(1.0370 \right) , \quad (16)$$

$$F_4 = \frac{e^2}{1089 \cdot 4} \left(\frac{2 \cdot 3}{5} - \frac{2}{4} + \frac{2}{3^4 \cdot 4 \cdot 5} \right) = \frac{e^2}{1089 \cdot 4} \left(0.7012 \right), \quad (17)$$

$$F_6 = \frac{e^2}{7361.6 \cdot 4} \left(\frac{2 \cdot 3}{7} - \frac{2}{6} + \frac{2}{3^6 \cdot 6 \cdot 7} \right) = \frac{e^2}{7361.6 \cdot 4} \left(0.5239 \right) \quad (18)$$

with

$$F_4/F_2 = 0.1397 \quad (19a)$$

and

$$F_6/F_2 = 0.01544 . \quad (19b)$$

6. Evaluation of F_k Ratios Using Hydrogenic Radial Distribution Functions for $4f^{12}$, TmIV.

The F_4/F_2 and F_6/F_2 ratios have been evaluated for the f^n configuration by Elliott, Judd, and Runciman, for a hydrogenic distribution.[7] We wish to present here the straightforward integration methods used to evaluate the F_4/F_2 and F_6/F_2 ratios for TmIV, with $Z^* = (Z-\sigma) = 35$. Using $\sigma = 34$ as given by Elliott, Judd, and Runciman,[7] we have

$$F_k = \left(e^2/D_k\right) \int R^2_{4f}(1)\, R^2_{4f}(2) \left(r_<^k / r_>^{k+1}\right) r_1^2 \cdot r_2^2 \, dr_1 \, dr_2 \,, \tag{20}$$

$$F_2 = \int_0^\infty R_1^2 \, R_2^2 \left(r_<^k / r_>^{k+1}\right) r_1^2 \, r_2^2 \, dr_1 \, dr_2 \,, \tag{21}$$

$$F_2 = \int_0^\infty R_1^2 \, r_1^2 \left[\int_0^{r_1} R_2^2 \, r_2^2 \left(r_2^k / r_1^{k+1}\right) dr_2\right] dr_1$$

$$+ \int_0^\infty R_1^2 \, r_1^2 \left[\int_{r_1}^\infty R_2^2 \, r_2^2 \left(r_1^k / r_2^{k+1}\right) dr_2\right] dr_1 \,, \tag{22}$$

and

$$F_2 = \int_0^\infty R^2_{f}(1) \, r_1^2 \left[\int_0^{r_1} R_{f}(2) \, r_2^2 \left(r_2^2 / r_1^3\right) dr_2\right] dr_1$$

$$+ \int_0^\infty R_1^2 \, r_1^2 \left[R_2^2 \, r_2^2 \left(r_1^2 / r_2^3\right) dr_2\right] dr_1 \,. \tag{23}$$

We wish to put all electrostatic interaction terms in terms of F_2. Thus we need only the ratios F_4 / F_2 and F_6 / F_2:

$$F_4 / F_2 = \frac{\displaystyle\int_0^\infty R_1^2\, r_1^2 \left[\int_0^{r_1} R_2^2\, r_2^2 \left(r_2^4 / r_1^5\right) dr_2\right] dr_1 + \int_0^\infty R_1^2\, r_1^2 \left[\int_{r_1}^\infty R_2^2\, r_2^2 \left(r_1^4 / r_2^5\right) dr_2\right] dr_1}{\displaystyle\int_0^\infty R_{\underline{f}(1)}^2\, r_1^2 \left[\int_0^{r_1} R_2^2\, r_2^2 \left(r_2^2 / r_1^3\right) dr_2\right] dr_1 + \int_0^\infty R_1^2\, r_1^2 \left[R_2^2\, r_2^2 \left(r_1^2 / r_2^3\right) dr_2\right] dr_1} \tag{24}$$

$$F_6 / F_2 = \frac{\displaystyle\int_0^\infty R_1^2\, r_1^2 \left[\int_0^{r_1} R_2^2\, r_2^2 \left(r_2^6 / r_1^7\right) dr_2\right] dr_1 + \int_0^\infty R_1^2\, r_1^2 \left[\int_{r_1}^\infty R_2^2\, r_2^2 \left(r_1^6 / r_2^7\right) dr_2\right] dr_1}{\displaystyle\int_0^\infty R_1^2\, r_1^2 \left[\int_0^{r_1} R_2^2\, r_2^2 \left(r_2^2 / r_1^3\right) dr_2\right] dr_1 + \int_0^\infty R_1^2\, r_1^2 \left[R_2^2\, r_2^2 \left(r_1^2 / r_2^3\right) dr_2\right] dr_1} \tag{25}$$

For TmIV, $4f^{12}$, with $Z = 69$, $\ell = 3$, and $Z^* = (69-\sigma)$, we have

$$R_{43}(r) = \frac{(Z-\sigma)^{3/2}}{96\sqrt{35}\,a_0^{3/2}} \cdot \frac{8(Z-\sigma)}{64\,a_0^3}\, r^3\, e^{-(Z-\sigma)r/4a_0} . \tag{26}$$

Putting in values for $R_{43}(r)$, $\sigma = 34$, we obtain

$$R_{43}(r) = 55.83\, a_0^{-9/2}\, r^3\, e^{-8.75\,(r/a_0)} . \tag{27}$$

Using Eq. (27) in Eq. (24) and (25), we obtain final ratios of

$$F_4/F_2 = 0.138 \tag{28a}$$

and

$$F_6/F_2 = 0.0151 , \tag{28b}$$

which agree with values obtained by Elliott, Judd, and Runicman.[7]

When the electrostatic equations written in terms of F_2 are normalized to $^3H = 0$ as the ground state, according to Hund's rules we obtain the pure electrostatic energy levels that are recorded in Table I.

Table I. Pure electrostatic energy levels, $4f^{12}$ configuration, TmIV

Level	Electrostatic equations in terms of Slater integrals	Electrostatic equations in terms of F_2 (a)	Energy levels normalized to $^3H = 0$
^3H	$F_0 - 25\,F_2 - 51\,F_4 - 13\,F_6$	$F_0 - 32.3\,F_2$	$0.00\,F_2$
^3F	$F_0 - 10\,F_2 - 33\,F_4 - 286\,F_6$	$F_0 - 18.9\,F_2$	$13.4\,F_2$
^1G	$F_0 - 30\,F_2 + 97\,F_4 + 78\,F_6$	$F_0 - 15.5\,F_2$	$16.8\,F_2$
^1D	$F_0 + 19\,F_2 - 99\,F_4 + 715\,F_6$	$F_0 + 16.3\,F_2$	$48.4\,F_2$
^1I	$F_0 + 25\,F_2 + 9\,F_4 + F_6$	$F_0 + 26.3\,F_2$	$58.6\,F_2$
^3P	$F_0 + 45\,F_2 + 33\,F_4 - 1287\,F_6$	$F_0 + 30.3\,F_2$	$62.6\,F_2$
^1S	$F_0 + 60\,F_2 + 198\,F_4 + 1716\,F_6$	$F_0 + 113.2\,F_2$	$145.5\,F_2$

(a) $F_4 = 0.138\,F_2$, and $F_6 = 0.0151\,F_2$.

7. Hartree-Fock F_k Ratios

Recently (1960), Ridley has published the results of a Hartree-Fock self-consistent field treatment (without exchange or relativistic corrections) for PrIV and TmIV.[23] Since the shape of the 4f wave functions she obtained for PrIV and TmIV are of some interest, we have plotted her values of $4\pi r^2 R^2$ vs r for TmIV in Fig. 1 and $\sum r_i^2 R^2_{n\ell_i}$ vs r in Fig. 2. Ridley found that the form of the radial distribution function of PrIV is far from hydrogen-like, since it has a much greater concentration in the exponential portion of the function. At the position of the principal maximum of R (5s;r), R^2(4f;r) is reduced from its maximum value by a factor of 0.40. The principal maximum of R (4f;r) falls just outside that of R (4d;r). In TmIV,

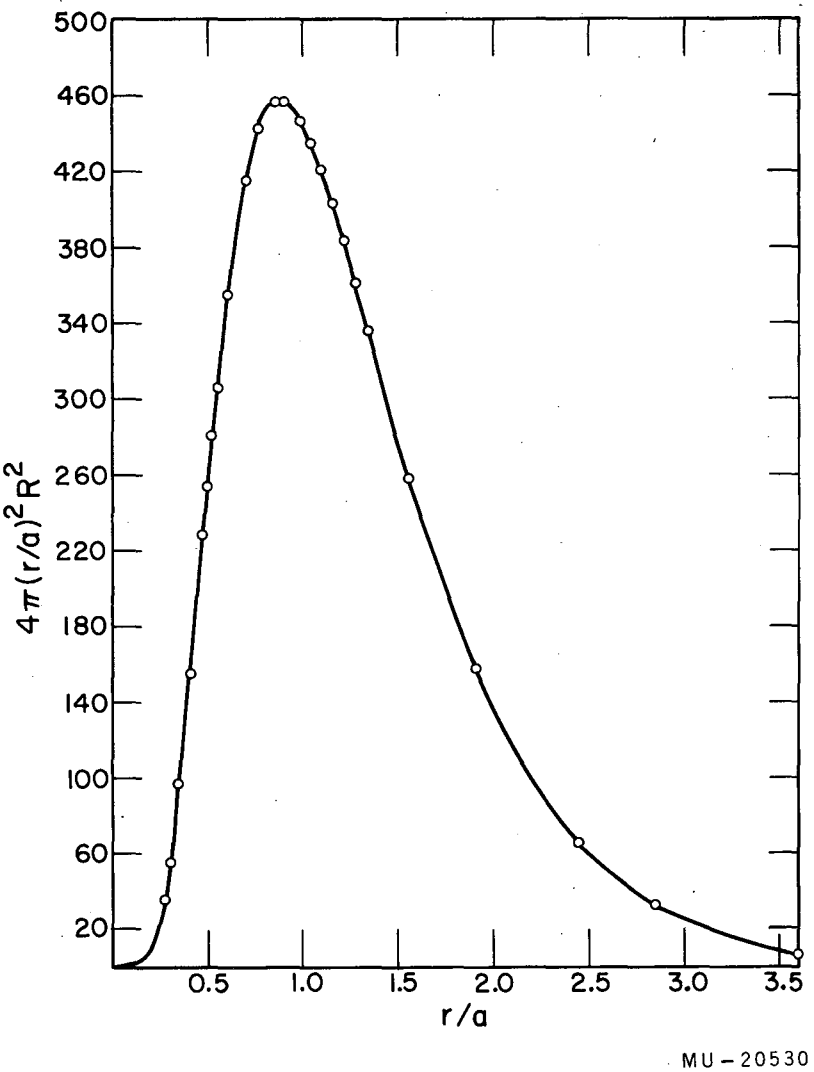

Fig. 1. Hartree-Fock radial-distribtuion function for TmIV, $4f^{12}$. Here $4\pi r^2R^2$ is plotted against r in angstroms. The values for R and r are taken from Ridley's tables of calculations (see text).

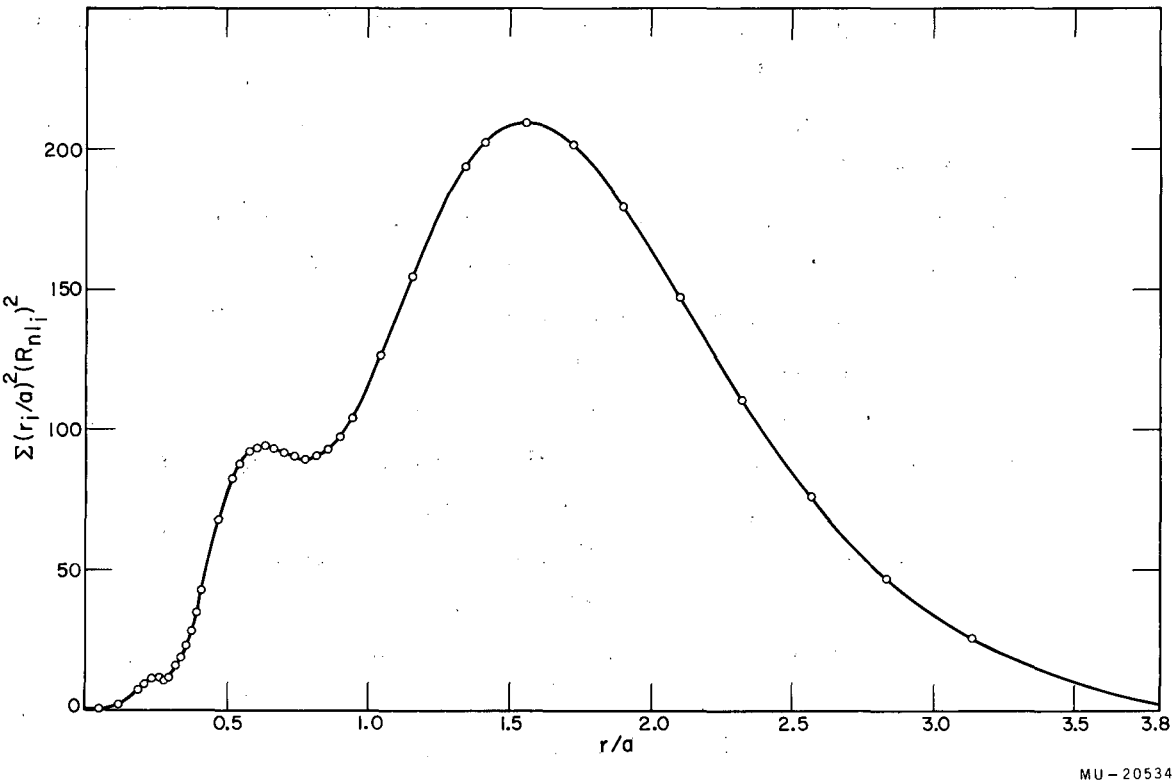

Fig. 2. The $\sum r_i^2 (R_{n,\ell_i})^2$ functions vs r for TmIV, $4f^{12}$.

the charge concentration in the tail of the 4f function is much less, and at the principal maximum of R (5s;r), R^2(4f;r) is only 0.25 of its maximum value. The importance of this concentration of 4f charge density relative to R(4d;r), R (5s;4), and R (5p;r) is shown by the value of the screening constant σ (4f) which is 40.6 in PrIV and 42.96 in TmIV.

As a result of her calculations, Ridley presents the ratios $F_4/F_2 = 0.129$ and $F_6/F_2 = 0.0137$. The hydrogenic values of these ratios given in the previous section are some 8% larger. A deviation in this direction would be expected, because the 4f functions in PrIV and TmIV are more diffuse than hydrogenic functions, and F_k therefore decreases more rapidly with k than in the hydrogenic case. The ratios change by less than 0.5% in going from PrIV to TmIV, even though the values for TmIV are closer to the hydrogenic case.

Fortunately, a rather critical test of Ridley's results can be made by using the experimental results of Johnsen,[25] and Gruber and Conway.[22] The positions of the $^3F_2$ and $^3F_3$ have been identified by polarization and Zeeman studies to be some 300 cm^{-1} apart with the $^3F_2$ higher in energy. Also the positions of the $^3P_{2,1,0}$, $^1D_2$, $^1G_4$, $^3F_4$, $^3H_4$, and $^3H_5$ have been identified. If Ridley's F_k ratios and ζ_{4f} values used in the spin-orbit matrices, we obtain, in general, poorer agreement with experimental values than if we had used the calculated 4f hydrogenic F_k ratios. At this point we find ourselves in a dilemma. If we use the hydrogenic ratios mentioned earlier, we are ignoring the exact solution to the Schrödinger wave equation, and if we use the Ridley ratios, we have ignored correlation effects and configuration-interaction effects. Since neither of the sets of F_k ratios represents the "true" set, we have selected the 4f hydrogenic ratios because they give better agreement with experimental values.

C. Evaluation of L-S Term Energies for AmIV, $5f^6$

1. The Racah Classification of States for f^n

When the calculation of pure electrostatic energy levels for configurations with more than two f electrons is carried out by the methods of Condon and Shortley, we find the work exceedingly tedious and laborious.[17] However, Racah has pointed out how states of f^n may be classified by group-theoretical methods.[4] We give in this section only a brief outline of the group theory since an excellent presentation has been given by Dr. B.R. Judd in a series of lectures on complex spectra.[15]

Racah first classifies all the orbital states of f^n according to the irreducible representations of the group U_7 of all unitary transformations in the seven-dimensional space covered by the orbital states of an f electron, having $m_\ell = -3, -2, -1, 0, +1, +2,$ and $+3$. These representations are characterized by the partition of n into seven integral parts. If we restrict the group U_7 to its subgroup R_3, the group of rotations in three-dimensional space, then the representation of U_7 which corresponds to the partition [n] breaks down into the irreducible representations $\mathcal{D}_L$ of R_3. Thus, we can enumerate states of angular momenta L associated with partition [n]. The orbital states can then be classified according to the irreducible representations of the rotation group R_7 in the seven-dimensional space spanned by the orbital states of an f electron.

When U_7, the total group, is restricted to its subgroup R_7, the representations of U_7 break down into representations $\mathcal{D}_W$ of R_7, which can be characterized by a partition of n into three integers w_1, w_2, and w_3. We may view $W \equiv (w_1\ w_2\ w_3)$ as a set of quantum numbers, where the w's are integers, $w_1 \geq w_2 \geq w_3 \geq 0$ and $w_1 \leq 2$ must hold for f^n LS states.

Now there exists the subgroup G_2 of R_7 which in turn contains R_3 as a subgroup. Thus, if we restrict R_7 to its subgroup G_2, the representations $\mathcal{D}_W$ of R_7 break down into the irreducible representations $G(u_1, u_2)$ of G_2. These may also be broken down into the

irreducible representations $\mathcal{D}_L$ of R_3. The representations $G(u_1, u_2)$ can be characterized by the set $U \equiv (u_1, u_2)$, where we consider U as another set of quantum numbers.

With few exceptions these labels serve to distinguish all states of the $\underline{f}$ shell. Using the symbol τ to indicate additional quantum numbers that we may yet need, we write the wave functions

$$\psi\,(\underline{f}^n \tau\, W\, U\, S\, L\, S_z\, L_z)\,. \tag{29}$$

Racah also defines a "seniority number," v, to label the states. If a and b are defined such that $w_1 = \cdots = w_a = 2$, $w_{a+1} = \cdots = w_{a+b} = 1$, $w_{a+b+1} = \cdots = w_3 = 0$, then we have $a = (v - S)/2$, $b = \min(2S,\ 2\ell + 1 - v)$, and $\psi\,(\underline{f}^n \tau\, U\, v\, S\, L\, S_z\, L_z)$. For the particular case of AmIV, $5\underline{f}^6$, we list in Table II the classification of states for $\underline{f}^6$.

Having expressed the wave function in terms of useful quantum numbers, let us now expand a state of configuration $\underline{f}^n$ in terms of products of states of the first (n-1) particles with those of the nth particle as follows:

$$\psi\,(\underline{f}^n \tau\, U\, v\, S\, L\, S_z\, L_z) = \sum_{\bar{\tau}\bar{U}\bar{v}\bar{S}\bar{L}} \left(\underline{f}^n (\tau U v S L) \quad \{\,|\, \underline{f}^{n-1} (\bar{\tau}\,\bar{U}\,\bar{v}\,\bar{S}\,\bar{L})\right) \tag{30}$$

$$\sum_{\bar{S}_z \bar{L}_z s_z \ell_z} (\bar{S}\,\tfrac{1}{2}\, S S_z \,|\, \bar{S}\,\tfrac{1}{2}\,\bar{S}_z\, s_z)$$

$$(\bar{L}\ell\, L L_z \,|\, \bar{L}\ell\,\bar{L}_z \ell_z)\, \bar{\psi}\,(\underline{f}^{n-1}\, \bar{\tau}\,\bar{U}\,\bar{v}\,\bar{S}\,\bar{L}\,\bar{S}_z\,\bar{L}_z)$$

$$\phi\,(\ell\, s_z\, \ell_z)\,.$$

Table II. Classification of states, f^6 configuration

S	n	v	W	U	SL
3	6	6	(100)	(10)	^{7}F
2	6	6	(210)	(11)	^{5}PH
				(20)	^{5}DGI
				(21)	^{5}DFGHKL
2	6	4	(111)	(00)	^{5}S
				(10)	^{5}F
				(20)	^{5}DGI
1	6	6	(221)	(10)	^{3}F
				(11)	^{3}PH
				(20)	^{3}DGI
				(21)	^{3}DFGHKL
				(30)	^{3}PFGHIKM
				(31)	$\left\{\begin{matrix}^3\text{PDFFGHH} \\ ^3\text{IIKKLMNO}\end{matrix}\right\}$
1	6	4	(211)	(10)	^{3}F
				(11)	^{3}PH
				(20)	^{3}DGI
				(21)	^{3}DFGHKL
				(30)	^{3}PFGHIKM
1	6	2	(110)	(10)	^{3}F
				(11)	^{3}PH

Table II. (Cont.)

S	n	v	W	U	SL
0	6	6	(222)	(00)	^{1}S
				(10)	^{1}F
				(20)	^{1}DGI
				(30)	^{1}PFGHIKM
				(40)	$\{^1$SDFGGHII, ^{1}KLLMNQ$\}$
0	6	4	(220)	(20)	^{1}DGI
				(21)	^{1}DFGHKL
				(22)	^{1}SDGHILN
0	6	2	(200)	(20)	^{1}DGI
0	6	0	(000)	(00)	^{1}S

The second sum in the expansion performs the vector coupling of the total S and L values, while the first coefficients, $\left(\underline{f}^n\,(\tau\, U v\, S\, L)\,\{\,|\underline{f}^{n-1}(\bar{\tau}\,\bar{U}\,\bar{v}\,\bar{S}\,\bar{L})\right)$, are the coefficients of fractional parentage (c.f.p.). These coefficients may be factored into the following three parts,

$$\left(\underline{f}^n\,(\tau\, U v S L)\,\{\,|\underline{f}^{n-1}(\bar{\tau}\,\bar{U}\,\bar{v}\,\bar{S}\,\bar{L})\right) = \left(\underline{f}^n\, v\, S\,\{\,|\underline{f}^{n-1}\,\bar{v}\,\bar{S} + \underline{f}\right) \tag{31}$$

$$(W\, U\,|\,\bar{W}\,\bar{U} + \underline{f})$$

$$(U\,\tau\, L\,|\,\bar{U}\,\bar{\tau}\,\bar{L} + \underline{f})\,.$$

Racah has discussed the properties of the c.f.p. and has given tables for the calculation of each part with the exception of $U \equiv (31)$, (40) states.[4] With an evaluation of the c.f.p., we can begin to write down the eigenfunctions that are useful in the calculation of the electrostatic energy terms. Let us now consider in some measure the energy matrices of the electrostatic interaction as they are evaluated by the methods of Racah.

2. Setting Up the Electrostatic Energy Matrices, $\underline{f}^6$, Configuration

In Section II B the electrostatic energy levels were calculated by expanding the interaction between electrons in Legendre polynomials of the cosine of the angle between electrons. As a result, we were able to write a linear combination of Slater radial integrals for even k,

$$E = \sum_{k=0}^{2\ell} f^k F_k\,. \tag{32}$$

In the $\underline{f}^6$ configuration, however, we have, for example, nine ^3H terms, and the method of Slater gives only the average electrostatic energy of these nine terms.[17] Racah's method does give directly the diagonal and off-diagonal elements of the electrostatic interactions as

a matrix of the degree equal to the number of terms. Using tensor operators and the calculated c.f.p., Racah has constructed new operators which have simple transformation properties under the group used.[4] Let us consider the operator,

$$\mathcal{E} = \sum_{k=0}^{\ell} e_k E^k , \tag{33}$$

where e_k are expectation values of the new operators and E^k are linear combinations of the Slater integrals, F_k. Racah defines for the configurations f^n,

$$e_0 = f^0 = n(n-1)/2 , \tag{34}$$

$$e_1 = 9f^0/7 + f^2/42 + f^4/77 + f^6/462 , \tag{35}$$

$$e_2 = 143\, f^2/42 - 130\, f^4/77 + 35\, f^6/462 , \tag{36}$$

$$e_3 = 11\, f^2/42 + 4f^4/77 - 7\, f^2/462 . \tag{37}$$

The term $9f^0/7$ was added for convenience in e_1 without changing its tensorial properties, since both f^0 and e_1 are scalars in the seven-dimensional space.

The general expression of the energy matrices of f^n will be,

$$e_0 E^0 + e_1 E^1 + e_2 E^2 + e_3 E^3 \tag{38}$$

instead of

$$f^0 F_0 + f^2 F_2 + f^4 F_4 + f^6 F_6 . \tag{39}$$

For $n = 6$, f^6, the e_i are matrices whose order equals the number of allowed states for a given SL. We note that e_0 is a function only of n, the number of f equivalent electrons. Since e_0 is the same for all matrices of f^6, namely $e_0 = 15$, we can omit it in our calculations. The e_1 operator is a scalar with respect to R_7,

G_2 , and R_3 . That is e_1 is diagonal in the Racah v USL scheme, and its eigenvalues must be independent of L and U. Thus we have

$$(\underline{f}^n \; v \; U \; S \; L \; | \; e_1 \; | \underline{f}^n \; v \; U \; S \; L) = \frac{9}{2}(n - v) + \frac{v(v+2)}{4} - S(S+1) \; . \tag{40}$$

Racah has shown that e_2 is diagonal with respect to seniority, and is zero for all terms of maximum multiplicity in $\underline{f}^n$. We can write,

$$(\underline{f}^n \; v \; U \; S \; L \; | \; e_2 \; | \underline{f}^n \; v \; U' \; SL) = \pm (W \; U \; L \; | \; e_2 \; | \; W \; U' \; L) \; , \tag{41}$$

where the upper or lower sign is taken according to whether $v + 2S$ is less than or greater than seven. The matrix is factorized by writing

$$(W \; U \; L \; | \; e_2 \; | \; W \; U' L) = \sum_{\gamma} \chi_{\gamma} \; (W, UU') \; (U | \; \chi_{\gamma} \; (L) \; | \; U') \; . \tag{42}$$

Tables of these matrix elements can be found in Racah's fourth paper.[4]

In evaluating e_3 , Racah simplified the problem by considering the eigenvalues of $e_3 + \Omega$, where Ω is defined as

$$\Omega = \frac{1}{2} \; L \; (L+1) - 12 \; G(G_2) \; , \tag{43}$$

with

$$\omega \; (U, L) = \frac{1}{2} \; L \; (L+1) - 12 \; g(U) \; . \tag{44}$$

Racah gives the following formula for evaluating $e_3 + \Omega$:

$$(\underline{f}^n \; v \; U \; S \; L \; | \; e_3 + \Omega \; | \underline{f}^n \; v \; U' \; SL) = a \; (n, v) \; (\underline{f}^n \; v \; U \; S \; L \; | e_3 + \Omega \; | \underline{f}^n \; v \; U' \; SL) \; , \tag{45}$$

$$a\,(v+2,\,v) = (1-v)/(7-v)\,,\quad a\,(v+4,\,v) = -4/\,(7-v)\,, \tag{46}$$

$$(\underline{f}^6\ v\ USL\ |\ e_3 + \Omega\ |\ \underline{f}^6\ v'\ U'S\,L) = y\ (\underline{f}^6,\ v\ SU,\ v'SU')\ (U\ |\ \phi(L)\ |\ U')\,. \tag{47}$$

Again, these matrix elements are given in Racah's fourth paper.[4] Thus we can construct the matrices for the pure electrostatic energy terms for $\underline{f}^6$. These matrices are listed in Table III.

Elliott, Judd, and Runciman have re-evaluated all the pure electrostatic energy levels from $\underline{f}^2$ to $\underline{f}^4$ and the two lowest multiplicities of the $\underline{f}^5$ and $\underline{f}^6$ configurations.[7] Also B.G. Wybourne has calculated the doublet electrostatic energy matrices for $\underline{f}^5$ and triplet and singlet matrices for $\underline{f}^6$.[8] The matrices presented in Table III were calculated independently and were completed before hearing of Wybourne's work.

Table III. Electrostatic energy-level matrices for the f^6 configuration

	$f_6^6(100)(10)$	$f_4^6(111)(00)$	$f_6^6(210)(11)$	$f_6^6(210)(21)$	$f_6^6(210)(21)$
^7F	$15E^0 = 0$				
^5S		$9E^1$			
^5P			$6E^1 + 11E^3$		
^5L				$6E^1 - 105E^2 - 15E^3$	
^5K					$6E^1 + 135E^2 - 7E^3$

	$f_6^6(210)(21)$	$f_6^6(210)(11)$
^5H	$6E^1 - 21E^2 + 6E^3$	$-12\sqrt{455}\,E^2$
		$6E^1 - 3E^3$

	$f_6^6(210)(20)$	$f_4^6(111)(20)$
^5I	$6E^1 + 30E^2 - 7E^3$	$-2\sqrt{14}\,E^3$
		$9E^1 + 7E^3$

	$f_6^6(210)(21)$	$f_4^6(111)(10)$
^5F	$6E^1 - 195E^2 + 15E^3$	$-6\sqrt{11}\,E^3$
		$9E^1$

	$f_6^6(210)(20)$	$f_6^6(210)(21)$	$f_4^6(111)(20)$
^5D	$6E^1 + \frac{858}{7}E^2 + 11E^3$	$\frac{468}{7}\sqrt{33}\,E^2$	$\frac{22}{7}\sqrt{14}\,E^3$
		$6E^1 - \frac{1131}{7}E^2 + 18E^3$	$\frac{12}{7}\sqrt{462}\,E^3$
			$9E^1 - 11E^3$

Table III (Cont'd)

	f_6^6 (210)(20)	f_6^6 (210)(21)	f_4^6 (111)(20)
^5G	$6E^1 - \frac{780}{7} E^2 + 4E^3$	$-\frac{24}{7}\sqrt{4290}\,E^2$	$\frac{8}{7}\sqrt{14}\,E^3$
		$6E^1 + \frac{1683}{7} E^2 + 11 E^3$	$\frac{2}{7}\sqrt{15015}\,E^3$
			$9 E^1 - 4E^3$

	f_6^6 (221)(31)
^3N	$10E^1 - 76 E^2 - 23 E^3$

	f_6^6 (221)(31)
^3O	$10 E^1 - 10 E^2 - 34 E^3$

Table III (Cont'd)

	$f_6^6(221)(30)$	$f_6^6(221)(31)$	$f_4^6(211)(30)$
^3M	$10E^1 + \frac{25}{2} E^2 - 21E^3$	$\frac{63}{2}\sqrt{35}\,E^2$	$\sqrt{2}\,E^3$
		$10E^1 + \frac{473}{22} E^2 - 13\,E^3$	$3\sqrt{70}\,E^3$
			$13\,E^1 + 50\,E^2 - 23\,E^3$

	$f_6^6(221)(21)$	$f_6^6(221)(31)$	$f_4^6(211)(21)$
^3L	$10E^1 + \frac{1285}{11} E^2 - 15E^3$	$\frac{72}{11}\sqrt{380}\,E^2$	$-\frac{32}{11}\sqrt{11}\,E^3$
		$10E^1 + \frac{2356}{11} E^2 - 4\,E^3$	$-\frac{6}{11}\sqrt{1045}\,E^3$
			$13\,E^1 - 85\,E^2 - 11\,E^3$

Table III (Cont'd)

	$f_6^6(221)(20)$	$f_6^6(221)(21)$	$f_6^6(221)(31)$	$f_4^6(211)(20)$	$f_4^6(211)(21)$
^3D	$10E^1 - \frac{286}{7}E^2 + 11E^3$	$-\frac{780}{7}\sqrt{3}E^2$	$\frac{72}{7}\sqrt{1638}E^2$	$\frac{66}{7}\sqrt{2}E^3$	$6\sqrt{\frac{44}{147}}E^3$
		$10E^1 + \frac{3055}{77}E^2 + 18E^3$	$\frac{180}{11}\sqrt{\frac{78}{7}}E^2$	$-\frac{44}{7}\sqrt{6}E^3$	$\frac{304}{77}\sqrt{11}E^3$
			$10E^1 - \frac{2396}{11}E^2 + 29E^3$	0	$\frac{6}{11}\sqrt{6006}E^3$
				$13E^1 - \frac{1144}{7}E^2 + \frac{143}{7}E^3$	$-\frac{156}{7}\sqrt{66}E^2 + \frac{16}{7}\sqrt{66}E^3$
					$13E^1 + \frac{1781}{7}E^2 + \frac{88}{7}E^3$

Table III (Cont'd)

	$f_6^6(221)(11)$	$f_6^6(221)(30)$	$f_6^6(221)(31)$	$f_4^6(211)(11)$	$f_4^6(211)(30)$	$f_2^6(110)(11)$
^3P	$10E^1+11E^3$	$26\sqrt{110}E^2$	$-6\sqrt{1430}E^2$	$-\frac{121}{15}\sqrt{5}E^3$	$-\frac{\sqrt{55}}{3}E^3$	$-\frac{11}{5}\sqrt{30}E^3$
		$10E^1-26E^2+23E^3$	$-114\sqrt{13}E^2$	$-\frac{19}{3}\sqrt{\frac{11}{2}}E^3$	$\frac{83}{6}\sqrt{2}E^3$	$\sqrt{33}E^3$
			$10E^1+302E^2+31E^3$	$\frac{1}{2}\sqrt{286}E^3$	$-\frac{17}{2}\sqrt{26}E^3$	$3\sqrt{429}E^3$
				$13E^1+\frac{484}{15}E^3$	$-130\sqrt{11}E^2+\sqrt{\frac{11}{3}}E^3$	$-\frac{11}{5}\sqrt{6}E^3$
					$13E^1-104E^2-\frac{14}{3}E^3$	$\sqrt{66}E^3$
						$18E^1-\frac{132}{5}E^3$

Table III (Cont'd)

	$f_6^6(221)(20)$	$f_6^6(221)(30)$	$f_6^6(221)(31)$	$f_6^6(221)(31)$	$f_4^6(211)(20)$	$f_4^6(211)(30)$
^3I	$10E^1-10E^2-7E^3$	$-30\sqrt{3}E^2$	$-270\,E^2$	0	$-6\sqrt{2}E^3$	$4\sqrt{6}E^3$
		$10E^1+\frac{25}{2}E^2+3E^3$	$\frac{171}{2}\sqrt{3}E^2$	$-27\sqrt{102}E^2$	$8\sqrt{6}E^3$	$7\sqrt{2}E^3$
			$10E^1+\frac{1151}{10}E^2+11E^3$	$\frac{153}{5}\sqrt{34}E^2$	0	$-15\sqrt{6}E^3$
				$10E^1-\frac{788}{5}E^2+11E^3$	0	0
					$13E^1-40E^2-13E^3$	$120\sqrt{3}E^2-4\sqrt{3}E^3$
						$13E^1+50E^2-11E^3$

Table III (Cont'd)

${}^3K$	$f_6^6(221)(21)$	$f_6^6(221)(30)$	$f_6^6(221)(31)$	$f_6^6(221)(31)$	$f_4^6(211)(21)$	$f_4^6(211)(30)$
	$10E^1-\frac{2091}{11}-E^2-7E^3$	$\frac{20}{11}\sqrt{374}\,E^2$	$\frac{156}{253}\sqrt{14858}E^2$	$\frac{1008}{253}\sqrt{3036}$ E^2	$\frac{32}{33}\sqrt{11}E^3$	$-\frac{16}{3}\sqrt{\frac{17}{11}}\,E^3$
		$10E^1-47E^2$ $-4E^3$	$741\sqrt{\frac{19}{253}}\,E^2$	$-\frac{219}{46}\sqrt{2346}E^2$	$-\frac{10}{3}\sqrt{34}E^3$	$-\frac{14}{3}\sqrt{2}E^3$
			$10E^1-\frac{123506}{506}$ E^2+4E^3	$-\frac{72}{253}\sqrt{21318}$ E^2	$-\frac{14}{253}\sqrt{163438}$ E^3	$-\frac{2}{11}\sqrt{9614}$ E^3
				$10E^1+\frac{85096}{506}$ E^2 $+4E^3$	$\frac{42}{23}\sqrt{69}E^3$	0
					$13E^1+219E^2$ $-\frac{25}{3}E^3$	$-8\sqrt{17}E^2$ $-\frac{16}{3}\sqrt{17}E^3$
						$13E^1-188E^2$ $+\frac{16}{3}E^3$

Table III (Cont'd)

	$f_6^6(221)(20)$	$f_6^6(221)(21)$	$f_6^6(221)(30)$	$f_6^6(221)(31)$	$f_4^6(211)(20)$	$f_4^6(211)(21)$	$f_4^6(211)(30)$
^3G	$10E^1+\frac{260}{7}E^2+4E^3$	$\frac{40}{7}\sqrt{390}E^2$	$13\sqrt{15}E^2$	$-\frac{45}{7}\sqrt{1305}E^2$	$\frac{24}{7}\sqrt{2}E^3$	$\frac{\sqrt{210210}}{147}E^3$	$\frac{8}{3}\sqrt{30}E^3$
		$10E^1-\frac{981}{7}E^2$ $+11E^3$	$-40\sqrt{26}E^2$	$-552\sqrt{\frac{2}{7}}E^2$	$-\frac{22}{21}\sqrt{195}$ E^3	$-\frac{80}{21}\sqrt{11}E^3$	$-\frac{4}{3}\sqrt{13}E^3$
			$10E^1-26$ E^2 $+14E^3$	$-30\sqrt{91}E^2$	$\frac{16}{3}\sqrt{30}E^3$	$-\frac{5}{6}\sqrt{286}$ E^3	$\frac{10}{3}\sqrt{2}E^3$
				$10E^1+122E^2$ $+22E^3$	0	$11\sqrt{\frac{7}{22}}E^3$	$-2\sqrt{182}E^3$
					$13E^1+\frac{1040}{7}$ E^2 $+\frac{52}{7}E^3$	$\frac{16}{7}\sqrt{2145}$ E^2	$-52\sqrt{15}E^2$ $-\frac{8}{3}\sqrt{15}E^3$
						$13E^1-\frac{1089}{7}$ E^2 $+\frac{341}{21}E^3$	$16\sqrt{143}E^2$ $-\frac{4}{3}\sqrt{143}$ E^3
							$13E^1-104$ E^2 $+\frac{22}{3}E^3$

Table III (Cont'd)

	$f_6^6(221)(10)$	$f_6^6(221)(21)$	$f_6^6(221)(30)$	$f_6^6(221)(31)$	$f_6^{'6}(221)(31)$	$f_4^6(211)(10)$
^3F	$10E^1$	0	$-5\sqrt{143}\,E^2$	0	$15\sqrt{429}E^2$	0
		$10E^1+\frac{10465}{77}E^2$ $+15\,E^2$	$-\frac{60}{11}\sqrt{4290}\,E^2$	$\frac{936}{11}\sqrt{10}$ E^2	$-\frac{36}{11}\sqrt{1430}\,E^2$	$\frac{46}{15}\sqrt{15}\,E^3$
			$10\,E^1+19E^2$ $+\,18E^3$	$72\sqrt{\frac{39}{11}}\,E^2$	$147\sqrt{3}\,E^2$	0
				$10\,E^1-\frac{2210}{11}$ E^2 $+\,26\,E^3$	$-\frac{168}{11}\sqrt{143}$ E^2	$-8\sqrt{6}\,E^3$
					$10E^1+41\,E^2$ $+26\,E^3$	0
						$13\,E^1$

Table III (Cont'd)

	$f_4^6(211)(21)$	$f_4^6(211)(30)$	$f_2^6(110)(10)$
^3F (cont.)	$-\sqrt{\frac{110}{3}}\ E^3$	0	0
	$-\frac{48}{11}\sqrt{11}\ E^3$	$\frac{4}{33}\sqrt{2145}\ E^3$	$-\frac{48}{5}\sqrt{10}\ E^3$
	$\frac{5}{6}\sqrt{390}\ E^3$	$-12\sqrt{2}\ E^3$	0
	$-\frac{18}{11}\sqrt{110}\ E^3$	$\frac{8}{11}\sqrt{858}\ E^3$	$-36\ E^3$
	$-\frac{3}{2}\sqrt{130}\ E^3$	$-12\sqrt{6}\ E^3$	0
	$-\frac{8}{15}\sqrt{165}\ E^3$	$-20\sqrt{143}\ E^2$	0
	$13\ E^1+65\ E^2$ $+21\ E^3$	$24\sqrt{195}\ E^2$ $+\frac{4}{3}\sqrt{195}\ E^3$	$-\frac{6}{5}\sqrt{110}\ E^3$
		$13\ E^1+76\ E^2$ $+42\ E^3$	0
			$18\ E^1$

Table III (Cont'd)

	$f_6^6(221)(11)$	$f_6^6(221)(21)$	$f_6^6(221)(30)$	$f_6^6(221)(31)$	$f_6^{'6}(221)(31)$	$f_4^6(211)(11)$
^3H	$10E^1-3E^3$	$-\frac{14}{11}\sqrt{10010}\,E^2$	$-2\sqrt{390}\,E^2$	$-2\sqrt{3315}\,E^2$	$\frac{50}{11}\sqrt{3003}\,E^2$	$\frac{11}{5}\sqrt{5}\,E^3$
		$10\,E^1+\frac{977}{11}E^2$ $+6\,E^3$	$-10\sqrt{231}\,E^2$	$-\frac{31}{11}\sqrt{7854}\,E^2$	$-\frac{103}{11}\sqrt{30}\,E^2$	0
			$10\,E^1+44\,E^2$ $+9\,E^3$	$30\sqrt{34}\,E^2$	$6\sqrt{770}\,E^2$	$-\frac{19}{6}\sqrt{78}\,E^3$
				$10\,E^1+92E^2$ $+17\,E^3$	$\frac{24}{11}\sqrt{6545}\,E^2$	$\frac{1}{12}\sqrt{2652}\,E^3$
					$10\,E^1-\frac{1340}{11}E^2$ $+17\,E^3$	$\frac{\sqrt{60060}}{60}\,E^3$
						$13\,E^1-\frac{44}{5}$ E^3

Table III (Cont'd)

	$f_4^6(211)(21)$	$f_4^6(211)(30)$	$f_2^6(110)(11)$
^3H (cont.)	0	$-\frac{1}{3}\sqrt{195}\,E^3$	$\frac{3}{5}\sqrt{30}\,E^3$
	$\frac{80}{11}\sqrt{11}\,E^3$	$-\frac{8}{33}\sqrt{462}\,E^3$	0
	$-\frac{10}{3}\sqrt{21}\,E^3$	$-\frac{5}{2}\sqrt{2}\,E^3$	$3\sqrt{13}\,E^3$
	$-\sqrt{\frac{714}{9}}\,E^3$	$-\frac{1}{2}\sqrt{17}\,E^3$	$\frac{3}{2}\sqrt{442}\,E^3$
	$-\frac{37}{33}\sqrt{330}\,E^3$	$-\frac{31}{22}\sqrt{385}\,E^3$	$\frac{3}{10}\sqrt{10010}\,E^3$
	$10\sqrt{182}\,E^2$	$10\sqrt{39}\,E^2$ $+\frac{1}{3}\sqrt{39}\,E^3$	$\frac{3}{5}\sqrt{6}\,E^3$
	$13\,E^1 - 197E^2$ $- 4\,E^3$	$22\sqrt{42}\,E^2$ $-\frac{8}{3}\sqrt{42}\,E^3$	0
		$13E^1+176\,E^2$ $+ 14\,E^3$	$3\sqrt{26}\,E^3$
			$18\,E^1$ $+\frac{36}{5}\,E^3$

Table III (Cont'd)

^1P

$f_6^6(222)(30)$
$12\,E^1 + 156\,E^2 + 23\,E^3$

^1Q

$f_6^6(222)(40)$
$12\,E^1 + 6\,E^2 - 42\,E^3$

^1M

$f_6^6(222)(40)$	$f_6^6(222)(30)$
$12\,E^1 - 291E^2 - 9\,E^3$	$-9\sqrt{165}\,E^2$
	$12\,E^1 - 75\,E^2 - 21E^3$

^1N

$f_6^6(222)(40)$	$f_4^6(220)(22)$
$12E^1 + 144\,E^2 - 19\,E^3$	$-2\sqrt{230}\,E^3$
	$15\,E^1 + 60\,E^2 - 39\,E^3$

^1K

$f_6^6(222)(30)$	$f_6^6(222)(40)$	$f_4^6(220)(21)$
$12\,E^1 + 282\,E^2 - 4E^3$	$-84\sqrt{3}\,E^2$	$4\sqrt{51}\,E^3$
	$12\,E^1 - 36E^2 + 8E^3$	$-2\sqrt{17}\,E^3$
		$15\,E^1 - 129\,E^2 - 3\,E^3$

Table III (Cont'd)

	$f_6^6(222)(10)$	$f_6^6(222)(30)$	$f_6^6(222)(40)$	$f_4^6(220)(21)$
^1F	$12E^1$	$-3\sqrt{1430}E^2$	$9\sqrt{1430}E^2$	$3\sqrt{22}E^3$
		$12E^1 - 114E^2 + 18E^3$	$90E^2$	$-3\sqrt{65}E^3$
			$12E^1 + 294E^2 + 30E^3$	$3\sqrt{65}E^3$
				$15E^1 - 195E^2 - 3E^3$

	$f_6^6(222)(30)$	$f_6^6(222)(40)$	$f_4^6(220)(21)$	$f_4^6(220)(22)$
^1H	$12E^1 - 264E^2 + 9E^3$	$-72\sqrt{42}E^2$	$2\sqrt{126}E^3$	0
		$12E^1 - 192E^2 + 21E^3$	$-12\sqrt{3}E^3$	$6\sqrt{26}E^3$
			$15E^1 + 183E^2 + 36E^3$	$-36\sqrt{78}E^2$
				$15E^1 + 156E^2 - 3E^3$

Table III (Cont'd)

^1L	$f_6^6(222)(40)$	$f_6^6(222)(40)$	$f_4^6(220)(21)$	$f_4^6(220)(22)$
	$12E^1+\frac{1164}{31}E^2$	$\frac{252}{31}\sqrt{1995}E^2$	$22\sqrt{\frac{15}{31}}E^3$	$8\sqrt{\frac{627}{341}}E^3$
		$12E^1+\frac{3210}{31}E^2$	$-\frac{12}{31}\sqrt{4123}E^3$	$\frac{24}{31}\sqrt{1085}E^3$
			$15E^1+15E^2-27E^3$	$-24\sqrt{95}E^2$
				$15E^1-54E^2+18E^3$

^1S	$f_6^6(222)(00)$	$f_6^6(222)(40)$	$f_4^6(220)(22)$	$f_0^6(000)(00)$
	$12E^1$	$-30\sqrt{143}E^2$	$-\frac{4}{5}\sqrt{165}E^3$	0
		$12E^1-384E^2+36E^3$	$4\sqrt{195}E^3$	0
			$15E^1+390E^2-6E^3$	$-\frac{36}{5}\sqrt{110}E^3$
				$27E^1$

Tabel III (Cont'd)

	$f_6^6(222)(20)$	$f_6^6(222)(40)$	$f_4^6(220)(20)$	$f_4^6(220)(21)$	$f_4^6(220)(22)$	$f_2^6(200)(20)$
^1D	$12E^1+78E^2+11E^3$	$-72\sqrt{26}E^2$	$\frac{61}{70}\sqrt{770}E^3$	$\frac{12}{7}\sqrt{7}E^3$	$-\frac{3}{2}\sqrt{78}E^3$	$-\frac{6}{5}\sqrt{55}E^3$
		$12E^1-12E^2+33E^3$	$-\frac{6}{35}\sqrt{5005}E^3$	$-\frac{6}{7}\sqrt{182}E^3$	$18\sqrt{3}E^3$	$\frac{6}{5}\sqrt{1430}E^3$
			$15E^1+\frac{429}{14}E^2+\frac{3971}{140}E^3$	$-\frac{117}{7}\sqrt{110}E^2-\frac{48}{35}\sqrt{110}E^3$	$-\frac{9}{14}\sqrt{15015}E^2+\frac{3}{20}\sqrt{15015}E^3$	$-\frac{33}{350}\sqrt{350}E^3$
				$15E^1-\frac{2535}{7}E^2+\frac{240}{7}E^3$	$\frac{135}{7}\sqrt{546}E^2$	$-\frac{24}{35}\sqrt{385}E^3$
					$15E^1-\frac{75}{2}E^2+\frac{39}{4}E^3$	$-\frac{3}{10}\sqrt{4290}E^3$
						$20E^1+286E^2+\frac{143}{5}E^3$

Table III (Cont'd)

	$f_6^6(222)(20)$	$f_6^6(222)(30)$	$f_6^6(222)(40)$	$f_6^{'6}(222)(40)$	$f_4^6(220)(20)$	$f_4^6(220)(22)$	$f_2^6(200)(20)$
^1I	$12E^1+\frac{210}{11}E^2$ $-7E^3$	$-\frac{90}{11}\sqrt{462}E^2$	$\frac{306}{341}\sqrt{64790}E^2$	$-\frac{108}{341}\sqrt{110670}E^2$	$-\frac{61}{110}\sqrt{770}E^3$	$-\frac{3}{22}\sqrt{1870}$ E^3	$\frac{42}{55}\sqrt{55}$ E^3
		$12E^1-75E^2$ $+3E^3$	$-\frac{9}{31}\sqrt{61845}E^2$	$\frac{756}{341}\sqrt{28985}E^2$	$\frac{24}{5}\sqrt{15}E^3$	0	$\frac{6}{5}\sqrt{210}$ E^3
			$12E^1-\frac{669}{31}E^2$ $+15E^3$	$\frac{180}{341}\sqrt{74613}E^2$	$-\frac{42}{217}\sqrt{4123}E^3$	$\frac{6}{31}\sqrt{10013}$ E^3	$\frac{42}{31}\sqrt{1178}$ E^3
				$12E^1+\frac{108264}{341}$ E^2 $+15E^3$	$-\frac{18}{341}\sqrt{17391}$ E^3	$\frac{150}{341}$ $\sqrt{7161}$ E^3	$\frac{18}{341}$ $\sqrt{243474}$ E^3
					$15E^1+\frac{15}{2}E^2$ $-\frac{361}{20}E^2$	$-\frac{45}{2}$ $\sqrt{119}E^2$ $+\frac{3}{4}\sqrt{119}$ E^3	$\frac{3}{10}\sqrt{14}$ E^3
						$15E^1-\frac{543}{2}$ E^2 $-\frac{3}{4}E^3$	$-\frac{3}{2}\sqrt{34}E^3$
							$20E^1+70E^2$ $-\frac{91}{5}E^3$

Table III (Cont'd)

	$f_6^6(222)(20)$	$f_6^6(222)(30)$	$f_6^6(222)(40)$	$f_6^6(222)(40)$	
^1G	$12E^1 - \frac{780}{11}E^2 + 4E^3$	$\frac{39}{11}\sqrt{2310}E^2$	$\frac{477}{297}\sqrt{38610}E^2$	$\frac{63}{297}\sqrt{835380}E^2$	
		$12E^1 + 156E^2 + 14E^3$	$-16\sqrt{91}E^2$	$\frac{64}{11}\sqrt{4862}E^2$	
			$12E^1 - \frac{1520}{3}E^2 + 26E^3$	$-\frac{34}{33}\sqrt{2618}E^2$	
				$12E^1 + \frac{10942}{33}E^2 + 26E^3$	

Table III (Cont'd)

	$f_4^6(220)(20)$	$f_4^6(220)(21)$	$f_4^6(220)(22)$	$f_2^6(200)(20)$
^1G (cont.)	$\frac{122}{385}\sqrt{770}\,E^3$	$\frac{1}{7}\sqrt{910}\,E^3$	$-\frac{2}{11}\sqrt{1430}\,E^3$	$-\frac{24}{55}\sqrt{55}\,E^3$
	$16\sqrt{3}\,E^3$	$\sqrt{429}\,E^3$	0	$4\sqrt{42}\,E^3$
	$\frac{24}{189}\sqrt{2457}\,E^3$	$-\frac{131}{189}\sqrt{2079}\,E^3$	$-\frac{8}{27}\sqrt{27}\,E^3$	$-\frac{24}{27}\sqrt{702}\,E^3$
	$-\frac{2}{33}\sqrt{14586}\,E^3$	$\frac{17}{9}\sqrt{102}\,E^3$	$-\frac{34}{99}\sqrt{7854}\,E^3$	$\frac{4}{33}\sqrt{51051}\,E^3$
	$15\,E^1-\frac{195}{7}\,E^2+\frac{361}{35}\,E^3$	$\frac{60}{7}\sqrt{143}\,E^2-\frac{8}{7}\sqrt{143}\,E^3$	$\frac{285}{7}\sqrt{91}\,E^2+\sqrt{91}\,E^3$	$-\frac{6}{35}\sqrt{14}\,E^3$
		$15\,E^1+\frac{2211}{7}\,E^2-\frac{33}{7}\,E^3$	$\frac{36}{7}\sqrt{77}\,E^2$	$-\frac{2}{7}\sqrt{2002}\,E^3$
			$15\,E^1+141E^2+57\,E^3$	$-2\sqrt{26}\,E^3$
				$20\,E^1-260\,E^2+\frac{52}{5}\,E^3$

3. Evaluation of Electrostatic Energy Matrices

The energy matrices just discussed are in terms of the parameters E^0, E^1, E^2, and E^3, which Racah has defined as:

$$E^0 = F_0 - 10F_2 - 33F_4 - 286\,F_6 \tag{48}$$

$$E^1 = \frac{1}{9}\left(70\,F_2 + 231\,F_4 + 2002\,F_6\right) \tag{49}$$

$$E^2 = \frac{1}{9}\left(F_2 - 3F_4 + 7\,F_6\right) \tag{50}$$

$$E^3 = \frac{1}{3}\left(5\,F_2 + 6F_4 - 91\,F_6\right) . \tag{51}$$

Thus, to obtain actual energy values for the terms, we must evaluate F_k, the Slater radial-distribution function. One method is to assume a distribution function, evaluate the Slater ratios, and compare F_4/F_2 and F_6/F_2 with experimental data. This method was outlined in Section IIB. Another method is to take analyzed experimental data for a specific ion and by a least-squares calculation, obtain the best experimental value of E^0, E^1, E^2 and E^3. This approach, carried out by B.G. Wybourne for NdIV, $4f^3$, has given reasonable results.[26]

Since little is known about the radial distribution function for an actinide ion ($5f^n$), we present the term energies based on three different F_k ratio assumptions. The first assumption based on 4f hydrogenic ratios was used principally to check the matrices in Table III by giving term energies for the quintets that could be checked directly with the Elliott, Judd, and Runciman values.[7] Two numerical errors were found in Table III of Elliott et al: ^5I should be 78.0 and 144.4 not 73.3 and 149.3.[7] For $4f^6$, the 4f hydrogenic radial-distribution function yields, $F_4/F_2 = 0.1381$ and $F_6/F_2 = 0.01511$; for $5f^6$, the 5f hydrogenic radial distribution function yields $F_4/F_2 = 0.1422$, and $F_6/F_2 = 0.01610$; and from Cohen's relativistic Hartree-Fock calculation for the normal uranium atom, Marrus et al. obtained from an IBM-704 program, $F_4/F_2 = 0.159$ and $F_6/F_2 = 0.0204$.[27,28] In addition, it is assumed that the F_k ratios

obtained from the Hartree-Fock calculation will not change appreciably in going from the uranium atom with three $\underline{f}$ electrons to the AmIV, $5\underline{f}^6$, for example. However, one should expect the probability-density-distribution function to become sharper in going from an atom to the ion, which has a less completely filled $\underline{f}$ shell of electrons, but the question of whether the F_k ratios will become larger or smaller cannot be answered simply. A Hartree-Fock calculation for a transuranium ion is sorely needed. Thus, the use of these uranium-atom ratios may be open to error, but at least it will give use some indication of the shift of the pure electrostatic energy-level spectrum as we go from the $4\underline{f}^6$ to the $5\underline{f}^6$ configuration.

We have listed the results in Tables IV, V and VI. Each table gives the configuration considered and the assumption made for that calculation. We shall use these tables later in Section IVB on the comparison of theory with data. From Figs. 3 through 8, which show the electrostatic energy-level spectra, we note the marked change in position of terms as we go from a $4\underline{f}^6$ configuration to a $5\underline{f}^6$ configuration. The spectrum on the right is that of a $5\underline{f}^6$ configuration, based on the uranium-atom Hartree-Fock (H-F) F_k ratios. All spectra are normalized to the ground term, $^7F = 0$. In general, as we go from $4\underline{f}^6$ to $5\underline{f}^6$, the energy spectrum moves in the direction of greater F_2. In many cases, quintets, triplets, and singlets appear in different order from the ground term.

Table IV. Pure electrostatic energy levels for the $4f^6$ configuration. A 4f hydrogenic radial distribution-function is assumed. Energy levels are in terms of F_2.

Term	Energy	Term	Energy	Term	Energy	Term	Energy	Term	Energy
^7F	0	^1I	114.5	^3H	148.3	^3H	181.7	^3H	250.4
^5D	51.70	^3D	114.6	^5F	148.6	^1L	183.6	^1G	251.4
^5L	57.64	^1N	117.5	^1M	148.7	^1H	185.0	^3G	253.6
^5G	60.69	^3H	118.2	^3D	151.3	^3M	186.7	^1I	257.7
^5H	68.93	^3G	118.9	^1I	151.6	^3L	194.3	^3G	268.3
^5I	78.03	^3M	121.7	^1F	153.4	^3I	198.8	^3P	269.1
^5F	78.89	^3K	121.8	^1G	154.5	^3K	199.3	^1S	269.7
^5K	88.05	^1L	122.6	^1K	155.8	^3P	200.0	^1D	277.2
^3P	88.57	^3I	126.7	^3I	157.6	^1G	202.6	^1L	277.6
^3O	95.37	^1G	126.8	^3K	162.3	^1L	203.4	^1G	277.7
^5G	96.52	^3L	128.2	^3F	163.6	^3G	204.0	^3D	278.7
^3M	97.67	^3H	130.1	^1F	164.5	^1N	208.2	^1F	279.4
^3K	99.56	^1M	130.8	^3H	167.1	^3F	213.4	^3F	300.4
^5D	99.73	^3F	131.2	^1S	168.4	^1F	221.7	^1D	304.4
^3F	101.2	^5S	132.2	^1G	170.1	^1P	222.5	^1G	322.8
^3H	101.4	^3P	132.7	^3P	170.6	^3H	222.8	^1H	325.5
^3I	101.5	^1H	133.2	^1D	171.4	^3D	228.3	^3F	334.3
^5P	104.5	^3I	135.6	^3D	174.9	^1H	233.9	^3P	337.2
^3N	106.7	^3L	136.1	^3G	175.0	^1D	236.4	^1I	337.4
^3G	107.5	^1D	136.7	^5G	177.3	^3I	237.5	^3H	337.9
^5H	110.1	^3F	137.7	^3F	178.6	^3F	241.1	^1G	372.3
^3K	112.6	^1I	142.1	^5D	180.7	^1I	241.3	^1D	395.3
^1S	113.9	^5I	144.4	^1K	180.9	^3K	242.6	^1S	462.2
^1Q	114.1	^3G	145.7	^1I	181.4	^1K	246.5		

Table V. Pure electrostatic energy levels for the $5f^6$ configuration. A 5f hydrogenic radial distribution function is assumed. Energy levels are in terms of F_2

Term	Energy	Term	Energy	Term	Energy	Term	Energy	Term	Energy
^7F	0	^1S	120.2	^5F	150.8	^1I	185.4	^3H	253.4
^5D	54.76	^1I	120.5	^3H	151.7	^1L	188.1	^1G	255.1
^5L	60.04	^3H	122.6	^1M	152.9	^1H	189.3	^3G	255.7
^5G	63.56	^3G	122.9	^3D	154.7	^3M	190.4	^1I	261.8
^5H	71.03	^1N	123.2	^1I	156.4	^3L	197.7	^3G	270.9
^5I	80.21	^3K	125.6	^1F	158.4	^3I	202.0	^3P	272.6
^5F	81.29	^3M	125.7	^1G	159.2	^3P	203.8	^1S	273.8
^5K	90.06	^1L	127.9	^1K	160.7	^3K	204.4	^1D	280.7
^3P	94.53	^3I	130.5	^3I	161.0	^1G	206.5	^3D	280.7
^5G	98.73	^1G	131.9	^3K	166.5	^3G	207.6	^1L	281.0
^3O	99.50	^3L	132.0	^3F	167.3	^1L	207.7	^1G	282.0
^5D	101.8	^3H	133.8	^1F	168.5	^1N	212.4	^1F	282.1
^3M	102.0	^3F	134.7	^3H	170.7	^3F	216.6	^3F	303.8
^3K	104.0	^5S	135.0	^1S	172.6	^1F	225.2	^1D	307.5
^3I	105.7	^1M	135.3	^3P	173.9	^1P	225.6	^1G	326.4
^3F	105.8	^3P	136.6	^1G	174.4	^3H	226.0	^1H	328.3
^5P	106.1	^1H	137.6	^1D	175.4	^3D	231.3	^3F	336.3
^3H	106.2	^3I	139.6	^3G	178.1	^1H	238.1	^3P	338.8
^3N	110.6	^3L	140.1	^3D	178.3	^3I	240.0	^1I	341.2
^5H	111.8	^3F	141.6	^5G	178.7	^1D	240.7	^3H	341.4
^3G	112.0	^1D	142.4	^5D	181.7	^3K	243.5	^1G	374.6
^3K	115.8	^1I	147.0	^3F	181.8	^3F	244.1	^1D	399.1
^3D	118.5	^5I	147.0	^1K	184.5	^1I	244.8	^1S	467.7
^1Q	119.0	^3G	148.9	^3H	185.4	^1K	250.0		

Table VI. Pure electrostatic energy levels for the $5f^6$ configuration. Slater ratios from a Hartree-Fock calculation for the normal uranium atom are assumed. Energy levels are in terms of F_2

Term	Energy	Term	Energy	Term	Energy	Term	Energy	Term	Energy
^7F	0	^3H	140.4	^3H	166.3	^1I	205.9	^1K	266.5
^5D	67.21	^3G	140.6	^1I	168.0	^3M	206.9	^3H	266.9
^5L	70.14	^3K	141.2	^3D	169.6	^1L	207.6	^1G	272.0
^5G	72.24	^3M	142.8	^1M	171.4	^1H	208.0	^1I	280.0
^5H	80.01	^1I	144.8	^3I	176.0	^3L	213.1	^3G	283.6
^5I	89.52	^1S	145.5	^1I	176.7	^3I	216.7	^3P	288.5
^5F	91.36	^3I	146.2	^1F	179.0	^3K	217.5	^3D	291.3
^5K	98.83	^1N	147.2	^1G	179.6	^3P	220.5	^1S	292.7
^5G	108.4	^5S	147.6	^3K	180.2	^3G	223.5	^1F	295.1
^5D	111.2	^3L	147.9	^1K	181.9	^1G	223.9	^1D	296.7
^5P	113.4	^3F	149.8	^3F	183.1	^1L	226.7	^1L	296.8
^3O	116.8	^3H	149.9	^5G	185.3	^3F	231.0	^1G	301.3
^3P	118.5	^1L	149.9	^3H	185.7	^1N	231.5	^3F	319.6
^5H	119.4	^3P	152.5	^1F	186.2	^1P	239.8	^1D	322.6
^3M	119.9	^1G	153.1	^5D	187.7	^3H	240.6	^1H	342.0
^3I	123.5	^1M	154.2	^3P	188.2	^1F	240.6	^1G	343.6
^3K	123.5	^1H	156.2	^1S	191.1	^3D	244.7	^3F	347.3
^3F	124.5	^3I	157.3	^3G	192.1	^3I	252.2	^3P	348.5
^3H	125.5	^3L	157.5	^1D	192.6	^1H	256.8	^3H	357.8
^3N	127.0	^3F	158.5	^3D	193.0	^3F	257.7	^1I	359.7
^3G	130.4	^5I	158.7	^1G	193.3	^3I	259.4	^1G	387.6
^3K	131.6	^5F	160.7	^3F	195.8	^1D	259,8	^1D	418.2
^3D	134.6	^3G	162.8	^1K	201.3	^1I	260.6	^1S	494.6
^1Q	139.9	^1D	166.3	^3H	202.0	^3G	266.0		

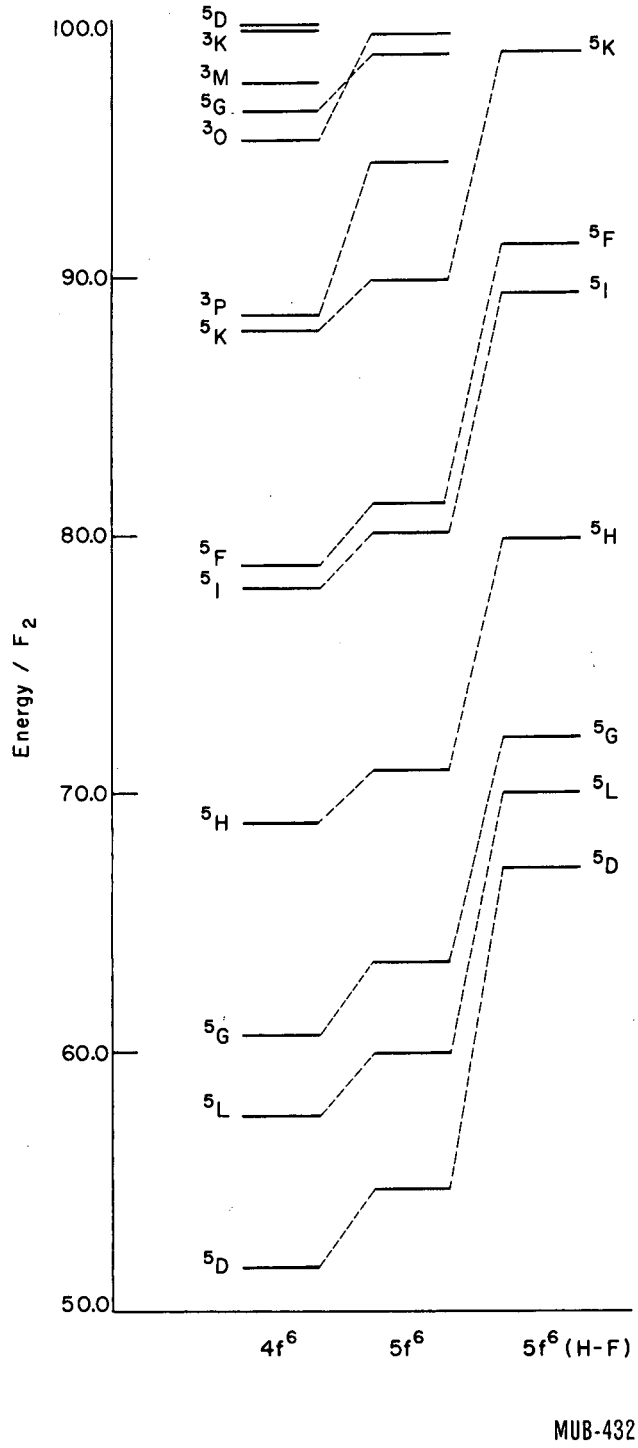

Fig. 3. Pure electrostatic energy-level spectra based on the 4f and 5f hydrogenic F_k ratios, and the 5f F_k ratios obtained from a Hartree-Fock calculation. Energy levels are in terms of F_2.

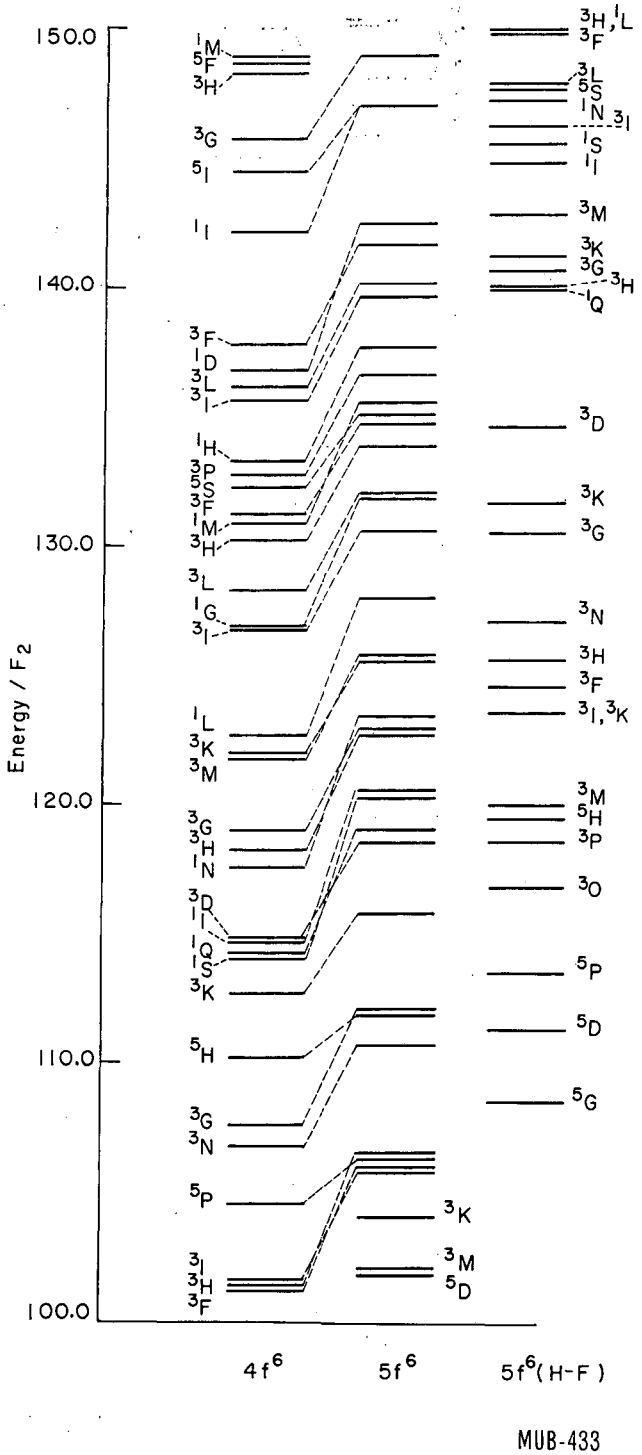

Fig. 4. Pure electrostatic energy-level spectra based on the 4f and 5f hydrogenic F_k ratios, and the 5f F_k ratios obtained from a Hartree-Fock calculation. Energy levels are in terms of F_2.

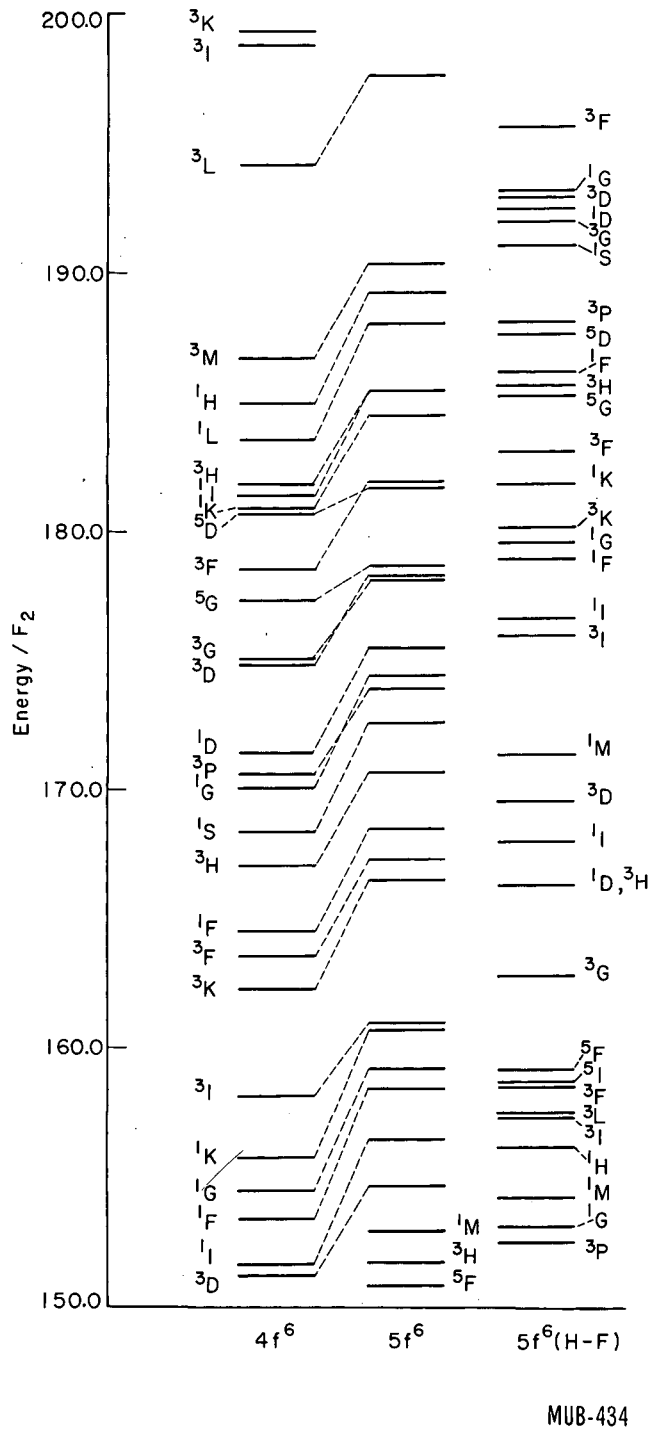

Fig. 5. Pure electrostatic energy-level spectra based on the 4f and 5f hydrogenic F_k ratios, and the 5f F_k ratios obtained from a Hartree-Fock calculation. Energy levels are in terms of F_2.

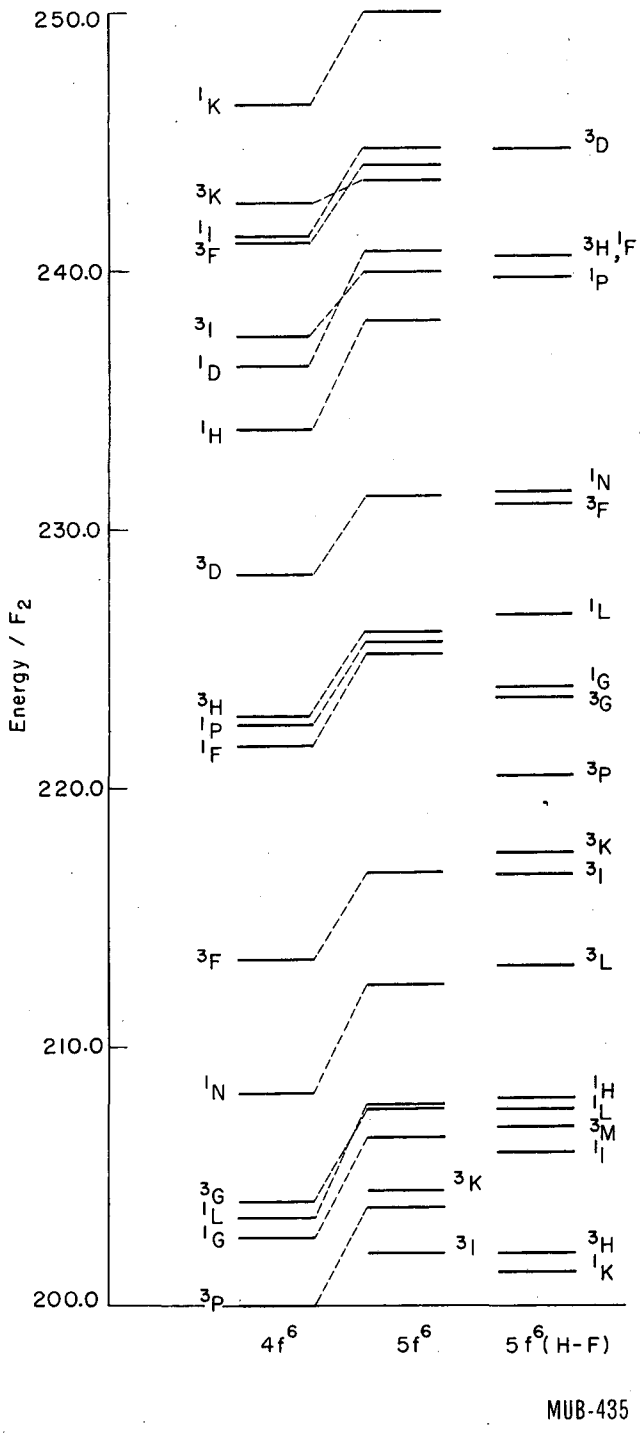

Fig. 6. Pure electrostatic energy-level spectra based on the 4f and 5f hydrogenic F_k ratios, and the 5f F_k ratios obtained from a Hartree-Fock calculation. Energy levels are in terms of F_2.

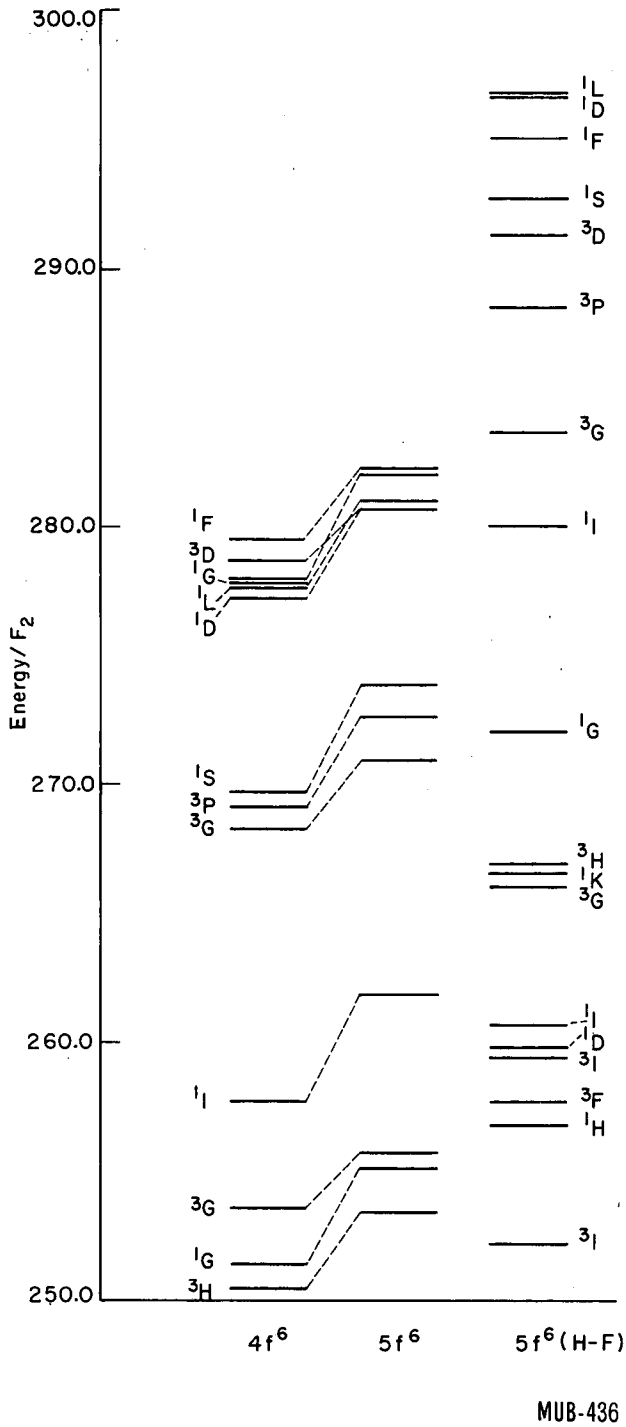

Fig. 7. Pure electrostatic energy-level spectra based on the 4f and 5f hydrogenic F_k ratios, and the 5f F_k ratios obtained from a Hartree-Fock calculation. Energy levels are in terms of F_2.

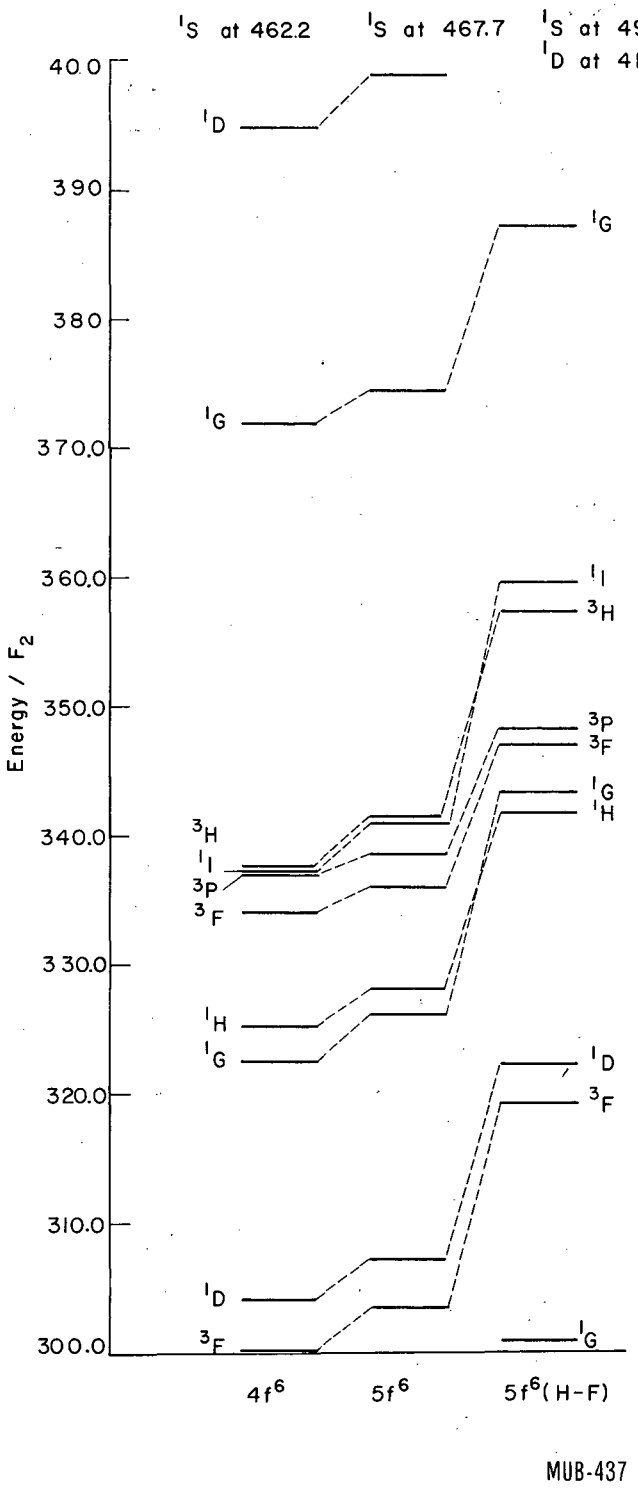

Fig. 8. Pure electrostatic energy-level spectra based on the 4f and 5f hydrogenic F_k ratios, and the 5f F_k ratios obtained from a Hartree-Fock calculation. Energy levels are in terms of F_2.

D. A Modified Classical Method of Evaluating Spin-Orbit Matrices

In addition to the electrostatic interactions between equivalent f electrons, there is the interaction of the magnetic moment of the spin of an electron with its own orbit. If this interaction is reasonably small compared with the coulombic interactions and other perturbations, we may couple $\vec{\ell}_i$, the orbital angular momentum of the ith electron, and $\vec{s}_i$, the spin angular momentum, in the following manner:

$$H_{S\text{-}O} = \sum_i \xi(r_i)\, \vec{s}_i \cdot \vec{\ell}_i \,. \tag{52}$$

Here $\vec{s}_i \cdot \vec{\ell}_i$ is a scalar product, and the quantity $\xi(r_i)$ is given by

$$\xi(r_i) = \frac{\hbar^2}{2m^2c^2} \frac{1}{r_i} \left(\frac{\partial U(r_i)}{\partial r_i}\right) \,, \tag{53}$$

where m is the mass of the electron, c is the velocity of light, and $U(r_i)$ is the electrostatic potential that is seen by the ith electron at a distance r.

Since an accurate theoretical value of $U(r_i)$ or $\left[\frac{\partial U(r_i)}{\partial r_i}\right]$ is usually not available, $\xi(r_i)$ is commonly considered as a variable parameter. If the spin-orbit-split energy levels of the ion or atom are close to the L-S coupling predictions, a reasonable value for this parameter can be obtained from analyzed experimental spectroscopy data. Usually, however, we consider the parameter $\zeta_{n\ell}$, or ζ rather than $\xi(r_i)$, where

$$\xi_{n\ell} = \hbar^2 \int_0^\infty R_{n\ell}^2 \; \xi(r_i)\, dr \,. \tag{54}$$

The presence of more than one electron complicates the calculation of the matrix elements. This is because $\vec{\ell}_i$ and $\vec{s}_i$ are only ordinary vector operators with respect to rotations of space and spin coordinates, whereas in the one-electron problem, they were the

total angular momentum corresponding to these respective rotations. In the one-electron case such as CeIV or PaV, $\vec{l}$ and $\vec{s}$ are diagonal in l and s. For the many-electron spin-orbit matrices, however, a study of the reduced matrix elements provides matrix elements of $\Delta L = \pm 1$, $\Delta S = \pm 1$, $\Delta L = 0$, and $\Delta S = 0$ for $\vec{l}_i$ and $\vec{s}_i$. Thus for example, in $4f^{12}$, TmIV, we may expect off-diagonal matrix elements between $^3F_4$ (L=3), $^1G_4$(L=4), and $^3H_4$(L=5), and between $^1I_6$ (L=6) and $^3H_6$(L=5). Before actually evaluating the matrix elements, let us show that the operator J commutes with H_{S-O}.

In the L-S scheme, we have J=L+S, and if J_z commutes, then J_x and J_y will also commute. Thus, we can write

$$j_z(\vec{s}\cdot\vec{l}) = \sum_{i\neq k} j_{zk}\,\vec{s}_i\cdot\vec{l}_i + \sum_i j_{zi}\,\vec{s}_i\cdot\vec{l}_i\,, \qquad (55)$$

$$j_z(\vec{s}\cdot\vec{l}) = (s_z + l_z)(s_x l_x + s_y l_y + s_z l_z) \qquad (56)$$

$$= (s_x s_z + i s_y) l_x + (s_y s_z - i s_x) l_y + s_z l_z s_z$$

$$+ s_x (l_x l_z + i l_y) + s_y (l_y l_z - i l_x) + s_z l_z l_z\,,$$

and

$$j_z(\vec{s}\cdot\vec{l}) = (\vec{s}\cdot\vec{l})\, j_z\,. \qquad (57)$$

Thus J commutes with H_{S-O}, and the spin-orbit matrices are diagonal in J and independent of $M_J = J_z$.[15]

If we use the raising and lowering operators mentioned in most textbooks on quantum mechanics,

$$\vec{s}\cdot\vec{l} = s_z l_z + s_y l_y + s_x l_x\,. \qquad (58)$$

and if we have

$$\ell_x = \frac{1}{2} (\ell_+ + \ell_-) \tag{59a}$$

and

$$\ell_y = \frac{1}{2i} (\ell_+ - \ell_-) \tag{59b}$$

then we can write

$$\vec{s} \cdot \vec{\ell} = s_z \ell_z + \frac{1}{4} \left[s_+ + s_- \right] \left[\ell_+ + \ell_- \right] - \frac{1}{4} \left[s_+ - s_- \right] \left[\ell_+ - \ell_- \right] , \tag{60}$$

or

$$\vec{s} \cdot \vec{\ell} = s_z \ell_z + \frac{1}{2} \left[s_+ \ell_- + s_- \ell_+ \right] . \tag{61}$$

With these ideas in mind, we can calculate the spin-orbit matrix elements. For $4\underline{f}^2 \equiv 4\underline{f}^{12}$, let us consider $(^3H_6, 6 \mid H_{S-O} \mid {}^3H_6, 6)$. The determinantal product state will be (3^+2^+), and the matrix element written out in full will be

$$\int (3^+2^+)^* \sum_{i=1}^{2} \xi (r_i) \vec{s}_i \cdot \vec{\ell}_i (3^+2^+) \, d\tau . \tag{62}$$

This integral is equal to

$$\frac{1}{2} \int \left[\psi_1^* (3^+) \, \xi (r_1) \, s_i \cdot \ell_1 \, \psi_1 (3^+) \right] d\tau$$

$$+ \frac{1}{2} \int \left[\psi_1^* (2^+) \, \xi (r_1) \, s_1 \cdot \ell_1 \, \psi_1 (2^+) \right] d\tau$$

$$+ \frac{1}{2}\int\left[\psi_2^*(2^+)\ \xi(r_2)\ s_2 \cdot \ell_2\ \psi_2(2^+)\right] d\tau$$

$$+ \frac{1}{2}\int\left[\psi_2^*(3^+)\ \xi(r_2)\ s_2 \cdot \ell_2\ \psi_2(3^+)\right] d\tau \ . \tag{63}$$

Since the coordinates of electron 2 are the same as electron 1 once the integration is performed, we can collect expression (63) into two integrals. The $1/2\ [s_+ \ell_- + s_- \ell_+]$ part of $\vec{s} \cdot \vec{\ell}$ will be zero in this case because of orthonormality condition $\int \phi_A \phi_B\, d\tau = 0$ for $A \neq B$, and $\int \phi_A \phi_B\, d\tau = 1$ for $A = B$. Thus integral (62) becomes

$$\int (3)\left(\frac{1}{2}\right)\ \psi_1^*(3^+)\ \xi(r_1)\ \psi_1(3^+)\, d\tau \ ,$$

where $\ell_z = 3$ and $s_z = 1/2$,

$$+ \int (2)\left(\frac{1}{2}\right)\ \psi_1^*(2^+)\ \xi(r_1)\ \psi_1(2^+)\ d\tau \ ,$$

where $\ell_z = 2$ and $s_z = 1/2$.

We may write the eigenfunctions as

$$\psi_1(3^+) = \frac{1}{r_1}\ R_{nf}\ Y_{3,3}(\theta,\phi), \quad \text{and} \quad \psi_1(2^+) = \frac{1}{r_i}\ R_{nf}\ Y_{3,2}(\theta,\phi) \ . \tag{65}$$

Thus we have

$$\int\left(\frac{3}{2}\right)\frac{1}{r_1}\ R_{nf}\ Y_{3,3}(\theta,\phi)\ \xi(r_1)\ \frac{1}{r_1}\ R_{nf}\ Y_{3,3}(\theta,\phi)\, d\tau \tag{66}$$

$$+ \int \left(\frac{2}{2}\right) \frac{1}{r_i} \; R_{nf} \; Y_{3,2} \; (\theta,\phi) \; \xi \; (r_1) \; \frac{1}{r_1} \; R_{nf} \; Y_{3,2} \; (\theta,\phi) \; d\tau \; .$$

Since the spherical harmonics $Y_{3,3}\,(\theta,\phi)$ and $Y_{3,2}\,(\theta,\phi)$ are orthogonal, our equation becomes

$$\frac{3}{2} \int R_{nf}^2 \; \xi \; (r_1) \; dr_1 + \frac{2}{2} \int R_{nf}^2 \; \xi \; (r_1) \; dr_1 \; . \qquad (67)$$

From the definition of $\zeta_{n\ell}$ given in Eq. (54), we have

$$\left({}^3H_6 \; , \; 6 \; | \; H_{S\text{-}O} \; | \; {}^3H_6 \; , \; 6 \right) = \left(\frac{3}{2} + \frac{2}{2} \right) \; \zeta_{4\underline{f}} \; = \frac{5}{2} \; \zeta_{\underline{f}}$$

(68)

To obtain the diagonal matrix element for ${}^3P_2$, we can write the following determinantal product states:

$$\left| \, {}^3P_2 \; , \; M_J = 2 \right) \; = a \; (3^+ - 2^+) + b \; (2^+ - 1^+) + c(1^+ 0^+) \; . \qquad (69)$$

Since $M_J = M_S + M_L$ is a maximum, we can obtain these coefficients because we have $J_+ = L_+ + S_+ \equiv 0$ and $L_+ \, (k_1 \, k_2 \cdots k_n) = \sum_i \left[\ell_i \, (\ell_i + 1) - m_{\ell_i} \, (m_{\ell_i} + 1) \right]^{1/2} (k_1, k_2, \cdots k_{n-1})$. Then we can write

$$\sqrt{10} \; a \; (3^+ - 1^+) + \sqrt{6} \; b \; (3^+ - 1^+) = 0 \; , \qquad (70a)$$

$$\sqrt{12} \; b \; (2^+ 0^+) \; + \sqrt{10} \; c \; (2^+ 0^+) = 0 \; , \qquad (70b)$$

and

$$aa^* + bb^* + cc^* = 1 \; , \qquad (71)$$

or

$$\left| {}^3P_2 , M_J = 2 \right) = \sqrt{\frac{3}{14}} \, (3^+ - 2^+) - \sqrt{\frac{5}{14}} \, (2^+ - 1^+) + \sqrt{\frac{6}{14}} \, (1^+ 0^+) . \tag{72}$$

Thus we have

$$\left({}^3P_2 , 2 \left| H_{S-O} \right| {}^3P_2 , 2 \right) = \frac{3}{14} \left[\frac{1}{2} \cdot 3 - \frac{1}{2} \cdot 2 \right] + \frac{5}{14} \left[\frac{1}{2} \cdot 2 - \frac{1}{2} \cdot 1 \right] + \frac{6}{14} \left[\frac{1}{2} \cdot 1 \right] = \frac{1}{2} \zeta_{\underline{f}} . \tag{73}$$

In like manner we find

$$\left| {}^3F_4, 4 \right) = \sqrt{\frac{1}{3}} \, (3^+ 0^+) - \sqrt{\frac{2}{3}} \, (2^+ 1^+) , \tag{74}$$

and

$$\left({}^3F_4 , 4 \left| H_{S-O} \right| {}^3F_4 , 4 \right) = \frac{1}{3} \left[\frac{1}{2} \cdot 3 + 0 \right] + \frac{2}{3} \left[\frac{1}{2} \cdot 2 + \frac{1}{2} \cdot 1 \right] = \frac{3}{2} \zeta_{\underline{f}} . \tag{75}$$

By using the raising and lowering operators, we may find the coefficients of the determinental product states, and then proceed to calculate all the diagonal as well as off-diagonal matrix elements. F. H. Spedding (1940), following Condon and Shortley (1935), worked out the matrices for $\underline{f}^2$.[29] In that paper Spedding used $\zeta = 2 \zeta_{\underline{f}}$. Therefore to be consistent with his calculations we need only multiply our matrix elements by a factor of two.

For the $\underline{f}^{12}$ configuration we need only change the sign in front of each ζ value. Then each term and ζ may be divided by F_2, and the variable $\chi = \zeta / F_2$ introduced. The results of such modification yield the spin-orbit matrices given in Table VII. The secular equations may then be solved for energy divided by F_2 as a function of χ.

Since all except the three-by-three equations were solved by hand, it is possible to give complete analytical expressions (see Table VIII). The values for the three-by-three equations were obtained from an IBM 650 program. The results of the calculations appear in Fig. 9.

Table VIII. Spin orbit matrices for $4f^{12}$.

For J = 6

	$^1I_6$	$^3H_6$
$^1I_6$	I/F_2	$-\sqrt{6}\,\chi$
$^3H_6$	$-\sqrt{6}\chi$	$(H/F_2) - 5\chi$

J = 5

	$^3H_5$
$^3H_5$	$H/F_2 + \chi$

J = 4

	$^3H_4$	$^1G_4$	$^3F_4$
$^3H_4$	$H/F_2 + 6\chi$	$\sqrt{40/3}\chi$	0
$^1G_4$	$\sqrt{40/3}\chi$	(G/F_2)	$-\sqrt{44/3}\chi$
$^3F_4$	0	$-\sqrt{44/3}\chi$	$(F/F_2) - 3\chi$

J = 3

	$^3F_3$
$^3F_3$	$F/F_2 + \chi$

J = 2

	$^3F_2$	$^1D_2$	$^3P_2$
$^3F_2$	$F/F_2 + 4\chi$	$\sqrt{24}\chi$	0
$^1D_2$	$\sqrt{24}\chi$	(D/F_2)	$-\sqrt{18}\chi$
$^3P_2$	0	$-\sqrt{18}\chi$	$(P/F_2) - \chi$

J = 1

	$^3P_1$
$^3P_1$	$P/F_2 + \chi$

J = 0

	$^3P_0$	$^1S_0$
$^3P_0$	$P/F_2 + 2\chi$	$\sqrt{48}\chi$
$^1S_0$	$\sqrt{48}\chi$	(S/F_2)

Table VIII. Analytical expressions for $E/F_2 = f(\chi)$

Levels	$E/F_2 = f(\chi)$
$^3H_5$	χ
$^3F_3$	$13.4 + \chi$
$^3P_1$	$62.5 + \chi$
$^1S_0$	$104 + \chi + 1/2\,(196\chi^2 - 332\chi + 6824)^{1/2}$
$^3P_0$	$104 + \chi - 1/2\,(196\chi^2 - 332\chi + 6824)^{1/2}$
$^1I_6$	$29.3 - 2.5\chi + 1/2\,(49\chi^2 + 586\chi + 3440)^{1/2}$
$^3H_6$	$29.3 - 2.5\chi - 1/2\,(49\chi^2 + 586\chi + 3440)^{1/2}$

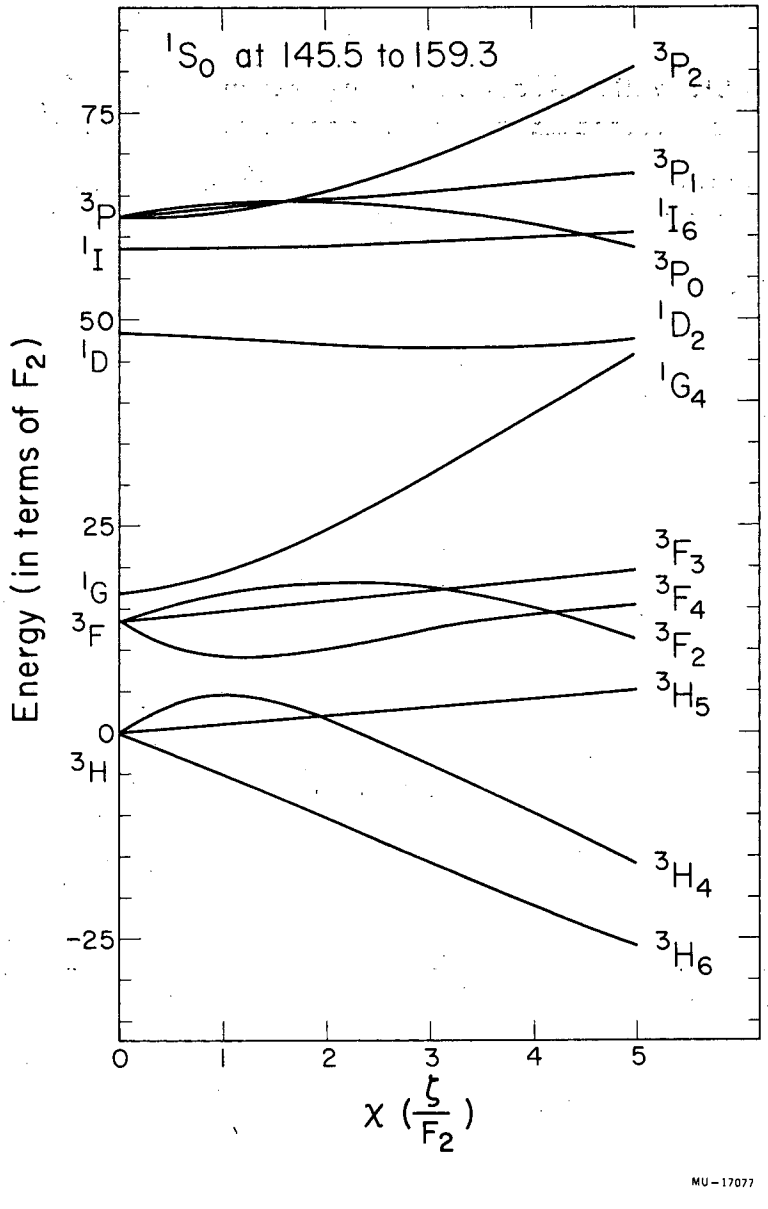

Fig. 9. Energy-level diagram for TmIV in intermediate coupling. The $^1S_0$ level varies from 145.5 F_2 at $\chi = 0$ to 159.3 F_2 at $\chi = 5$. Good agreement between theory and experiment is obtained at $\chi = 3$.

E. Crystal-Field Splitting of Electronic Energy Levels

1. The Pure Electrostatic-Potential Model

An ion in a crystalline solid is in general exposed to a strong anisotropic electrostatic field arising from charges located on neighboring ions. The isotropy of the ion in free space is thus reduced. In group theoretical language we say that the symmetry group is reduced from a full three-dimensional rotation group to some finite group of rotations through finite angles. This allows the degeneracy associated with complete rotational symmetry to be lifted, and the free-ion J levels to be split by the crystalline electric field into $\leq 2J+1$ sublevels called crystal quantum states. If the crystal-field splitting is small compared with spin-orbit splitting, we may simply add a term to our free-ion Hamiltonian and proceed according to first-or second-order perturbation theory.

By assuming a simple electrostatic model, we can compute the potential at the ion site in a given crystalline environment by replacing each of the neighbors by a point charge, or point dipole if the neighbors are H_2O molecules as in the case of $Tm(C_2H_5SO_4)_3 \cdot 9H_2O$. The model is a rather naive one which assumes that (a) the center ion is surrounded by pure electrostatic point charges or dipoles (anions or H_2O molecules), each of which has no zero point motion in the lattice; (b) the point symmetry, which for all cases presented in this paper is assumed to be D_{3h} or C_{3h}, is truly descriptive of the environment of the impurity ion in a cation site; (c) all exchange forces or covalent forces together have an effect small enough that these contributions appear in a few lattice parameters, $A_n^m \langle r^n \rangle$; (d) there are no appreciably large cation-cation electrostatic repulsion terms, or additional anion-anion interaction terms which might perturb the energy levels of the central ion.

In our present problem, the electrostatic interactions between ions in a crystal seem to be the most important type of interaction. Certainly the more subtle types of interactions mentioned above may be of some importance in our understanding of crystal physics, but at present we cannot expect much more from our model than that it has satisfactorily explained the order and magnitude of separation of the crystal quantum states.

2. The Crystalline Electrostatic Potential

The crystalline electrostatic potential can be expanded as a series of spherical harmonics. We carry out this expansion not because the spherical harmonics satisfy Laplace's equation, but because they form a complete set. For C_{3h} point symmetry, where we consider the central cation to be surrounded by nine point charges at a distance r from the center ion (see Fig. 10), we obtain the following perturbation-energy expression as given by Stevens:[11]

$$V = A_2^0 \sum (3z^2 - r^2) + A_4^0 \sum (35z^4 - 30 r^2 z^2 + 3r^4)$$

$$+ A_6^0 \sum (231 z^6 - 315 r^2 z^4 + 105 r^4 z^2 - 5 r^6)$$

$$+ A_6^6 \sum (x^6 - 15x^4 y^2 + 15 x^2 y^4 - y^6), \qquad (76)$$

where the summations are taken over the coordinates of all electrons. If we stay within a given configuration, we can exclude from Eq. (76) all terms of odd parity and higher k since these vanish in the calculations. It can be shown that the term V_3^0 is zero in this case. Thus we can write Eq. (76) in the form $f(r)\, P_n^m(\theta, \phi)$ which transforms under rotations according to the irreducible representation Θ_n of the rotation group. The quantities A_n^m are characteristic of the lattice and always appear with the quantities $\langle r^n \rangle$, the mean value of r^n for a single f electron. The products $A_n^m \langle r^n \rangle$ are called crystal-field parameters and are determined empirically. The selection of these parameters is discussed later.

3. The Operator Equivalent Method

As Stevens has shown, within a given manifold of J the matrix elements of the potential form V_n^m associated with the parameter A_n^m are related to the matrix elements of certain angular-momentum operators through a factor $\theta_n \langle r^n \rangle$.[11] Here θ_n is the so-called

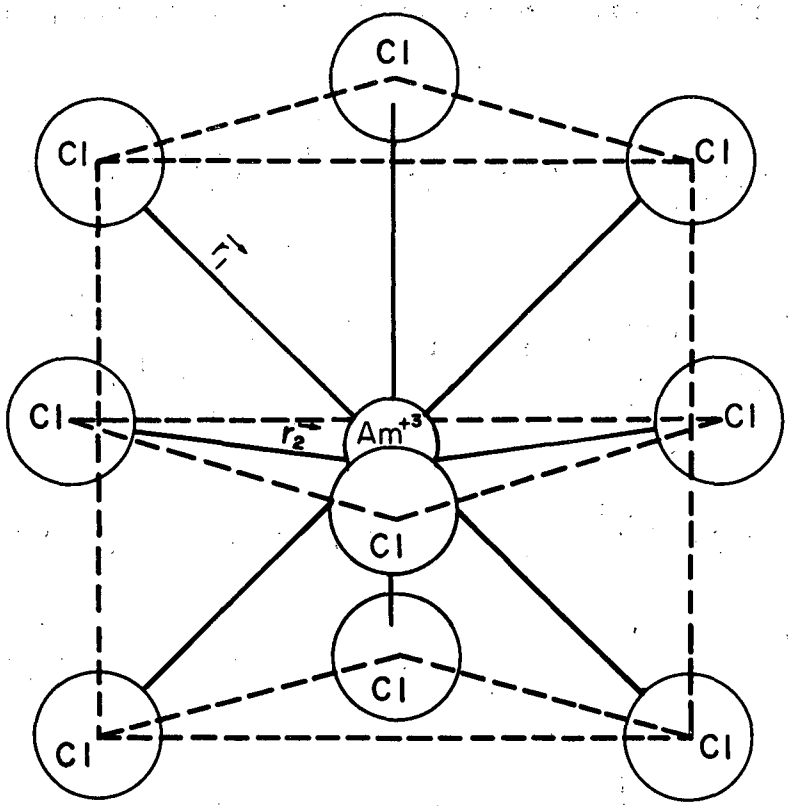

MU-22135

Fig. 10. The AmIV cation site in $LaCl_3$ - $AmCl_3$.

"operator equivalent" factor usually written as α, β, and γ for n=2, 4, and 6, respectively. This theory has been generalized by Elliott, Judd, and Runciman for all rare earth ions.[7]

The operator-equivalent factors α, β, and γ as defined by Stevens are

$$\left(\psi_{JJ_z} \left| \sum (3 z^2 - r^2) \right| \psi'_{JJ_z}\right) = \alpha \left\langle r^2 \right\rangle \left[3J_z^2 - J(J+1) \right], \tag{77}$$

$$\left(\psi_{JJ_z} \left| \sum (35 z^4 - 30 r^2 z^2 + 3r^4) \right| \psi'_{JJ_z}\right) \tag{78}$$

$$= \beta \left\langle r^4 \right\rangle \left[35 J_z^4 - 30 J(J+1) J_z^2 + 25 J_z^2 - 6J(J+1) + 3J^2(J+1)^2 \right],$$

$$\left(\psi_{JJ_z} \left| \sum (231 z^6 - 315 r^2 z^4 + 105 r^4 z^2 - 5r^6 \right| \psi'_{JJ_z}\right)$$

$$= \gamma \left\langle r^6 \right\rangle \Big[231 J_z^6 - 315 J(J+1) J_z^4 + 735 J_z^4$$

$$+ 105 J^2(J+1)^2 J_z^2 - 525 J(J+1) J_z^2 + 294 J_z^2 - 5J^3(J+1)^3$$

$$+ 40 J^2 (J+1)^2 - 60 J(J+1) \Big], \tag{79}$$

$$\left(\psi_{JJ_z} \left| \sum (x^6 - 15x^4y^2 + 15x^2y^4 - y^6) \right| \psi'_{JJ_z}\right)$$

$$= \gamma \left\langle r^6 \right\rangle \frac{1}{2} \left\{ J_+^6 + J_-^6 \right\}, \tag{80}$$

where $\left\langle r^n \right\rangle$ is the mean value of r^n for a single $\underline{f}$ electron. Here the wave function ψ represents the set of quantum numbers $\underline{f}^n \tau U v S L$.

We can write the operator-equivalent factors α, β, and γ as $(\psi_J \,||\, \alpha \,||\, \psi'_J)$ or simply $\langle J \,||\, \alpha \,||\, J \rangle$. Elliott et al.[7] have shown that the Stevens method of calculating these reduced matrix elements is related to a tensor-operator method by the following equations:

$$(\psi_J \,||\, \alpha \,||\, \psi'_J) = -8\left[\frac{7(2J-2)!}{15(2J+3)!}\right]^{1/2} (\psi_J \,||\, U^2 \,||\, \psi'_J) \tag{81}$$

$$(\psi_J \,||\, \beta \,||\, \psi'_J) = 16\left[\frac{14(2J-4)!}{11(2J+5)!}\right]^{1/2} (\psi_J \,||\, U^4 \,||\, \psi'_J) \tag{82}$$

$$(\psi_J \,||\, \gamma \,||\, \psi'_J) = -640\left[\frac{7(2J-6)!}{429(2J+7)!}\right]^{1/2} (\psi_J \,||\, U^6 \,||\, \psi'_J), \tag{83}$$

where $(\,||\, U^k \,||\,)$ is the reduced matrix element of the tensor operator U^k_q which corresponds $V^q_k \equiv V^m_n$.[7] According to Elliott et al. we can write

$$(\psi_J \,||\, U^k \,||\, \psi'_J) = n\sum_{\overline{\psi}} (\psi \{\,|\overline{\psi}) (\psi' \{\,|\overline{\psi}) (-1)^{\overline{L}+k-3-L'} \{(2L+1)(2L'+1)\}^{1/2} W(3L3L'; \overline{L}k), \tag{84}$$

where $W(3L3L'; Lk)$ is a Racah coefficient, $(\underline{f} \,||\, U^k \,||\, \underline{f}) = 1$, and the coefficients of fractional parentage are as defined in section IIC.[7]

With this machinery one may then calculate all the L-S operator equivalents for the $\underline{f}^n$ configuration in general. Judd has given the equations for evaluating α, β, and γ for Pr^{+3} $(4\underline{f}^2)$.[30] He has reported these values for $^3H_4$, $^1G_4$, $^3F_4$, $^3F_3$, $^1D_2$, $^3P_2$, and

$^3P_1$ in the same paper with the crystal-field splitting results for Pr^{+3} in $LaCl_3$. For Tm^{+3} ($4f^{12}$), the α, β, and γ may be calculated from the Pr^{+3} set of equations. The only difference will be a change in sign.[31] The L-S operator equivalents for Am^{+3}, $5f^6$ which appear in Table IX have been evaluated from the preceding equations and agree with those obtained by B. R. Judd for Eu IV, $4f^6$.[32]

As a detailed example, let us calculate α, or $\langle || \alpha || \rangle$ for the level $^3P_2$. Since $A_2^0 \sum (3z^2 - r^2)$, which is an expression of the general form $\sum Y_{k,q}(\theta, \phi)$, transforms as a spherical tensor $\underset{\sim}{T}^{(k)}$, we seek to evaluate $(^3P_2, M_J \mid T_q^k \mid {}^3P_2, M_J)$.[33] If within a given J manifold, $\sum (3z^2 - r^2)$ approximates $3M_J^2 - J(J+1)$, then we have

$$\sum (3z^2 - r^2) \equiv \alpha \langle r^2 \rangle \left[3J_z^2 - J(J+1) \right]. \tag{85}$$

Thus we have

$$(^3P_2, M_J = 2 \mid \sum (3z^2 - r^2) \mid {}^3P_2, M_J = 2)$$

$$= \alpha \langle r^2 \rangle (^3P_2, 2 \mid 3J_z^2 - J(J+1) \mid {}^3P_2, 2), \tag{86}$$

or

$$(^3P_2, M_J = 2 \mid \sum (3z^2 - r^2) \mid {}^3P_2, M_J = 2) = 6 \alpha \langle r^2 \rangle . \tag{87}$$

Table IX. Operator equivalents for the ^7F ground term, AmIV, $5f^6$

Level	$\langle J \Vert \alpha \Vert J \rangle$	$\langle J \Vert \beta \Vert J \rangle$	$\langle J \Vert \gamma \Vert J \rangle$
$^7F_0$	0	0	0
$^7F_1$	$-\frac{1}{5}$	0	0
$^7F_2$	$\frac{-11}{315}$	$\frac{-2}{189}$	0
$^7F_3$	$\frac{-1}{135}$	$\frac{1}{33 \cdot 45}$	$\frac{-2}{27 \cdot 429}$
$^7F_4$	$\frac{1}{385}$	$\frac{23}{15 \cdot 33 \cdot 77}$	$\frac{2}{77 \cdot 429}$
$^7F_5$	$\frac{1}{135}$	$\frac{2}{99 \cdot 105}$	$\frac{-1}{189 \cdot 429}$
$^7F_6$	$\frac{1}{99}$	$\frac{-2}{11 \cdot 15 \cdot 99}$	$\frac{1}{11 \cdot 189 \cdot 429}$

If we write out the matrix element in terms of M_S and M_L, we have

$$\left({}^3P_2 ,\ M_S = 1,\ M_L = 1 \left| \sum (3z^2 - r^2) \right| {}^3P_2 ,\ M_S = 1,\ M_L = 1 \right) . \tag{88}$$

In order to find the equating coefficient, c, between $(3z^2 - r^2)$ and $3\ell_z - \ell(\ell+1)$, we must calculate the integrals described by the following matrix element,

$$(\underline{f},\ m_\ell = 0 \mid 3z^2 - r^2 \mid \underline{f},\ m_\ell = 0) = c\ (\underline{f},\ m_\ell = 0 \mid 3\ell_z^2 - \ell(\ell+1) \mid \underline{f},\ m_\ell = 0) , \tag{89}$$

or

$$\iiint Y^*_{3,0}(\theta,\phi)\ \{r^2(3\cos^2\theta - 1)\}\ Y_{3,0}(\theta,\phi)\ R^2_{4,3}(r)\, dr\, d(\cos\theta)\, d\phi = -12\, c. \tag{90}$$

Integrating the left-hand side, we have $\frac{8}{15} \langle r^2 \rangle = -12\, c$, or $c = -\frac{2}{45} \langle r^2 \rangle$. In section II D, Eq. (72) we evaluated $\left| {}^3P_2,\ M_S = 1,\ M_L = 1 \right)$ and found it to be

$$\left| {}^3P_2, 1, 1 \right) = \sqrt{\frac{3}{14}}\ (3^+ 2^+) - \sqrt{\frac{5}{14}}\ (2^+ 1^+) + \sqrt{\frac{6}{14}}\ (1^+ 0^+) . \tag{91}$$

Then we can write

$$\left({}^3P_2 ,\ 1,\ 1 \left| c \sum (3\ell_z^2 - \ell(\ell+1) \right| {}^3P_2 ,\ 1, 1 \right) = -\frac{2}{45} \langle r^2 \rangle \left(\frac{45}{14} - \frac{45}{14} - \frac{126}{14} \right) . \tag{92}$$

We obtain as our final answer

$$(^3P_2, 1, 1 \mid c\sum (3\ell_z^2 - \ell(\ell+1) \mid {}^3P_2, 1, 1) = \frac{2 \cdot 126}{45 \cdot 14} \langle r^2 \rangle = 6a \langle r^2 \rangle, \tag{93}$$

and

$$a = \frac{1}{15} . \tag{94}$$

Since we are interested in $4f^{12}$ rather than $4f^2$, we need only change the sign of a. This can be easily seen if we had used $|{}^3P_2, 1, 1)$ for $4f^{12}$ instead of $4f^2$. The value $a = -1/15$ is recorded in Table X, together with other operator equivalents obtained in the same manner.

4. Intermediate-Field Operator Equivalents

Recently, the electronic energy levels for TmIV in the intermediate field were obtained from a plot of E/F_2 vs. χ, where $\chi = \zeta/F_2$.[22] Here ζ is the spin-orbit parameter used by Spedding, and F_2 is a Slater integral. The best fit of theory to experiment was obtained at $\chi = 3$. The eigenvectors at $\chi = 3$ for $^3H_4$, $^3F_4$, and $^1G_4$, as well as $^3F_2$, $^3P_2$, and $^1D_2$ were obtained from and IBM 650 program. The eigenvectors for $^3H_6$ and $^1I_6$ were calculated by hand using the spin-orbit matrices given in Table VII.

It should be pointed out that these eigenvectors and eigenvalues are based on the assumption of $4f$ hydrogenic F_k ratios. However, spectroscopic studies on rare earth ions are showing that while this assumption is reasonable it is certainly not accurate. We could have chosen $\chi = 2.8$ or $\chi = 3.1$ just as well and obtained eigenvalues which fit the data rather well. However, there is a change of 3 to 5% in eigenvector values as we go from $\chi = 2.8$ to $\chi = 3.1$. This means that our uncertainty in the actual eigenvector value may be as large as 4% in some cases. If one varied the F_k ratios as well as the

Table X. Operator equivalents in the intermediate field, $Tm^{+3}(4f^{12})$

Level	$\langle J \Vert \alpha \Vert J \rangle$	$\langle J \Vert \beta \Vert J \rangle$	$\langle J \Vert \gamma \Vert J \rangle$
$^3P_1$	$\frac{1}{5}$ [1.000]	0	0
$^3P_2$	$\frac{-1}{15}$ [1.095]	$\frac{-4}{7 \cdot 27}$ [0.629][a]	0
$^1D_2$	$\frac{-22}{15 \cdot 21}$ [0.678]	$\frac{-4}{7 \cdot 27}$ [-0.105]	0
$^3F_2$	$\frac{-8}{21 \cdot 15}$ [1.636]	$\frac{2}{7 \cdot 81}$ [-1.859]	0
$^3F_3$	$\frac{-1}{90}$ [1.000]	$\frac{1}{45 \cdot 99}$ [1.000]	$\frac{1}{39 \cdot 99}$ [1.000]
$^3F_4$	$\frac{-1}{126}$ [-1.357]	$\frac{1}{45 \cdot 77}$ [1.527]	$\frac{-1}{13 \cdot 63 \cdot 99}$ [5.945]
$^1G_4$	$\frac{2}{11 \cdot 35}$ [1.799]	$\frac{46}{11 \cdot 45 \cdot 77}$ [0.866]	$\frac{4}{13 \cdot 33 \cdot 77}$ [0.537]
$^1I_6$	$\frac{2}{99}$ [0.995]	$\frac{-4}{11 \cdot 15 \cdot 99}$ [0.984]	$\frac{2}{13 \cdot 33 \cdot 21 \cdot 99}$ [0.967]
$^3H_6$	$\frac{1}{99}$ [1.010]	$\frac{8}{3 \cdot 11 \cdot 1485}$ [0.976]	$\frac{-5}{13 \cdot 33 \cdot 2079}$ [0.986]

[a] The pure L-S operator equivalent, β, is zero for $^3P_2$, since the corresponding Racah coefficient is zero. However, if we allow for intermediate coupling effects, the entry becomes $(-4/7 \cdot 27)$ [0.629].

$A_n^m \langle r^n \rangle$ parameters (a total of six parameters instead of four), a better fit would certainly be obtained. Table X includes values of α, β, and γ for TmIV, $4f^{12}$, with intermediate-field corrections in brackets.

Suppose we wish to calculate α, β, and γ for $^1G_4$ in the intermediate field at $\chi = 3$. In a $4f^{12}$ configuration there are three $J = 4$ levels. We write

$$|^1G_4'\rangle = 0.6119\,|^3H_4\rangle + 0.7260\,|^1G_4\rangle - 0.3137\,|^3F_4\rangle, \tag{95}$$

where 0.6119, 0.7260, and -0.3137 are the corresponding eigenvectors, and $|^1G_4'\rangle$ corresponds to the intermediate field $^1G_4$. Now we have

$$\begin{aligned}\left(^1G_4' \left|\left| \begin{matrix}\alpha\\ \beta\\ \gamma\end{matrix} \right|\right| {}^1G_4'\right) &= (0.6119)^2 \left(^3H_4 \left|\left| \begin{matrix}\alpha\\ \beta\\ \gamma\end{matrix} \right|\right| {}^3H_4\right) \\ &+ (0.7260)^2 \left(^1G_4 \left|\left| \begin{matrix}\alpha\\ \beta\\ \gamma\end{matrix} \right|\right| {}^1G_4\right) \\ &+ (0.3137)^2 \left(^3F_4 \left|\left| \begin{matrix}\alpha\\ \beta\\ \gamma\end{matrix} \right|\right| {}^3F_4\right) \\ &- 2(0.3137)(0.6119) \left(^3H_4 \left|\left| \begin{matrix}\alpha\\ \beta\\ \gamma\end{matrix} \right|\right| {}^3F_4\right).\end{aligned} \tag{96}$$

There will be no cross terms involving $^1G_4$ with $^3F_4$ and $^3H_4$, since matrix elements between different spin states are zero. Each of the pure L-S operator equivalents in Eq. (96) can be evaluated from the equations given by Judd.[30] It is possible to factor out $^1G_4$ L-S α, β, and γ expressions from the right-hand side of Eq. (96). This leaves a sum of numbers that denotes the importance of intermediate-field corrections to the L-S operator-equivalent values. In this way, $^3F_4$, $^3F_2$, $^3P_2$, $^1D_2$, and $^3H_6$ operator equivalents were calculated. The $^3P_1$, $^3F_3$, and $^3H_5$ operator equivalents are not affected by spin-orbit interaction.

5. Crystal-Field Splitting Matrices and Crystal Quantum Energies

Once the operator equivalents have been calculated, we can write down the crystal-field splitting matrices from tables given by Stevens,[11] and Elliott and Stevens.[34] Since the parameters $A_2^0\langle r^2\rangle$, $A_4^0\langle r^4\rangle$, $A_6^0\langle r^6\rangle$, and $A_6^6\langle r^6\rangle$ are determined from empirical and experimental data, we shall leave these as constants to be determined by methods explained in the sections dealing with the comparison of theory with data.

The matrices for $J = 1$ to $J = 6$ listed in Table XI are common to the TmIV and AmIV problems. In both cases we are dealing with the splitting of J levels from one to six since both f shells have an even number of electrons. However, the effect of configuration interaction is not the same in both cases.

For Tm^{+3}, the point symmetry is taken as C_{3h}. This assumption is based on Ketelaar's crystal-structure work on rare earth ethylsulfates[35] and on the recent work of Fitzwater and Rundle.[36] To determine whether the $AmCl_3$—$LaCl_3$ mixed-crystal system preserved C_{3h} symmetry about the cation sites, we added $PrCl_3$ to the mixture and found that the PrIV lines had the same positions as when no $AmCl_3$ was present. We concluded therefore that the symmetry about the americium ions very probably is C_{3h}.

In Tables XI and XII we list the matrices and the crystal-quantum energy levels. We leave the diagonal and off-diagonal elements in terms of the operator equivalents and crystal-field parameters. Blank spaces refer to matrix elements that are zero.

The matrices can be diagonalized easily, and the secular determinants obtained can be solved to give expressions no more complicated than quadratic equations. The axial terms V_n^0 cause a splitting of levels with differing $|J_z|$, whereas V_n^m mixes states for which $J_z - J_z' = q$. Thus we can define the crystal quantum number μ, where $J_z \equiv \mu \pmod{q}$. Matrix elements other than those for which $\Delta J_z = 0, \pm 6$ are zero in this case. The crystal-field splittings are given as analytical expressions of the diagonal and off-diagonal elements in Table XII. Numerical values for AmIV are given in the section devoted to a comparison of theory with data.

Table XI. The C_{3h} crystal-field splitting matrices for J = 1 to J = 6

J = 0 No splitting

J = 1

$$A = J_z(\pm 1) = A_2^0 \langle r^2 \rangle \alpha$$

$$B = J_z(0) = -2 A_2^0 \langle r^2 \rangle \alpha$$

$$\beta = \gamma = 0$$

J_z	-1	0	1
-1	A		
0		B	
1			A

J = 2

$$C = J_z(\pm 2) = 6 A_2^0 \langle r^2 \rangle \alpha + 12 A_4^0 \langle r^4 \rangle \beta$$

$$D = J_z(\pm 1) = -3 A_2^0 \langle r^2 \rangle \alpha - 48 A_4^0 \langle r^4 \rangle \beta$$

$$E = J_z(0) = -6 A_2^0 \langle r^2 \rangle \alpha + 72 A_4^0 \langle r^4 \rangle \beta$$

J_z	-2	-1	0	1	2
-2	C				
-1		D			
0			E		
1				D	
2					C

Table XI (Cont'd)

J = 3

$$F = J_z(\pm 3) = 15\, A_2^0 \langle r^2 \rangle \alpha + 180\, A_4^0 \langle r^4 \rangle \beta + 180\, A_6^0 \langle r^6 \rangle \gamma$$

$$G = J_z(\pm 2) = 0 - 420\, A_4^0 \langle r^4 \rangle \beta - 1080\, A_6^0 \langle r^6 \rangle \gamma$$

$$H = J_z(\pm 1) = -9\, A_2^0 \langle r^2 \rangle \alpha + 60\, A_4^0 \langle r^4 \rangle \beta + 2700\, A_6^0 \langle r^6 \rangle \gamma$$

$$I = J_z(0) = -12\, A_2^0 \langle r^2 \rangle \alpha + 360\, A_4^0 \langle r^4 \rangle \beta - 3600\, A_6^0 \langle r^6 \rangle \gamma$$

$$a_{1,7} = 360\, A_6^6 \langle r^6 \rangle \gamma$$

J_z	-3	-2	-1	0	1	2	3
-3	F						$a_{1,7}$
-2		G					
-1			H				
0				I			
1					H		
2						G	
3	$a_{1,7}$						F

Table XI (Cont'd)

J = 4

$$K = J_z(\pm 4) = 28\, A_2^0 \langle r^2 \rangle \alpha + 840\, A_4^0 \langle r^4 \rangle \beta + 5040\, A_6^0 \langle r^6 \rangle \gamma$$

$$L = J_z(\pm 3) = 7\, A_2^0 \langle r^2 \rangle \alpha - 1260\, A_4^0 \langle r^4 \rangle \beta - 21,420\, A_6^0 \langle r^6 \rangle \gamma$$

$$M = J_z(\pm 2) = -8\, A_2^0 \langle r^2 \rangle \alpha - 660\, A_4^0 \langle r^4 \rangle \beta + 27,720\, A_6^0 \langle r^6 \rangle \gamma$$

$$N = J_z(\pm 1) = -17\, A_2^0 \langle r^2 \rangle \alpha + 540\, A_4^0 \langle r^4 \rangle \beta + 1260\, A_6^0 \langle r^6 \rangle \gamma$$

$$N' = J_z(0) = -20\, A_2^0 \langle r^2 \rangle \alpha + 1080\, A_4^0 \langle r^4 \rangle \beta - 25,200\, A_6^0 \langle r^6 \rangle \gamma$$

$$b_{1,7} = 720\sqrt{7}\, A_6^6 \langle r^6 \rangle \gamma\,, \quad C_{2,8} = 2520\, A_6^6 \langle r^6 \rangle \gamma$$

J_z	-4	-3	-2	-1	0	1	2	3	4
-4	K						$b_{1,7}$		
-3		L						$c_{2,8}$	
-2			M						$b_{1,7}$
-1				N					
0					N'				
1						N			
2	$b_{1,7}$						M		
3		$c_{2,8}$						L	
4			$b_{1,7}$						K

Table XI (Cont'd)

J = 5

$$P = J_z(\pm 5) = 45A_2^0 \langle r^2 \rangle \alpha + 2520\, A_4^0 \langle r^4 \rangle \beta + 37{,}800\, A_6^0 \langle r^6 \rangle \gamma$$

$$Q = J_z(\pm 4) = 18\, A_2^0 \langle r^2 \rangle \alpha - 2520\, A_4^0 \langle r^4 \rangle \beta - 120{,}960\, A_6^0 \langle r^6 \rangle \gamma$$

$$R = J_z(\pm 3) = -3A_2^0 \langle r^2 \rangle \alpha - 2520\, A_4^0 \langle r^4 \rangle \beta + 73{,}080\, A_6^0 \langle r^6 \rangle \gamma$$

$$S = J_z(\pm 2) = -18\, A_2^0 \langle r^2 \rangle \alpha - 420\, A_4^0 \langle r^4 \rangle \beta + 90{,}720\, A_6^0 \langle r^6 \rangle \gamma$$

$$T = J_z(\pm 1) = -27A_2^0 \langle r^2 \rangle \alpha + 1680A_4^0 \langle r^4 \rangle \beta - 30{,}240\, A_6^0 \langle r^6 \rangle \gamma$$

$$U = J_z(0) = -30A_2^0 \langle r^2 \rangle \alpha + 2520\, A_4^0 \langle r^4 \rangle \beta - 100{,}800\, A_6^0 \langle r^6 \rangle \gamma$$

$$d_{1,7} = 360\sqrt{210}\, A_6^6 \langle r^6 \rangle \gamma ,$$

$$e_{2,8} = 5040\sqrt{3}\, A_6^6 \langle r^6 \rangle \gamma ,$$

$$f_{3,9} = 10{,}080\, A_6^6 \langle r^6 \rangle \gamma ,$$

Table XI. (Cont'd)

J_z	-5	-4	-3	-2	-1	0	1	2	3	4	5
-5	P						$d_{1,7}$				
-4		Q						$e_{2,8}$			
-3			R						$f_{3,9}$		
-2				S						$e_{2,8}$	
-1					T						$d_{1,7}$
0						U					
1	$d_{1,7}$						T				
2		$e_{2,8}$						S			
3			$f_{3,9}$						R		
4				$e_{2,8}$						Q	
5					$d_{1,7}$						P

J = 6

$$V = J_z(\pm 6)$$
$$= 66\, A_2^0 \langle r^2 \rangle \alpha + 5940\, A_4^0 \langle r^4 \rangle \beta + 166,320\, A_6^0 \langle r^6 \rangle \gamma$$

$$W = J_z(\pm 5)$$
$$= 33\, A_2^0 \langle r^2 \rangle \alpha - 3960\, A_4^0 \langle r^4 \rangle \beta - 415,800\, A_6^0 \langle r^6 \rangle \gamma$$

Table XI (Cont'd)

$$X = J_z(\pm 4) = 6A_2^0 \left\langle r^2 \right\rangle \alpha - 5760\, A_4^0 \left\langle r^4 \right\rangle \beta + 60{,}480\ A_6^0 \left\langle r^6 \right\rangle \gamma$$

$$Y = J_z(\pm 3) = -15\, A_2^0 \left\langle r^2 \right\rangle \alpha - 3240\, A_4^0 \left\langle r^4 \right\rangle \beta + 325{,}080\, A_6^0 \left\langle r^6 \right\rangle \gamma$$

$$Z = J_z(\pm 2) = -30\, A_2^0 \left\langle r^2 \right\rangle \alpha + 660\, A_4^0 \left\langle r^4 \right\rangle \beta + 166{,}320\, A_6^0 \left\langle r^6 \right\rangle \gamma$$

$$A' = J_z(\pm 1) = -39\, A_2^0 \left\langle r^2 \right\rangle \alpha + 3840\, A_4^0 \left\langle r^4 \right\rangle \beta - 151{,}200\, A_6^0 \left\langle r^6 \right\rangle \gamma$$

$$B' = J_z(0) = -42\, A_2^0 \left\langle r^2 \right\rangle \alpha + 5040\, A_4^0 \left\langle r^4 \right\rangle \beta - 302{,}400\, A_6^0 \left\langle r^6 \right\rangle \gamma$$

$$g_{1,7} = 720\sqrt{231}\, A_6^6 \left\langle r^6 \right\rangle \gamma\,, \quad h_{2,8} = 2520\sqrt{66}\, A_6^6 \left\langle r^6 \right\rangle \gamma$$

$$k_{3,9} = 5040\sqrt{30}\, A_6^6 \left\langle r^6 \right\rangle \gamma\,, \quad \ell_{4,10} = 30{,}240\ A_6^6 \left\langle r^6 \right\rangle \gamma$$

J_z	-6	-5	-4	-3	-2	-1	0	1	2	3	4	5	6
-6	V						$g_{1,7}$						
-5		W						$h_{2,8}$					
-4			X						$k_{3,9}$				
-3				Y						$\ell_{4,10}$			
-2					Z						$k_{3,9}$		
-1						A'						$h_{2,8}$	
0	$g_{1,7}$						B'						$g_{1,7}$
1		$h_{2,8}$						A'					
2			$k_{3,9}$						Z				
3				$\ell_{4,10}$						Y			
4					$k_{3,9}$						X		
5						$h_{2,8}$						W	
6							$g_{1,7}$						V

Table XII. Crystal quantum energy levels for J = 1 to J = 6

Field-free J level	Number of sub-levels	Crystal quantum sublevels μ	Energy expressions in terms of the symbols used in Table XI[a]
1	2	0	B [a]
		±1	A
2	3	0	E
		±1	D
		±2	C
3	5	0	I
		±1	H
		±2	G
		3	$F + a_{1,7}$
		3	$F - a_{1,7}$
4	6	0	N'
		±2	$\frac{1}{2}\left\{(K+M)+\left[(M-K)^2+4b_{1,7}^2\right]^{1/2}\right\}$
		±2	$\frac{1}{2}\left\{(K+M)-\left[(M-K)^2+4b_{1,7}^2\right]^{1/2}\right\}$
		±1	N
		3	$L + c_{2,8}$
		3	$L - c_{2,8}$

Table XII. (Cont'd)

Field-free J level	Number of sub-levels	Crystal quantum sublevels μ	Energy expressions in terms of the symbols used in Table XI[a]
5	7	0	U
		±1	$\frac{1}{2}\left\{(P+T)+\left[(P-T)^2+4d_{1,7}^2\right]^{1/2}\right\}$
		±1	$\frac{1}{2}\left\{(P+T)-\left[(P-T)^2+4d_{1,7}^2\right]^{1/2}\right\}$
		±2	$\frac{1}{2}\left\{(Q+S)+\left[(Q-S)^2+4e_{2,8}^2\right]^{1/2}\right\}$
		±2	$\frac{1}{2}\left\{(Q+S)-\left[(Q-S)^2+4e_{2,8}^2\right]^{1/2}\right\}$
		3	$R+f_{3,9}$
		3	$R-f_{3,9}$
6	9	0	V
		0	$\frac{1}{2}\left\{(V+B')+\left[(V-B')^2+8g_{1,7}^2\right]^{1/2}\right\}$
		0	$\frac{1}{2}\left\{(V+B')-\left[(V-B')^2+8g_{1,7}^2\right]^{1/2}\right\}$
		±1	$\frac{1}{2}\left\{(W+A')+\left[(W-A')^2+4h_{2,8}^2\right]^{1/2}\right\}$
		±1	$\frac{1}{2}\left\{(W+A')-\left[(W-A')^2+4h_{2,8}^2\right]^{1/2}\right\}$
		±2	$\frac{1}{2}\left\{(X+Z)+\left[(X-Z)^2+4k_{3,9}^2\right]^{1/2}\right\}$
		±2	$\frac{1}{2}\left\{(X+Z)-\left[(X-Z)^2+4k_{3,9}^2\right]^{1/2}\right\}$
		3	$Y+\ell_{4,10}$
		3	$Y-\ell_{4,10}$

[a] These capital and small letters stand for the corresponding diagonal and off-diagonal matrix elements.

F. Selection Rules

Using the group theoretical methods outlined by Tinkham, we can derive the selection rules for the D_{3h} and C_{3h} point symmetries.[18] Since C_{3h} is really a subgroup of the D_{3h} point group, we first derive the selection rules for D_{3h} and then modify these rules for the C_{3h} subgroup. For the irreducible representation nomenclature we use the notation of Eyring, Walter, and Kimble, along with the notation introduction by Hellwege.[37, 38]

Since the electric dipole moment $\vec{er}$ is a polar vector $\vec{V}$, we find it transforms like the coordinates. In a rotation through ϕ about the z axis, we have

$$\underset{\sim}{\Gamma}^{(\vec{V})}(\phi) = \begin{pmatrix} \cos\phi & -\sin\phi & 0 \\ \sin\phi & \cos\phi & 0 \\ 0 & 0 & 1 \end{pmatrix} , \tag{97}$$

where $\underset{\sim}{\Gamma}^{(\vec{V})}(\phi)$ gives the transformation properties of the x, y, and z components. We recall that the character of the "jth" representation is

$$\chi^{(j)}(R) = \sum_{\mu=1}^{\ell_j} \Gamma^{(j)}(R)_{\mu\mu} = \text{Tr. } \Gamma^{(j)}(R) , \tag{98}$$

so the character of Eq. (97) is

$$\chi^{(\vec{V})}(\phi) = 1 + 2\cos\phi . \tag{99}$$

All rotations by ϕ about any axis are in the same class and therefore have the same character.

The inversion operation can be combined with the rotation by ϕ. Thus we can write

$$\underset{\sim}{\Gamma}^{(\vec{V})}(\phi, i) = \begin{pmatrix} -\cos\phi & \sin\phi & 0 \\ -\sin\phi & -\cos\phi & 0 \\ 0 & 0 & -1 \end{pmatrix} \tag{100}$$

and

$$\chi^{(\vec{V})}(\phi, i) = -(1 + 2\cos\phi). \tag{101}$$

The magnetic dipole-moment operator $\vec{\mu}$ is an axial vector $\vec{A}$, which means it transforms like a polar vector under rotations but is invariant under inversion. Thus we have

$$\underset{\sim}{\Gamma}^{(\vec{A})}(\phi, i) = \underset{\sim}{\Gamma}^{(\vec{A})}(\phi) = \begin{pmatrix} \cos\phi & -\sin\phi & 0 \\ \sin\phi & \cos\phi & 0 \\ 0 & 0 & 1 \end{pmatrix} \tag{102}$$

and

$$\chi^{(\vec{A})}(\phi, i) = \chi^{(\vec{A})}(\phi) = 1 + 2\cos\phi\,. \tag{103}$$

In the determination of selection rules, parity (or inversion symmetry) is important. In the case of electric dipole transitions where $\vec{V}$ belongs to a $\underset{\sim}{u}$ representation, we find that transitions are forbidden between states of the same parity because $\Gamma_u \times \Gamma$ has the opposite parity to Γ and therefore cannot contain any representations of the same parity as Γ. However, magnetic-dipole transitions are not forbidden by parity since the operator $\vec{\mu}$ is invariant under inversion.

Experimentally, "forced" electric-dipole transitions are observed in rare earth and actinide spectra when the cation is located in a site not having inversion symmetry. For cations located in a site having inversion symmetry, vibrations of the cations in a site destroy the perfect inversion symmetry and parity is no longer a "good" quantum number. If pure electric and magnetic dipole transitions are allowed, we find that the electric-dipole transitions are roughly 10^4 times as intense as magnetic-dipole transitions. Thus even a small departure from inversion symmetry and the break-down of parity allows the electric-dipole transition probabilities to be larger in many cases.

For $D_{3h} = D_3 \times \sigma_h$, where (σ_h, E) is (i, E), we can calculate $\chi^{(\vec{A})}$ and $\chi^{(\vec{V})}$ in the following manner. For magnetic

dipole radiations we have

$$\chi^{(\vec{A})}(\phi, i) \quad \begin{array}{|cccccc|} \hline E & \sigma_h & 2C_3 & 2S_3 & 3C_2' & 3\sigma_v \\ \hline 3 & -1 & 0 & 2 & -1 & -1 \\ \hline \end{array} ,$$

and $\chi^{(\vec{A})}(\phi, i)$ transforms according to $A_2' + E'' = \Gamma_2 + \Gamma_6$. The allowed magnetic-dipole transitions for D_{3h} symmetry are given in Table XIII.

For electric-dipole radiations we have

$$\chi^{(\vec{V})}(\phi, i) \quad \begin{array}{|cccccc|} \hline E & \sigma_h & 2C_3 & 2S_3 & 3C_2' & 3\sigma_v \\ \hline 3 & 1 & 0 & -2 & -1 & 1 \\ \hline \end{array} ,$$

and $\chi^{(\vec{V})}(\phi, i)$ transforms according to $A_2'' + E' = \Gamma_4 + \Gamma_5$.

The allowed electric-dipole transitions for D_{3h} symmetry are given in Table XIII. For magnetic-dipole transitions we have $\Delta J = 0$ or ± 1 , and $0 \leftrightarrow 0$ is forbidden. Because C_{3h} is a subgroup of D_{3h} there is no longer any meaning to the subscripts on the nondegenerate states, A_1' and A_2' . Both states in C_{3h} symmetry have the simple A' character. We give the selection rules for electric- and magnetic-dipole radiation for C_{3h} in Tables XIV and XV. The results presented in these three tables are in agreement with the selection rules for D_{3h} and C_{3h} presented by Sayre and Freed.[39]

Table XIII. Magnetic- and electric-dipole transition selection rules for D_{3h} point symmetry

Magnetic-dipole transitions

A_2', σ polarization		E'', π and axial polarization	
$A_1' \times A_2' = A_2'$	$A_1' \leftrightarrow A_2'$	$A_1' \times E'' = E''$	$A_1' \leftrightarrow E''$
$A_1'' \times A_2' = A_2''$	$A_1'' \leftrightarrow A_2''$	$A_2' \times E'' = E''$	$A_2' \leftrightarrow E''$
$E' \times A_2' = E'$	$E' \leftrightarrow E'$	$E' \times E'' = E'' + A_1'' + A_2''$	$E' \leftrightarrow E''$
$E'' \times A_2' = E''$	$E'' \leftrightarrow E''$		$E' \leftrightarrow A_1''$
			$E' \leftrightarrow A_2''$

Electric-dipole transitions

E', σ and axial polarization		A_2'', π polarization	
$A_1' \times E' = E'$	$A_1' \leftrightarrow E'$	$A_1' \times A_2'' = A_2''$	$A_1' \leftrightarrow A_2''$
$A_2' \times E' = E'$	$A_2' \leftrightarrow E'$		$A_2' \leftrightarrow A_1''$
$E' \times E' = E' + A_1' + A_2'$	$E' \leftrightarrow E'$	$A_1'' \times A_2'' = A_2'$	$A_1'' \leftrightarrow A_2'$
	$E' \leftrightarrow A_1'$		$A_2'' \leftrightarrow A_1'$
	$E' \leftrightarrow A_2'$	$E' \times A_2'' = E''$	$E' \leftrightarrow E''$
$E'' \times E' = E'' + A_1'' + A_2''$	$E'' \leftrightarrow E''$		
	$E'' \leftrightarrow A_1''$		
	$E'' \leftrightarrow A_2''$		

Table XIV. Magnetic- and electric-dipole transition selection rules for C_{3h} point symmetry

Magnetic-dipole transitions

A', σ polarization		E'', π and axial polarization	
$A' \times A' = A'$	$A' \leftrightarrow A'$	$A' \times E'' = E''$	$A' \leftrightarrow E''$
$A'' \times A' = A''$	$A'' \leftrightarrow A''$	$E' \times E'' = E''$	$E' \leftrightarrow E''$
$E' \times A' = E'$	$E' \leftrightarrow E'$	$+ A''$	$E' \leftrightarrow A''$
$E'' \times A' = E''$	$E'' \leftrightarrow E''$		

Electric-dipole transitions

E', σ and axial polarization		A'', π polarization	
$A' \times E' = E'$	$A' \leftrightarrow E'$	$A' \times A'' = A''$	$A' \leftrightarrow A''$
$E' \times E' = E'$	$E' \leftrightarrow E'$	$E' \times A'' = E''$	$E' \leftrightarrow E''$
$+ A'$	$E' \leftrightarrow A'$		$E'' \leftrightarrow E'$
$E'' \times E' = E''$	$E'' \leftrightarrow E''$		
$+ A''$	$E'' \leftrightarrow A''$		

Table XV. Electric- and magnetic-dipole transition selection rules for C_{3h} point symmetry

Electric-dipole transitions

	μ'			
μ	0	± 1	± 2	3
0			σ, π	π
± 1		σ, a	π	σ, a
± 2	σ, a	π	σ, a	
3	π	σ, a		

Magnetic-dipole transitions

	μ'			
μ	0	± 1	± 2	3
0	σ	π, a		
±1	π, a	σ	π, a	
±2		π, a	σ	π, a
± 3			π, a	σ

III. EXPERIMENTAL PROCEDURES AND OBSERVATIONS

A. Spectrographic and Spectrophotometer Equipment

Absorption and fluorescence spectra of the crystals were observed with a Jarrell-Ash Wadsworth-mount 3.4-meter spectrograph having a speed of f/22. Two gratings were used in this instrument--one with 30,000 lines per inch and another with 15,000 lines per inch. In the first order, the reciprocal linear dispersion was 2.4 A/mm and 5.3 A/mm, respectively. The crystals were maintained at selected temperatures of 273°K (ice bath), 194°K (carbon dioxide and acetone), 77°K (liquid N_2), 20°K (liquid H_2), and 4°K (liquid He) in quartz and pyrex dewars. See Fig. 11.

Spectra taken on a Hilger fast spectrograph having a speed of f/4 indicated that selective excitation would help in the analysis of the AmIV fluorescence spectrum. Light sources included an air-cooled high-pressure mercury lamp (BH6), a water-cooled high pressure mercury lamp (AH6), a 100-watt tungsten lamp, and a commercially available Kistiakowsky-type hydrogen-discharge lamp. Three types of polarizers were employed: a Nicol, an Ahrein with ultraviolet transmitting cement, and a Wollaston. Iron and mercury lines served as wavelength references, and the photographic plates were measured on a precision screw-type comparator.

Solution spectra were taken on a Cary Model-14 recording spectrophotometer which was calibrated at the factory with an AH4 Hg arc. Some Nd^{+3}, and Am^{+3} standards were run in order to check the wave lengths. The calibration results indicated the instrument to be correct to 1.5 A in the region from 2700 to 4900A and 2A from 4900A to 2 μ. The resolving power of the monochromator is about 1.0A in the ultraviolet and visible ranges and about 3.0A in the near infrared. The wave length scale is reproducible to 0.5A.

Infrared spectra were observed on a Beckman IR-5 Infrared Spectrophotometer and a Perkin-Elmer Model 112-U Spectrometer. The latter is a single-beam instrument equipped with a double-pass monochromator and gives a resolution better than 1 cm^{-1} at 850 cm^{-1} (NaCl).

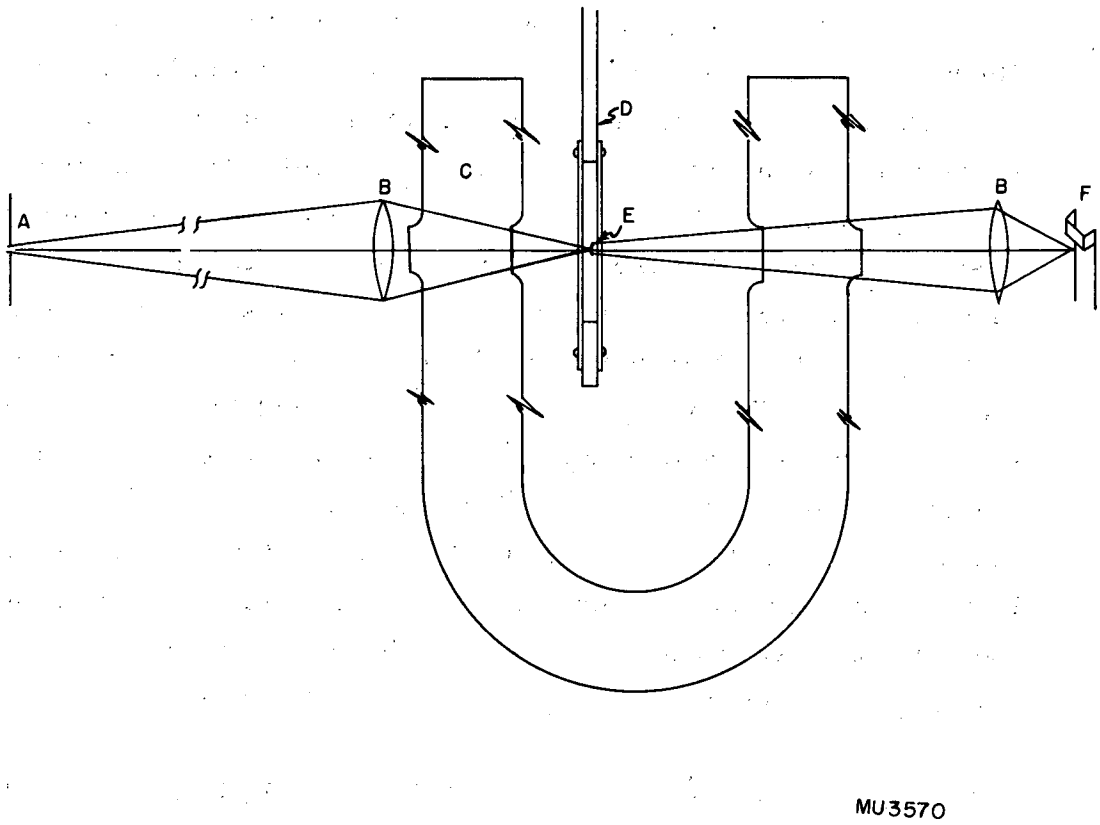

Fig. 11. Optical arrangement for obtaining low-temperature absorption spectra. (A) Slit, (B) condensing lens, (C) Dewar flask with optically flat windows, (D) sample holder, (E) position of sample, (F) Tungsten-filament lamp.

B. Preparation and Growth of Single Crystals

1. Single Crystals of $LaCl_3$ — $AmCl_3$

Pure La_2O_3 (99.9%) was obtained from Research Chemicals, Burbank, California, and dissolved in concentrated HCl. An emission-spectra analysis of this solution indicated no detectable amounts of other rare earths except $\leqslant 0.1\%$ Pr. The only other impurities found were Ca, Mg, and Si. The solution was evaporated in a desiccator over P_2O_5 under "house" vacuum. The crystals of hydrated $LaCl_3$ thus obtained were then placed in platinum trays which were inserted into a quartz tube held horizontally in a variac-controlled tube furnace, (see Fig. 12). The temperature was measured with an inserted chromel-alumel thermocouple. Dehydration was carried out by raising the temperature to 100°C for one hour, to 150°C for another hour, and finally to 250°C for two hours. Just before the heating was begun, a one-to-one mixture of dry tank HCl and Ar was passed over the trays at a slow rate. Passage of the HCl over the sample is necessary to prevent hydrolysis of the trichloride,

$$LaCl_3 \cdot x\,H_2O \rightleftharpoons LaOCl + 2\,HCl + (x-1)\,H_2O\,. \qquad (104)$$

Then a known volume of Am^{+3} in 2.0 M HCl was added to a quartz sublimation tube. The ion-exchange-purified Am^{+3} was found to be spectroscopically pure, and an α assay of the solution gave a reliable value for the concentration. The solution in the tube was then slowly evaporated on a vacuum line, and anhydrous $AmCl_3$ was formed by heating the hydrate slowly in the presence of dry HCl. After the tube was flushed repeatedly with dry argon, and the $AmCl_3$ completely dried, a known quantity of anhydrous $LaCl_3$ was added and the mixture thoroughly degassed (see Fig. 13). The chlorides were then melted to form a solution.

A portable tube furnace was then placed around the portion containing the dried chloride, the temperature slowly raised to 900°C, and the chloride sublimed into the cooler portion of the tube. Purification

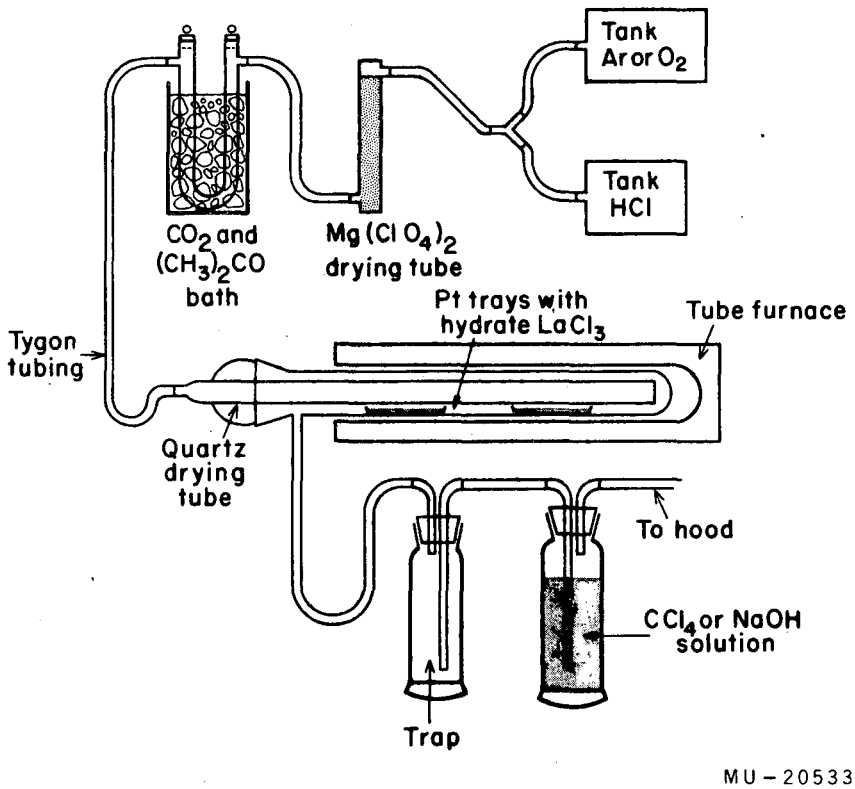

Fig. 12. Apparatus used to dry rare earth trichlorides. Tank HCl and Ar were passed through a drying tube to remove water, and through a carbon dioxide-acetone bath to remove certain organic material in the tank HCl.

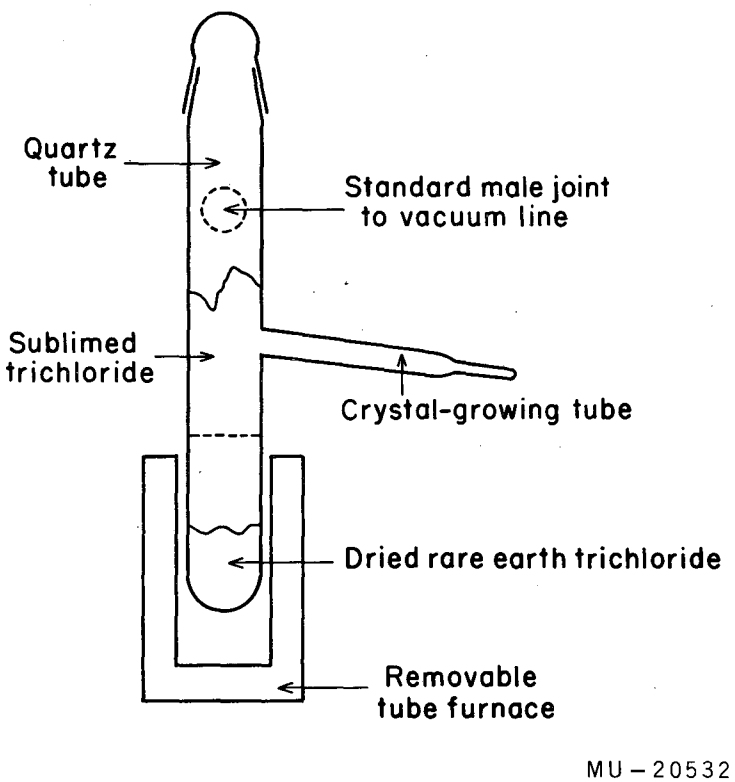

Fig. 13. All-quartz sublimation tube. The $AmCl_3$-$LaCl_3$ mixture is heated to 900°C in a tube furnace and sublimed into the cooler portion of the tube. The entire unit is rotated 120 deg, and the purified material is melted into the sidearm by using a torch. The tube is then sealed and drawn off the line under vacuum.

of the trichlorides apparently is required for the production of crystals of high optical quality. The nonvolatile residue usually contains some oxide (originating from the disproportion of oxychloride), carbon (from unidentified organic impurities in the HCl), and various impurity metal chlorides of low volatility.

When sublimation was complete, the tube was rotated 120 deg about a standard male joint, and the sublimate heated by a torch to the melting point (for $LaCl_3$, 860°C). The molten material was allowed to run into an attached sidearm which was previously shaped for growing single crystals. The weight of crystalline material was usually 1 to 3 g. After all the material was collected in the sidearm, the crystal-growing tube was sealed off under vacuum. A quartz hook was made at the top of the tube so that it could be suspended from a 5-mil platinum wire inside the crystal-growing furnance.

In order to grow single crystals of optical quality, the crystal-growing tubes were lowered by means of Kramer synchronous motors through a tube furnace set at 880°C near the center of the furnace.[40] At a drop rate of 0.2 cm hr^{-1}, seven days were required to lower the crystal growing tube through the furnace. In the narrow portion of the tube near the tip a small single crystal formed which grew larger and larger as the tube moved slowly through the thermal gradient.[40]

The tube furnace was set on end and had a nickel core with two quartz-lined holes running top to bottom. The furnace temperature was controlled to within ± 5°C electronically by a Wheelco Controller which fed in 60% of the current through a variac system while the remaining current passed through the control unit. Figure 14 shows the arrangement of the electronics used in growing single cyrstals and Figs. 15 through 18 give a more careful description of some essential units.

The crystals thus obtained were optically clear, with the c axis usually parallel to the length of the tube. Crossed polaroid sheets were used to locate the position of the c axis in these uniaxial crystals.

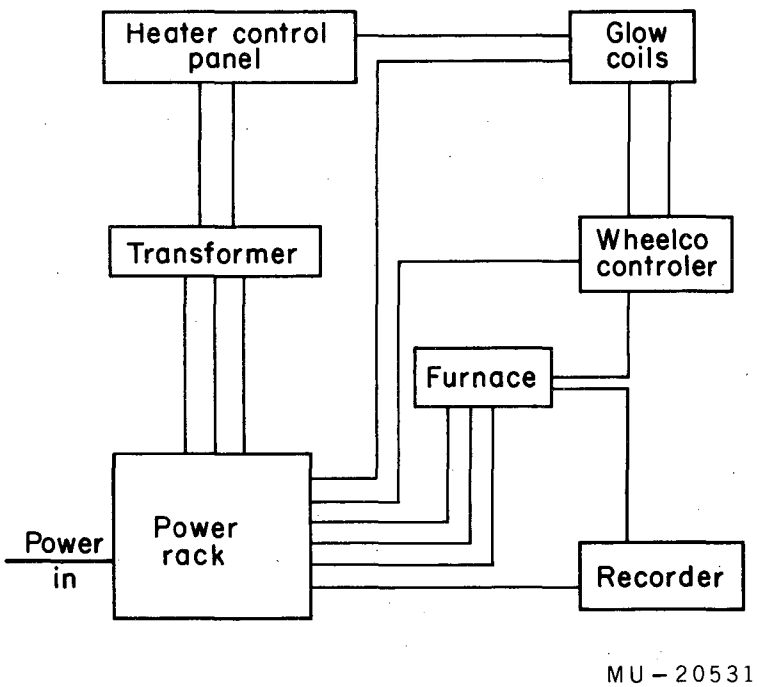

Fig. 14. Block diagram of apparatus used in growing single crystals from the melt.

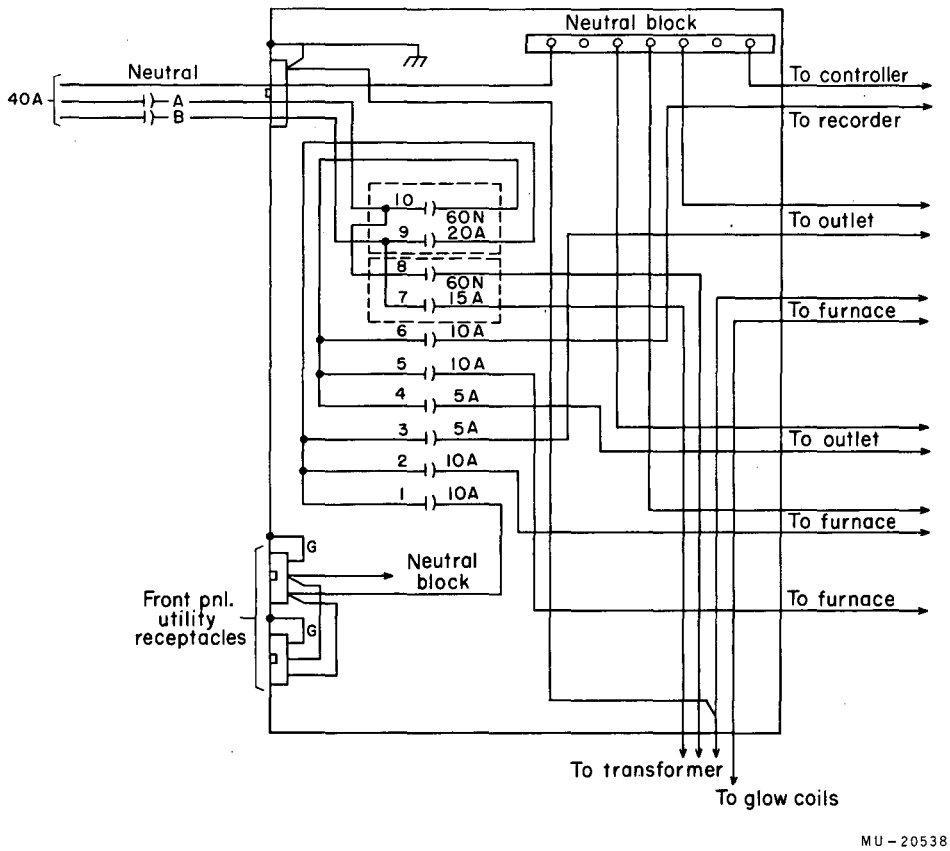

Fig. 15. Wiring diagram of power rack.

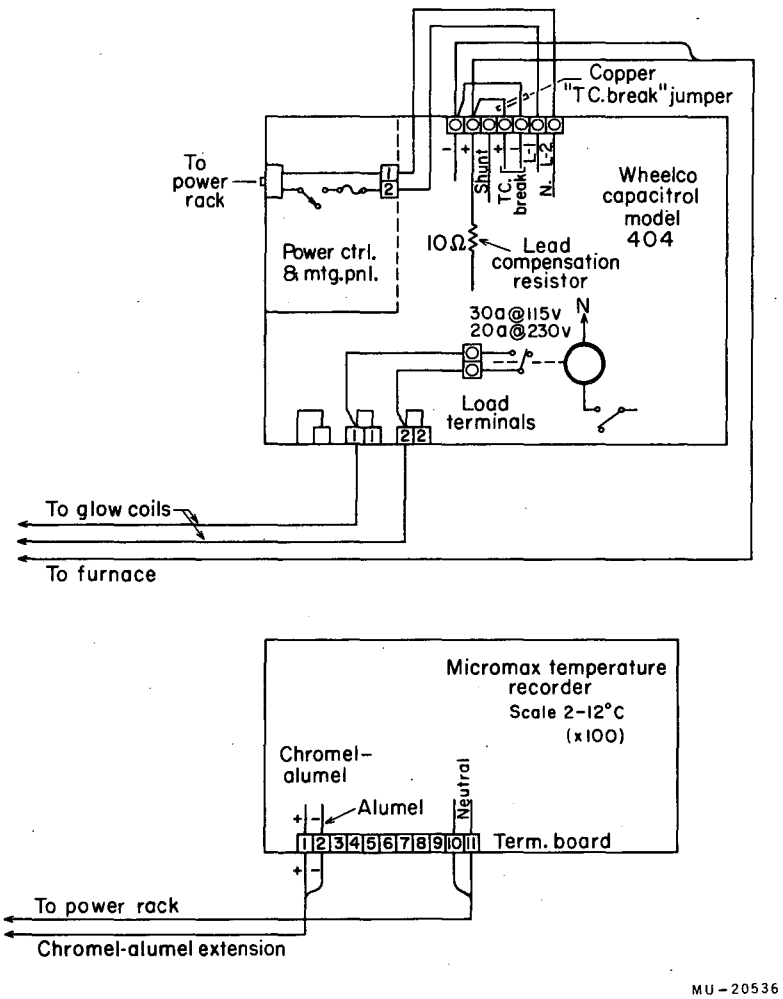

Fig. 16. Wiring diagram of Wheelco controller and temperature-recording unit.

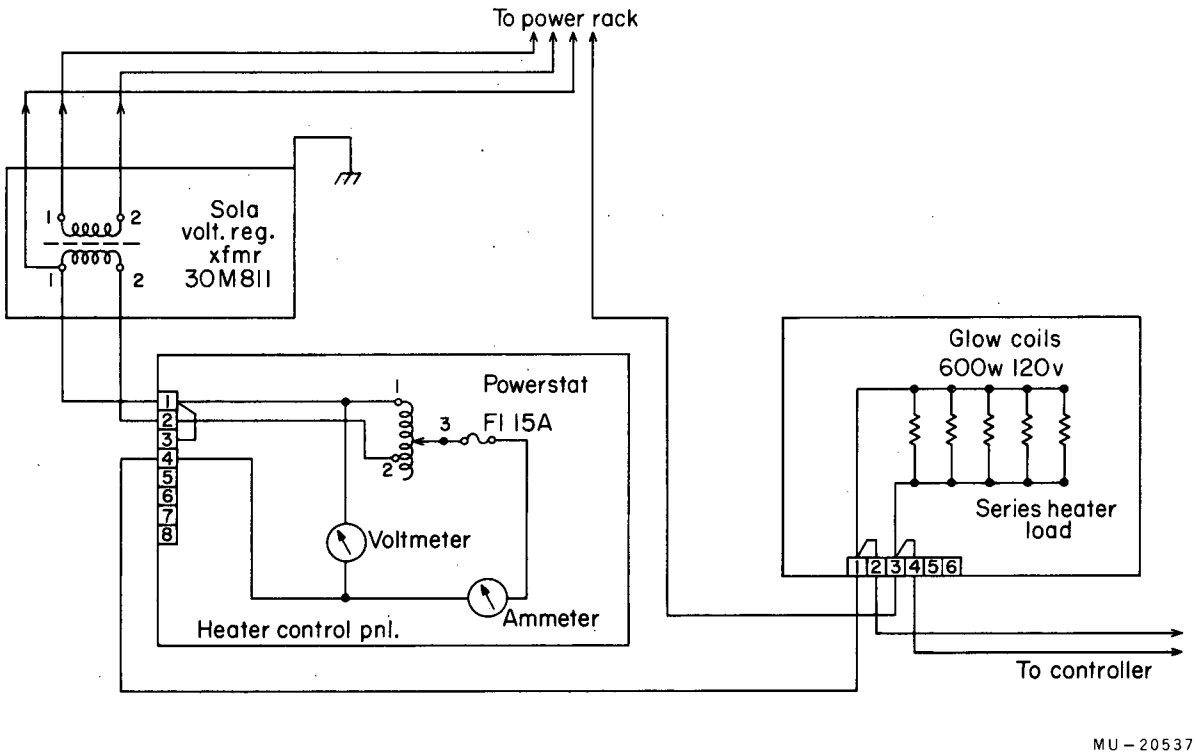

Fig. 17. Wiring diagram of Sola transformer, heater control panel, and glow coils.

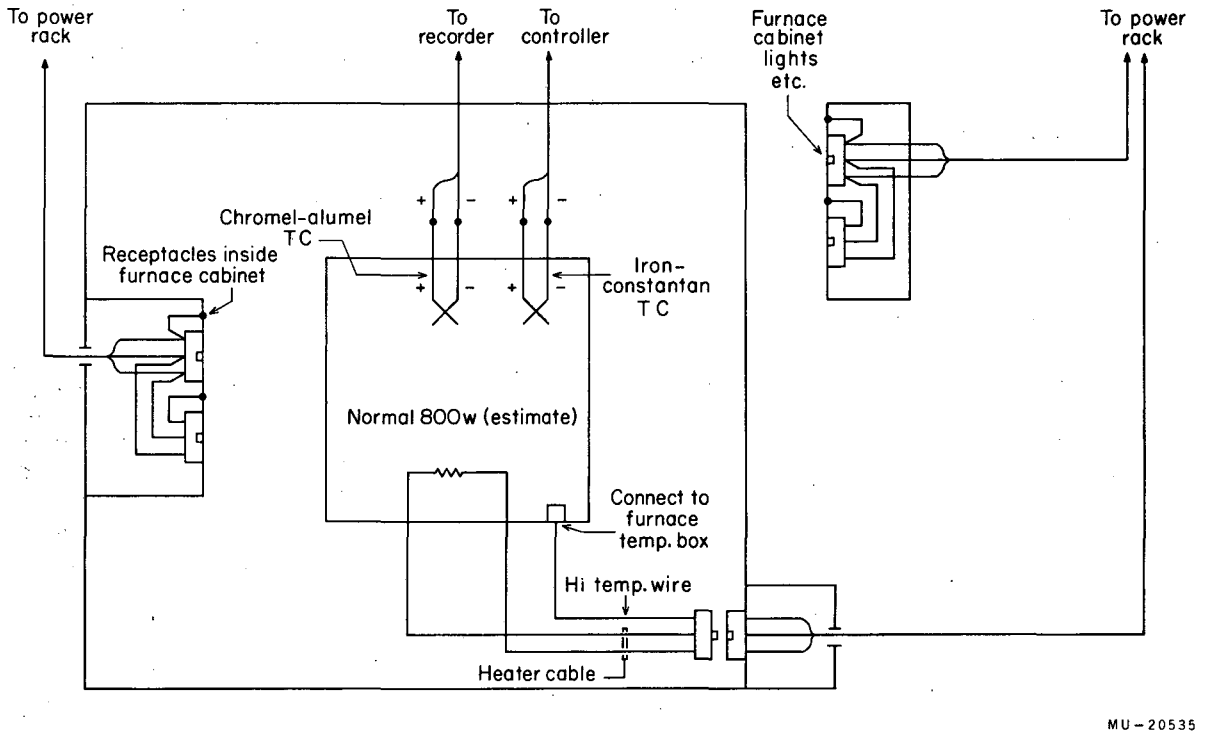

Fig. 18. Wiring diagram of the furnace cabinet used to grow radioactive single crystals.

2. Single Crystals of Rare Earth Ethylsulfates

Two methods were used to prepare single crystals of the rare earth ethylsulfates. In the first method the anhydrous rare earth trichloride was dissolved in pure ethanol. A stoichiometric quantity of sodium ethylsulfate was then dissolved in pure ethanol and added quantitatively to the chloride solution, so that the reaction

$$3\,NaC_2H_5SO_4 \cdot 9H_2O + TmCl_3 \xrightleftharpoons{\text{in ethanol}} Tm(C_2H_5SO_4 \cdot 9H_2O)_3 + 3\,NaCl \qquad (105)$$

would take place.

Since the solubility of NaCl in ethanol is much less than in water, the NaCl precipitates out in finely divided particles, leaving a solution of rare earth ethylsulfate saturated with NaCl. The remaining NaCl in solution is removed gradually in the process of recrystallization of the ethylsulfates.

The hydrogen ion activity must be carefully controlled to prevent hydrolsis of the ethylsulfate:

$$H_2O + C_2H_5SO_4^- \cdot 9H_2O \xrightleftharpoons{H^+} C_2H_5OH + HSO_4^- + 9\,H_2O\,. \qquad (106)$$

The presence of the hydrogen ion as a catalyst, increases the rate of hydrolysis. For this reason the solutions were maintained at a pH of six by adding very small amounts of NH_4OH. Crystal preparation had to be carried out below 35 °C to prevent decomposition of the ethylsulfate nonahydrate.

After the NaCl particles were removed from the ethylsulfate solution by eentrifuging or filtering, the supernatant liquid was poured into petri dishes which were placed in a vacuum desiccator over P_2O_5. The desiccator was then flushed several times with dry N_2, and the

crystals grown directly from the solution in 0.5 atm. of nitrogen and over P_2O_5 as a desiccant.

Another method of preparation is to dissolve the rare earth oxide in a mixture of HCl and H_2SO_4. The HCl was then removed by heating the solution on a steam bath. The slightly soluble rare earth sulfates were mixed with a large quantity of water, and to this solution a stoichiometric quantity of barium ethylsulfate was added. The solution was maintained at pH=6 by adding small amounts of NH_4OH. On mixing, $BaSO_4$ precipitated, and was removed by filtration. Unprecipitated barium sulfate was removed by repeated recrystallization. The method of growing crystals in petri dishes was the same as that discussed in the preceding paragraph. In this manner we were able to prepare single crystals of optical quality of the ethylsulfates of La^{+3}, Pr^{+3}, Dy^{+3}, Er^{+3}, Tm^{+3}, and Eu^{+3}.

3. Crystals of Hydrated Rare Earth Trichlorides

Hydrated rare earth trichlorides were grown quite simply from the HCl solution used to dissolve the oxide. Usually the solution was first diluted to 3 N acid, stirred well, and then poured into petri dishes. Excellent crystals were obtained on the first crystallization which was carried out in an evacuated desiccator over P_2O_5.

C. Absorption Spectra of TmIV

In recent years, several investigators have attempted to analyze the absorption spectrum of TmIV in the ethylsulfate matrix.[22, 25, 41] Usually the optical spectra are studied by substituting small amounts of thulium in yttrium or lanthanum ethylsulfate.[25, 41] The advantage of diluting the thulium into an optically clear matrix is that vibrational as well as "weak" electronic transitions are usually not seen, and the resulting simplicity of the spectrum aids the analysis. However, here we studied pure thulium ethylsulfate nonahydrate to observe the reportedly weak absorption lines due to transitions from $^3H_6 \rightarrow {}^1I_6$, and upper sublevels of $^3H_6 \rightarrow {}^3P_0$. Johnsen has identified the 0 and ±1 crystal quantum levels of the $^3H_6$ ground-state J-level and the upper multiplets of $^3F_{2,3,4}$ and $^1G_4$.[25] Our confirmation of these $^3H_6$ crystal quantum levels is given in Table XVI. Additional sublevels of the $^3H_6$ were found to be ±1 or 3 at 195 cm^{-1} and ±2 at 231 cm^{-1}. These sublevels are based on the polarized absorption spectrum of $^3P_{2,1,0}$, $^1D_2$, and $^1G_4$.

Spectra of the $^3P_{2,1,0}$ multiplet were taken at 77°K, 194°K, and 273°K. Enhanced intensities of certain lines at higher temperatures were observed, indicating the increased population of upper sublevels of the $^3H_6$. Three transitions in particular (2621.1 σ; 2623.4, π; 2634.6 π) identify the ±2 sublevel of $^3P_2$. These transitions are sharp with line widths of only several tenths A. Two additional transitions (2629.0, σ; 2640.0, σ) appear to be from the $^3H_6$ sublevels of ±1, and ±1' or 3 to the ±1 sublevel of $^3P_2$. Several weak and one rather strong line appear to the ultra violet of the $0 \rightarrow \pm 2$ transition. These σ lines are only several angstroms apart and could possibly be $\pm 1 \rightarrow \pm 1$ transitions. Thus the $^3P_2$, $\mu = \pm 1$ sublevel could be to the ultraviolet of the ±2. However, no manipulation of all the $^3P_2$ data gives a consistent position for ±1 to the ultraviolet of ±2. Since two and possibly three lines indicate 38,060 $cm^{-1} = \pm 1$, we suggest for $^3P_2$ a ±2 sublevel at 38,140 cm^{-1} and ±1 at 38,060 cm^{-1}.

Table XVI. Spectra, polarization, and crystal quantum transitions of $Tm(C_2H_5SO_4)_3 \cdot 9H_2O$

Term assignment	Crystal quantum transitions	Wavelengths, intensities, and polarization									Wave numbers (in vacuum)		
		λ(A) 77°K (in air)	I.	P.	λ(A) 194°K (in air)	I.	P.	λ(A) 273°K (in air)	I.	P.	77°K	194°K	273°K
$^3P_2$	0→±2	2621.1	8[b]	σ	2621.7	6[c]	σ				38,140	38,132	
	±1 →±2	2623.4	8[a]	π	2624.0	6[b]	π				38,107	38,099	
	±1→ ±1	2629.0	4[b]	σ	2629.3	6[b]	σ	2629.6	4[d]	σ	38,027	38,022	38,017
	3→±2	2634.6	4[b]	π	2635.1	6[b]	π	2635.4	5[d]	π	37,945	37,938	37,934
	3→±1	2640.0	1[a]	σ	2639.8	6[b]	σ	2640.1	6[d]	σ	37,866	37,870	37,866
$^3P_1$	±1→ ±1	2742.2	8[a]	σ	2743.1	5[b]	σ	2743.9	4[c]	σ	36,456	36,444	36,434
	3 →±1, 0	2754.4	3[a]	σ	2755.5	5[b]	σ				36,294	36,280	
$^3P_0$	3→0	2866.2	6[c]	π	2867.6	5[c]	π	2867.5	5[d]	π	34,879	34,863	34,862
	±2→0	2869.1	6[c]	σ	2870.4	5[d]	σ	2870.6	5[d]	σ	34,843	34,828	34,825
$^1D_2$	±1→±1	3578.3	9[d]	σ	3578.9	6[d]	σ	3579.0	6[d]	σ	27,938	27,934	27,933
	0→±2	3583.2	9[d]	σ							27,900		
	±1→±2	3587.4	9[c]	π	3587.9	6[c]	π	3589.7	4[d]	π	27,867	27,864	27,850
	3→±1	3599.2	5[b]	σ							27,776		
	3→±2	3608.6	4[b]	π	3608.7	6[b]	π	3608.4	8[b]	π	27,705	27,704	27,705
	±2→ 0	3616.2	3[b]	σ	3616.4	6[b]	σ	3616.9	8[b]	σ	27,645	27,644	27,640

Table XVI. (Cont'd)

$^1G_4$	0→ 3	4676.3	7[a]	π					21,379	
	±1→ 3	4683.4	7[b]	σ					21,346	
	0→ 3	4684.6	8[b]	π	4685.0	5[c]	π		21,341	21,339
	±1→ 3	4691.8	6[d]	σ					21,308	
	0→ ±2	4698.2	5[d]	σ	4698.0	3[d]	σ		21,279	21,277
	±1→ ±2	4705.5	6[a]	π	4708.7	3[d]	π		21,246	21,231
	0→ ±2	4723.0	6[b]	σ					21,168	
	±1→ ±2	4725.0	6[b]	σ	4724.6	5[d]	σ		21,158	21,160
	±1→ ±2	4730.2	6[b]	π					21,135	
	3→ ±2	4741.7	3[a]	π	4745.2	5[b]	π		21,084	21,068
	3→ 0	4747.1	3[b]	π					21,060	
	±2→ ±2	4749.3	2[c]	σ					21,049	
	±2→ 0	4754.8	2[b]	σ					21,025	
	±2→ ±2	4774.5	1[a]	σ					20,938	

[a] Line width: 0.1 to 0.5 A.

[b] Line width: 0.5 to 1.0 A.

[c] Line width: 1.0 to 2.0 A.

[d] Line width: 2.0 to 4.0 A.

One sharp intense σ line corresponds to a $\pm 1 \rightarrow \pm 1$ and a transition from $^3H_6$ to $^3P_1$. Additional weak lines to the red indicate transitions from 3 and ± 2 of $^3H_6$ to the sublevels ± 1 and 0 of $^3P_1$. Lines polarized σ and π and separated by only 10 cm^{-1} may indicate either an incomplete polarization or a vibrational satellite, or a small crystal-field splitting of $^3P_1$. Since no additional confirmation could be made, it is hard to estimate just how large the splitting is. However, several thousand cm^{-1} to the red, two reasonably intense lines (2866.2 , π ; 2869.1 σ) can be explained as transitions from 3 and ± 2 of $^3H_6$ to $\mu = 0$, $^3P_0$.

Very weak polarized lines are observed near the $^3P_0$ level. These may be due to the $^1I_6$ since no additional spectra are observed to the red until the $^1D_2$ grouping is reached. Four or five polarized lines confirmed the positions of the ± 1 and ± 2 sublevels of $^1D_2$. The position of the $^1G_4$ sublevels was found to be similar to that reported by Johnsen.[25]

It should be pointed out that differentation of the pure electronic transition from the vibronic transitions is not easy. Since experimental identification of a vibronic satellite is not unambiguous in many cases, the selection of a sublevel should not be made simply on the basis of a crystal-field-splitting calculation. Likewise, a careful study of possible impurity ions may show that they exhibit polarized absorption spectra in the region of interest. In our TmIV study, holmium and erbium ethylsulfate crystals were prepared and polarization spectra taken. Lines due to these impurities are excluded from Table XVI.

Table XVII gives the wave lengths and intensities for the lines appearing in the spectrum of $TmCl_3 \cdot 6\ H_2O$. The similarity in the spectra of the hydrated chloride and the ethylsulfate allows us to assign the multiplets, but the crystal quantum assignments cannot be made because the point symmetry of the Tm^{+3} ion in the hydrate is not known. Table XVIII gives the wave lengths and intensities for the $TmCl_3$ in $LaCl_3$. The only J levels seen are the $^1D_2$ and $^1G_4$.

Table XVII. Spectra of $TmCl_3 \cdot 6H_2O$

Term assignment	λ(A) 77°K (in air)	λ (cm^{-1}) 77°K (in vac.)	I	Term assignment	λ(A) 77°K (in air)	λ(cm^{-1}) 77°K (in vac.)	I
$^3P_2$	2590.9	38,585	8[a]	$^1G_4$	4629.2	21,596	8[c]
	2602.7	38,410	9[b]		4645.9	21,518	6[c]
	2611.5	38,281	8[a]		4649.5	21,502	9[b]
	2613.7	38,249	5[a]		4680.5	21,359	3[a]
	2622.0	38,127	4[c]		4709.8	21,226	4[a]
	2626.2	38,066	4[c]		4716.5	21,196	2[c]
					4719.8	21,181	1[a]
$^3P_1$	2734.3	36,562	4[c]				
	2743.5	36,439	6[d]	$^3F_2$[e]	6567	15,220	5[b]
	2747.1	36,391	6[d]		6586	15,180	5[a]
$^3P_0$	2879.3	34,721	5[a]	$^3F_3$	7058	14,160	6[a]
					7064	14,150	9[b]
$^1D_2$	3552.7	28,140	6[c]		7104	14,070	7[c]
	3556.5	28,110	9[a]		7116	14,050	7[c]
	3560.0	28,082	9[a]		7140	14,020	4[c]
	3569.3	28,008	6[d]		7147	13,990	3[a]
	3573.2	27,978	6[d]		7159	13,970	3[a]
	3579.1	27,932	3[c]				
				$^3F_4$	7709	12,970	3[b]
					7781	12,850	3[b]
					7793	12,830	2
					7828	12,770	2
					7910	12,640	2
					7922	12,620	1

[a] Line width: 0.8 to 1.5 A.

[b] Broad complex of unresolved vibrational and electronic lines.

[c] Line width: 0.3 to 0.8 A.

[d] Line width: 0.1 to 0.3 A.

[e] $F_{2,3,4}$ measured to nearest angstrom.

Table XVIII. Spectra and polarization of anhydrous $TmCl_3$ in $LaCl_3$

Term assignment	λ(A) 77°K (in air)	λ (cm^{-1}) 77°K (in vac.)	P	I
$^1D_2$	3609.3	27,689	σ	5[a]
	3614.2	27,661	σ	5[a]
	3618.2	27,630	π	4[b]
	3621.6	27,604	σ	3[c]
	3626.3	27,569	σ	3[c]
	3630.9	27,534	π	4[a]
$^1G_4$	4708.0	21,234	π	4[a]
	4714.1	21,207	π	4[a]
	4733.0	21,122	σ	2[c]
	4636.1	21,109	σ	2[c]
	4740.6	21,088	π	3[b]
	4743.7	21,075	π	3[b]
	4752.0	21,038	σ	1[a]

[a] Line width: 0.1 to 0.5 A.

[b] Line width less than 0.1 A.

[c] Line width: 0.5 to 1.5 A.

The continuous absorption in the ultraviolet masks the ^3P levels, and the ^3F levels are too weak for good measurements.

The spectrum of 203.0 mg of $TmCl_3$ in 10.0 ml of 0.10 M DCl in $\rangle$ 98.5% D_2O was measured between 1 and 2 μ on a recording Cary 14 spectrophotometer. An acid solution was necessary to prevent the hydrolysis of the Tm^{+3} ion. Ordinary-water absorption bands appear around 1.4 μ and 1.8 μ, making it difficult to employ H_2O as a solvent for absorption studies in the region from 1 to 2 μ. In the case of D_2O, the isotope shift is far enough to the red (to about 2.2 μ) to make D_2O a useful solvent for studies in the region where the $^3H_5$ and $^3H_4$ levels are expected. Two peaks (1.175 μ and 1.206 μ) and one shoulder (1.217 μ) were found for the $^3H_5$, and one peak (1.668 μ) and one shoulder (1.715 μ) were found for the $^3H_4$ (see Fig. 19).

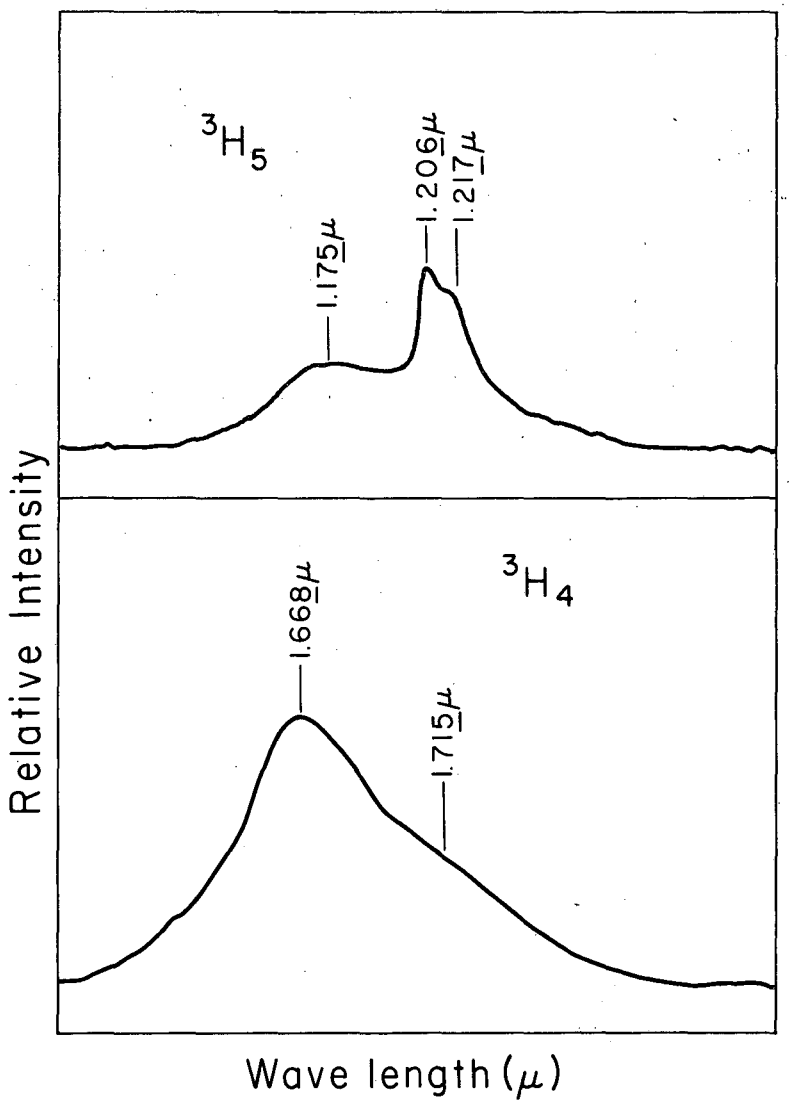

Fig. 19. The $^3H_5$ and $^3H_4$ levels of $TmCl_3$ in D_2O, DCl.

D. Absorption Spectrum of AmIV

The polarized absorption spectrum of Am IV in $LaCl_3$ has been studied from 0.2 μ to 16.0 μ at temperatures of 77°K (liquid N_2) and 4°K (liquid He). In almost every instance, spectral lines observed are sharp and completely polarized. Definite groupings of lines appear in every portion of the spectrum (see Fig. 20), and an analysis of the crystal-field splitting given later indicates that these groupings probably can be assigned to a given J manifold.

For the particular point symmetry, C_{3h}, which is consistent with experiment, the polarized transverse and the axial spectra indicate forced electric-dipole as well as magnetic-dipole transitions. Magnetic-dipole transitions are observed from $^7F_0$ (the ground level) to excited J = 1 levels, and forced electric-dipole transitions are observed from $^7F_0$ to the excited sublevels ±2 and 3 of J levels greater than one.

Many of the sharp lines in the near ultraviolet split into two components in a Zeeman field. Thus from the g values and from the total number of allowed transitions to doubly degenerate sublevels, we can establish a value for J. The sublevels split in a magnetic field are indicated in Table XIX.

The $^7F_1$ grouping consists of transitions to the sublevels 0(4.82 μ) and ±1 (4.55 μ). These two peaks in the infrared, (see Fig. 21 and Table 20) are properly polarized and have an axial spectrum that indicates magnetic-dipole transitions. Since these transitions appear in the region where quartz absorbs, the sample was inclosed in a tube having AgCl windows. The intense radioactivity of americium-241 as well as the hygroscopic nature of anhydrous $LaCl_3$ requires that we mount the crystal in a dry-nitrogen-atmosphere box suitably prepared for radioactive work.

The position of the $^7F_2$ level is somewhat uncertain. In this rather high symmetry, only one forced electric-dipole transition is allowed: $^7F_0$ ($\mu = 0$) to $^7F_2$ ($\mu = \pm 2$). A sharp peak at 2.75 μ was observed to have the proper polarized transverse spectrum. However,

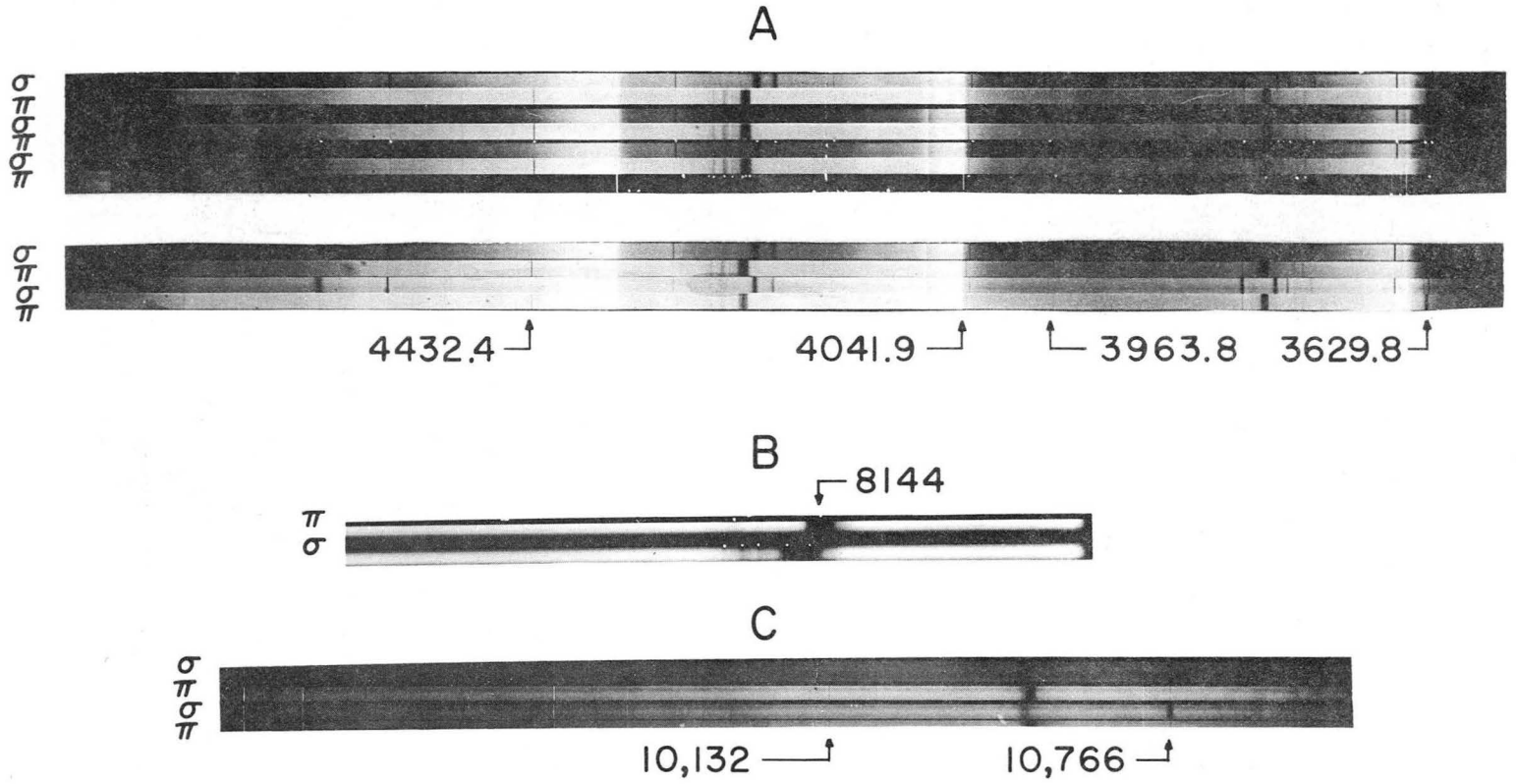

ZN-2614

Fig. 20. (A) Polarized absorption spectrum of AmIV in $LaCl_3$ taken at 77°K. This portion of the spectrum includes the ultraviolet region to 4600 A. The dispersion is 5.25 A/mm. (B) Polarized spectrum of the 8100 A groups. (C) Polarized spectrum of the 10,400 A group. The dispersion is 10.0 A/mm.

Table XIX. Visible and ultraviolet absorption spectra, polarization, and intensities of Am^{+3} in $LaCl_3$

Wave length(A) (in air) 77°K	Wave numbers (in vacuum) 77°K	P	I	Comments
5119.1	19,529	σ	7[a, b]	Intense, broad-line complex group. Could be a single state or several states of approximately the same energy.
5093.0	19,630	σ	10[c]	
5089.6	19,642	σ	4[d]	
5083.2	19,667	π	8[d]	
5075.0	19,699	π	10[c]	
4623.1	21,624	σ	5[b, e]	Broad; has unresolved structure.
4561.5	21,916	σ	8[a, f]	J=2
4432.4	22,555	π	6[a, g]	A possible J=3
4305.0	23,222	σ	6[a, b]	
4298.7	23,256	π	4[a, g]	
4262.5	23,454	π	3[d]	A complex structure. Could be a J=4, 5, 6, or 7
4260.0	23,468	π	3[h]	
4257.3	23,482	π	3[e]	
4245.2	23,549	π	7[h]	
4242.5	23,564	π	7[h]	
4239.9	23,579	π	7[h]	
4232.2	23,622	σ	7[d]	
4216.0	23,713	σ	6[i]	
4163.5	24,012	σ	4[a, f]	J=2
4041.9	24,734	π	5[g, j]	J=4, 5, 6, or 7
4038.8	24,753	σ	6[f, j]	
3968.2	25,193	σ	4[g, j]	
3963.8	25,221	π	4[f, j]	

Table XIX. (continued)

Wave length(A) (in air) 77°K	Wave numbers (in vacuum) 77°K	P	I	Comments
3795.3	26,344	σ	9[b, d]	
3775.4	26,480	π	10[i]	
3773.0	26,497	π	4[d]	Intense, sharp line complex group. Probably due to two or three J levels of approximately the same energy.
3771.8	26,505	π	4[d]	
3765.0	26,553	σ	8[b, h]	
3759.5	26,592	σ	3[b, h]	
3754.3	26,629	σ	5[a, f]	
3745.7	26,690	π	3[d]	
3740.5	26,727	π	3[h]	
3732.6	26,783	σ	4[b, i]	
3658.2	27,328	σ	8[a, f]	A possible J=2 and J=4, 5, 6, or 7
3632.7	27,520	σ	5[a, f]	
3629.8	27,542	π	7[a]	
3627.9	27,556	σ	6[a, f]	
3574.6	27,967	π	2[i]	
3418.5	29,244	π	4[e]	J=8
3410.3	29,315	σ	4[e]	
3388.2	29,506	σ	4[e]	
3380.9	29,569	σ	4[e]	
3377.3	29,601	π	6[e]	
3155.0	31,687	σ	6[j]	J=1
3153.2	31,705	π	6[j]	
3077.8	32,481	π	4[d]	J=3
3067.7	32,588	σ	4[a]	
3060.1	32,669	π	4[d]	

Table XIX. (continued)

Wave length(A) (in air) 77°K	Wave numbers (in vacuum) 77°K	P	I	Comments
2994.4	33,386	π	3[j]	
2993.6	33,395	σ	3[a]	
2986.4	33,475	σ	3[j]	
2939.2	34,013	σ	6[a]	A possible J=4, 5, 6, or 7
2934.0	34,073	π	10[d]	
2916.4	34,279	σ	7[a]	
2914.0	34,307	π	7[a]	

[a] Line width: 0.3 to 0.5A.

[b] Line broadened in magnetic field.

[c] Unresolved band structure.

[d] Line width: 0.5 to 1.0A.

[e] Line width: 2.0 to 5.0A: possible unresolved doublet.

[f] Absorption line split into two observable components in applied magnetic field.

[g] Line not broadened in magnetic field.

[h] Line width: 1.0 to 1.5A.

[i] Line width: 1.5 to 2.0A.

[j] Line width: 0.1 to 0.3A.

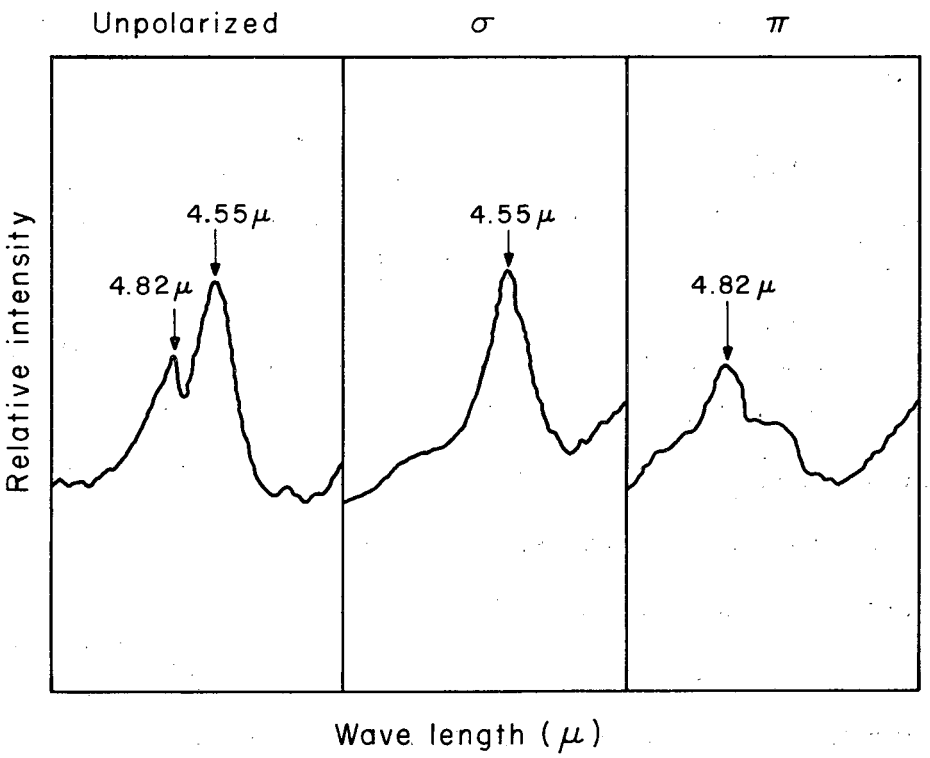

Fig. 21. Polarized absorption spectrum of the $^7F_1$ level of AmIV in $LaCl_3$.

Table XX. Infrared spectrum, polarization, and transitions of Am^{+3} in $LaCl_3$

Wave length(A) (in air) 77°K	Wave numbers (in vaccuum) 77°K	P	I	Trans. from $^7F_0(\mu=0)$ to:	Possible J-level assignment	Comments
48,200	2074	π, a	4	0		Magnetic-dipole transitions to this level from $^7F_0$.
45,500	2197	σ	5	±1	1	
27,500	3635	σ, a	3	±2	2	Electric-dipole transitions. Position of this level is somewhat uncertain.
19,200	5208	π	3	3		Electric-dipole transitions
18,840	5307	σ, a	6	±2	3	
18,730	5340	π	3	3		
10,766	9282	σ, a	9[a]	±2		Electric-dipole transitions. This grouping was observed in the photographic region of the infrared.
10,485	9535	π	10[a]	3	4	
10,474	9545	σ, a	8[a]	±2		
10,132	9867	π	5[b]	3		
8246	12,123	σ, a	3[a]	±2		Electric-dipole transitions. Several lines are rather broad; however, complete polarization was observed.
8159	12,253	π	10[a]	3	5	
8144	12,275	π	8[c]	3	and	
8123	12,307	σ, a	10[c]	±2	6	
8060	12,404	σ, a	10[a]	±2		
8055	12,411	π	5[b]	3		
7956	12,566	π	5[a]	3		
7950	12,575	σ, a	4[a]	±2		

[a] Line width 3 to 8A.

[b] Line width 1 to 3A.

[c] Line width 8 to 15A: unresolved band structure.

this peak is close to an absorption peak of an impurity in the windows, and a water band at 2.9 μ which has a very large molar-extinction coefficient. The AmIV spectrum in this region was never obtained completely free of these peaks.

The polarized absorption spectrum of $^7F_3$, which appears in Fig. 22, was taken at 77°K on a Perkin-Elmer instrument. This same J - level was observed when several milligrams of anhydrous $AmCl_3$ were dissolved in D_2O and the spectrum taken from 1.0μ to 2.5 μ on a Cary 14. When the blank was subtracted from the AmIV solution spectrum, a peak and a shoulder were observed near 1.85 μ. Also, single crystals of $LaCl_3$ containing AmIV still in the original quartz growing tube were studied because the samples were completely free from H_2O.

To make sure that the spectrum reported in Table XX was due solely to AmIV, the spectrum of a single crystal of pure $LaCl_3$ was taken in its original quartz growing tube. This spectrum indicated that the peaks reported in Table XX are due to AmIV.

The $^7F_4$, $^7F_5$, and $^7F_6$ J - levels may be studied in the photographic region of the infrared. Four clearly polarized lines (2σ and 2π) were observed at 1.05 μ, and as few as eight lines at 0.805 μ. At 77°K the spectrum is sharp, with only several lines considered broad (see Fig. 20). These line groupings from the basis of a crystal-field-splitting analysis.

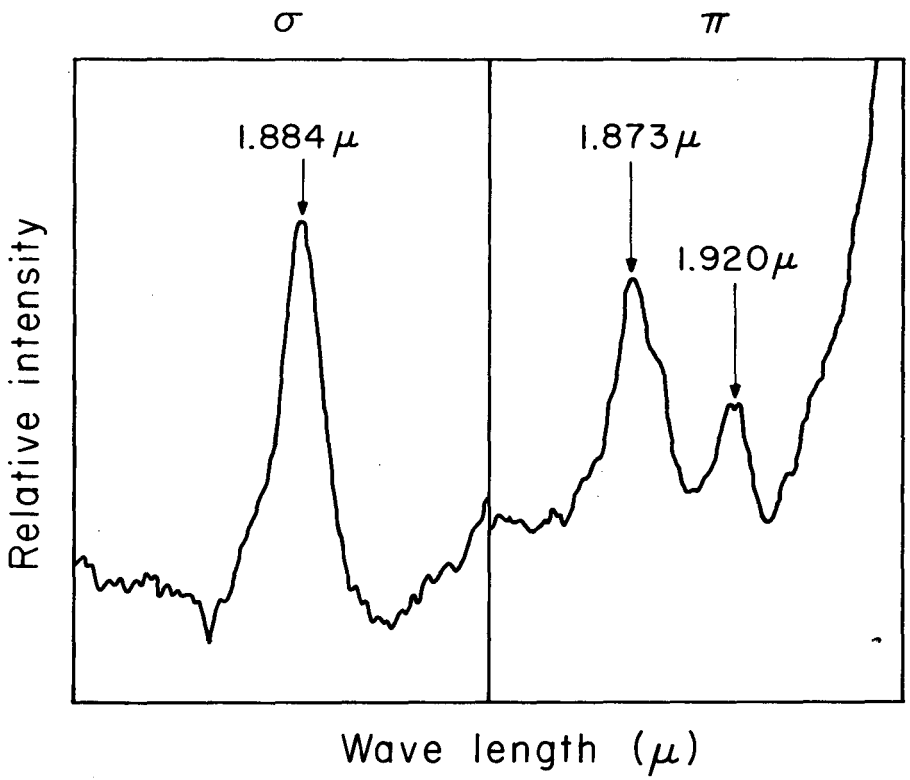

Fig. 22. Polarized absorption spectrum of the $^7F_3$ level of AmIV in $LaCl_3$ taken at 77°K.

IV. COMPARISON OF THEORY WITH EXPERIMENTAL RESULTS

A. Intermediate-Field J Levels for TmIV, $4f^{12}$

In the first sections of this thesis we outlined the theory needed to explain the observed absorption spectra of TmIV and AmIV. Now we should like to present the detailed results of our calculations, so that we may make a direct comparison with the experimental results reported in sections IIIC and IIID.

If we take the absorption spectrum of $Tm(C_2H_5SO_4)_3 \cdot 9H_2O$ and divide the experimental energy levels by F_2, we find that the "best" fit to the plot given in Fig. 9 is obtained around $\chi = 3$. This would imply $\zeta_{4f} = 1350\ cm^{-1}$, or $\zeta = 2700\ cm^{-1}$ and $F_2 = 450\ cm^{-1}$ Both of these values are consistent with results reported by other workers.[42, 43] Theoretical values for the different J levels in intermediate field at $\chi = 3$ and experimentally observed levels are listed in Table XXI. It should be remembered that the entry for the $^3H_4$ level was obtained from the room-temperature absorption spectrum of $TmCl_3$ in D_2O, DCl. That the environment about Tm^{+3} is different in a D_2O, DCl solution from that in the solid ethylsulfate, may explain part of the 600 cm^{-1} difference between theory and experiment. Other theoretical values appearing in Table XXI, however, differ from experiment only by some 200 cm^{-1}. Probable reasons for this disagreement are (a) the theoretical calculations for the field-free ion are good only to three significant figures ($\pm 100\ cm^{-1}$), (b) the perturbing influence of the neighboring ligands in the crystal will shift the centers of the stark-split levels from the predicted field-free levels, (c) the center of gravity of the crystal-field split level cannot be known without a detailed calculation of the crystal-field splitting, and (d) (probably the most important reservation of all) the theoretical model is based on assumed Slater F_k ratios which might better have been obtained by empirical methods rather than calculated on the assumption of 4f hydrogenic F_k ratios.

Table XXI. Comparison of theory with experiment for TmIV

Levels	Values for energy levels (cm^{-1})	
	Theory	Experiment
$^3H_6$	100	105
$^3H_4$	5320	5900[a]
$^3H_5$	8520	8390
$^3F_4$	12730	12673[b]
$^3F_3$	14550	14446[b]
$^3F_2$	15000	15092[b]
$^1G_4$	21120	21275[b]
$^1D_2$	28090	27926
$^1I_6$	33850	34,000
$^3P_0$	35600	35074
$^3P_1$	36640	36443
$^3P_2$	38440	38100
$^1S_0$	75030	--

[a]Estimated from solution data

[b]Values taken from Johnsen[25] (see text).

B. Preliminary Analysis of EuIV and AmIV

There is no question that an intermediate-field calculation of the 301 J levels for $\underline{f}^6$ is necessary to interpret the absorption spectrum of EuIV and AmIV completely. However, until the intermediate-field matrices are completed, we can use some pieces of experimental and theoretical information now at our disposal to give us at least a tentative term assignment for some of the J levels of EuIV and AmIV.[32, 39, 44, 45]

The Sayre and Freed J level assignments for EuIV are based on the polarized transverse and axial absorption spectra of $Eu(C_2H_5SO_4)_3 \cdot 9H_2O$.[39] Such data, consistent with a given point symmetry, identifies J levels 1, 2, and 3 uniquely and larger J values only indicatively.

If we put $\underline{5f}$ hydrogenic F_k ratios into the pure electrostatic energy matrices given in Table III, and use the reasonable values of $\zeta = 1360\ cm^{-1}$ and $F_2 = 370\ cm^{-1}$ for EuIV,[15] we obtain the L-S plot of energy levels in units of F_2 which appears in Fig. 23. We choose the $\underline{5f}$ hydrogenic ratios for EuIV only because of the remarkable degree of agreement between theoretical J levels and the experimental levels that appear in the visible and infrared. From a least-squares fit, Wybourne in his analysis of NdIV, also obtained Slater ratios close to the $\underline{5f}$ hydrogenic ratios.[26]

It should be pointed out that a term assignment in the intermediate field is based on that L-S level which provides the largest eigenvector contribution to a given J level. In Fig. 23 however, for EuIV we have made the assignments in terms of the parent L-S level, since only first-order-perturbation eigenvectors are known. The goodness of fit in some cases would indicate that the L-S level will probably have the same designation in the intermediate field.

On the basis of the EuIV data and assumptions just considered, we can make a limited number of assignments. The ^7F and $^5D_{0,\,1,\,2}$ levels, which have been studied and identified by various workers, agree rather well with our plot.[44] Also we presume

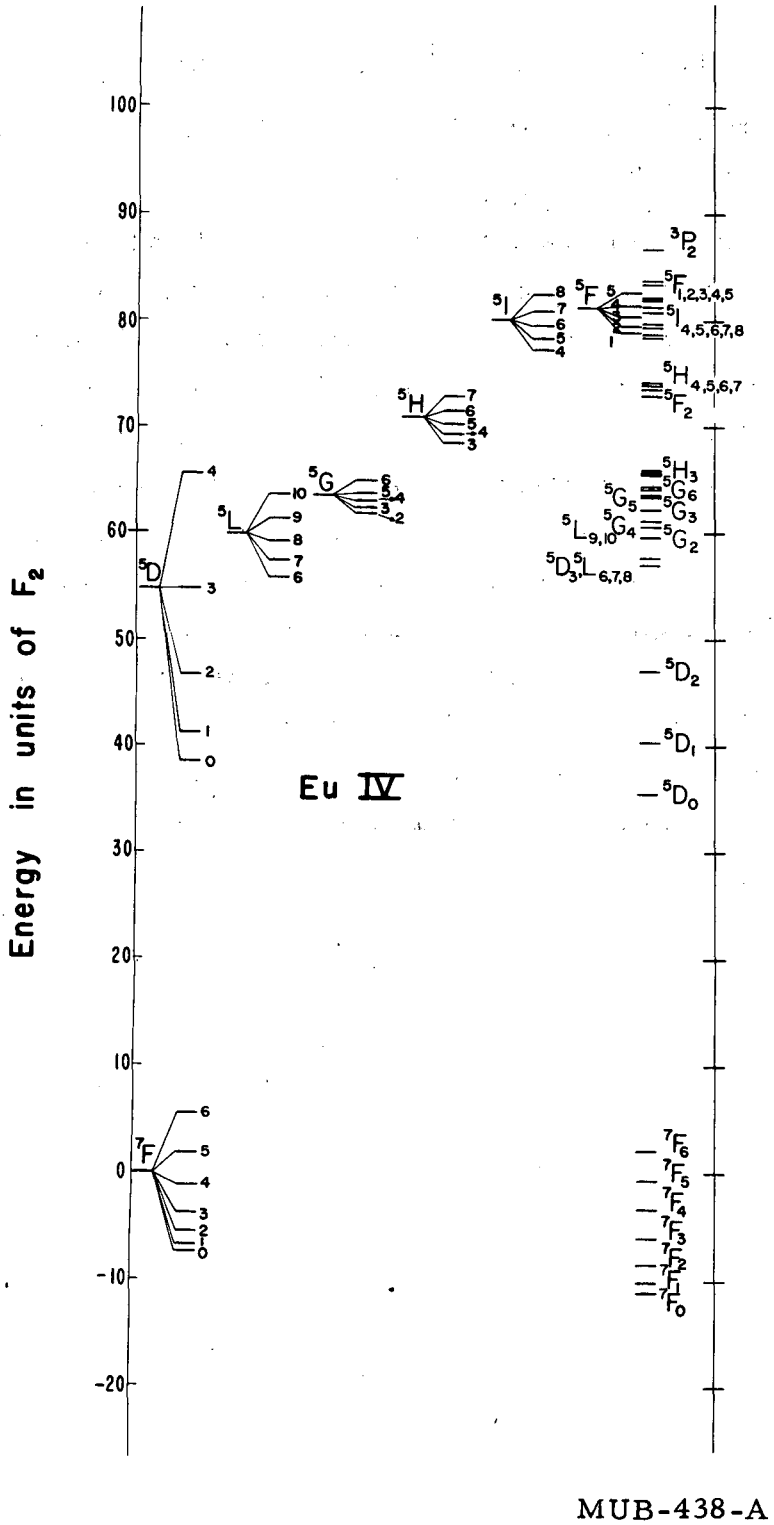

Fig. 23. Comparison of the L-S , Landé energy levels with experimental levels of EuIV.

to identify the $^5G_2$, $^5G_3$, $^5F_2$, $^3P_2$, and $^5H_3$ from the Sayre and Freed data.[39] However, it is impossible to unequivocally identify such levels as the $^5I_{4,5,6,7}$, $^5L_{6,7}$ and $^5H_{4,5,6,7}$, because of a similar number of transitions to each level and because of the overlap of levels which produces a complex absorption-spectrum pattern. Additional complications in the analysis of EuIV data result from the intermixing of crystal quantum sublevels of neighboring levels.

For AmIV a J level assignment has been given to the infrared absorption data appearing in Table XX. It is apparent that not much can be derived from the L-S model even in the ground state of AmIV. Since the polarized absorption spectra in the visible and ultraviolet appear in groupings, we have assigned experimental J levels. See Table XIX. However, since we are farther into intermediate coupling with AmIV than we are with EuIV, it would be better simply to indicate groupings now and see later how these groupings will fit the completed spin-orbit calculaations.

C. Crystal-Field Splitting of the Ground Term, ^7F, of AmIV

As an example of a detailed crystal-field splitting calculation, let us select the infrared absorption data of AmIV as giving the experimental crystal-field-split levels of a given J. We then seek to reproduce these values by following the theory outlined in Section IIE. Having found α, β, and γ for the ^7F levels, we can express the matrices given in section IIE in terms of the parameters $A_n^m \langle r^n \rangle$.

In addition to containing some physical significance as a scale factor for the crystalline electric potential, A_n^m is also the repository for errors due to neglect of configuration interaction and intermediate coupling effects. Since configuration interaction, and crystal-quantum sublevel interaction become more important as we go higher in energy, we should not expect the $A_n^m \langle r^n \rangle$ parameters to be quite the same for the ultraviolet groups as for the infrared groups.

However, the very close agreement of the theoretical calculations with the infrared data leads us to expect that the parameters will be only slightly changed in the ultraviolet region, provided the intermediate-field corrections are first made to the operator equivalents of the ultraviolet J levels. Also where multiplets lie close together, we need to consider the interaction of similar sublevels of the different J levels. These measures must be carried out before we can hope to fit the ultraviolet data.

The parameters that were found to fit the infrared absorption data are $A_2^0 \langle r^2 \rangle = 206\ cm^{-1}$, $A_4^0 \langle r^4 \rangle = -94.1\ cm^{-1}$, $A_6^0 \langle r_0^6 \rangle = -93.8\ cm^{-1}$, and $A_6^6 \langle r^6 \rangle = 1100\ cm^{-1}$. The selection of $A_2^0 \langle r^2 \rangle$ was made from the splitting of the $^7F_1$ level, and the $A_6^6 \langle r^6 \rangle$ parameter was taken from the experimental separation of the $\mu = 3$ sublevels of the $^7F_3$ level. The $A_4^0 \langle r^4 \rangle$ and $A_6^0 \langle r^6 \rangle$ parameters were selected to give the proper energy separation between the ± 2 and 3 sublevels of all levels. See Figs. 24 and 25.

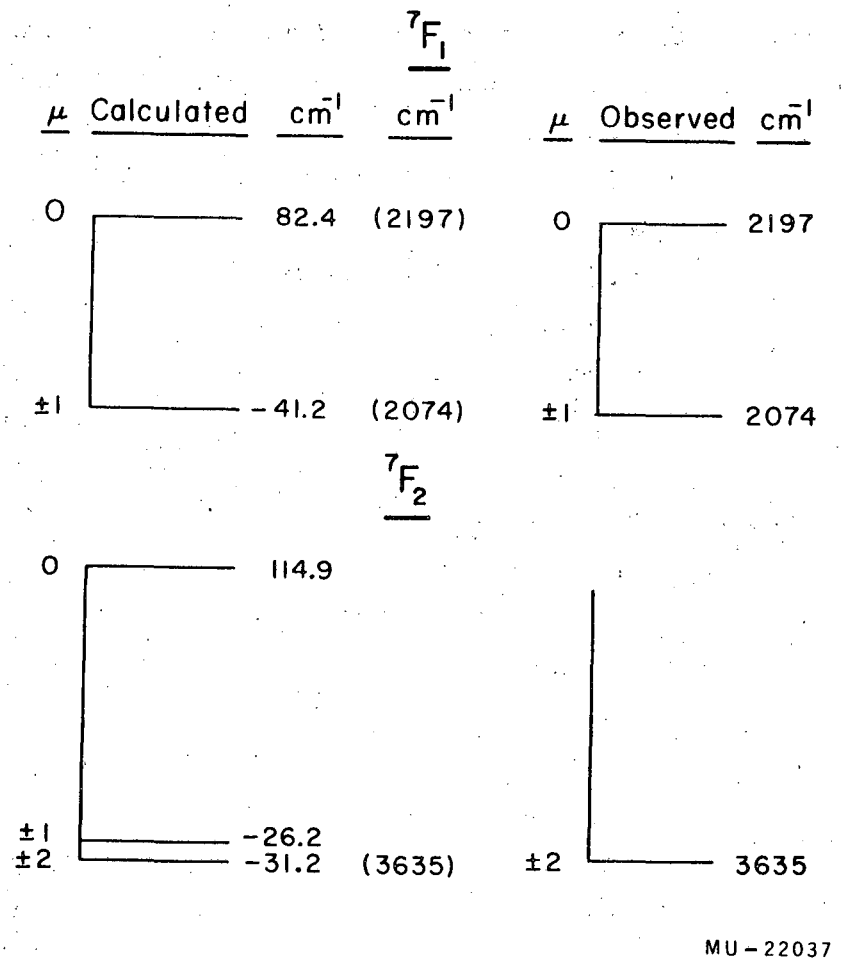

Fig. 24. The ^7F levels of AmIV in $LaCl_3$. The theoretical values are given on the left; the observed energy-level scheme, based on the absorption-spectrum data reported in this paper, is given on the right. Here μ is the crystal quantum number. Energy is expressed in wave numbers.

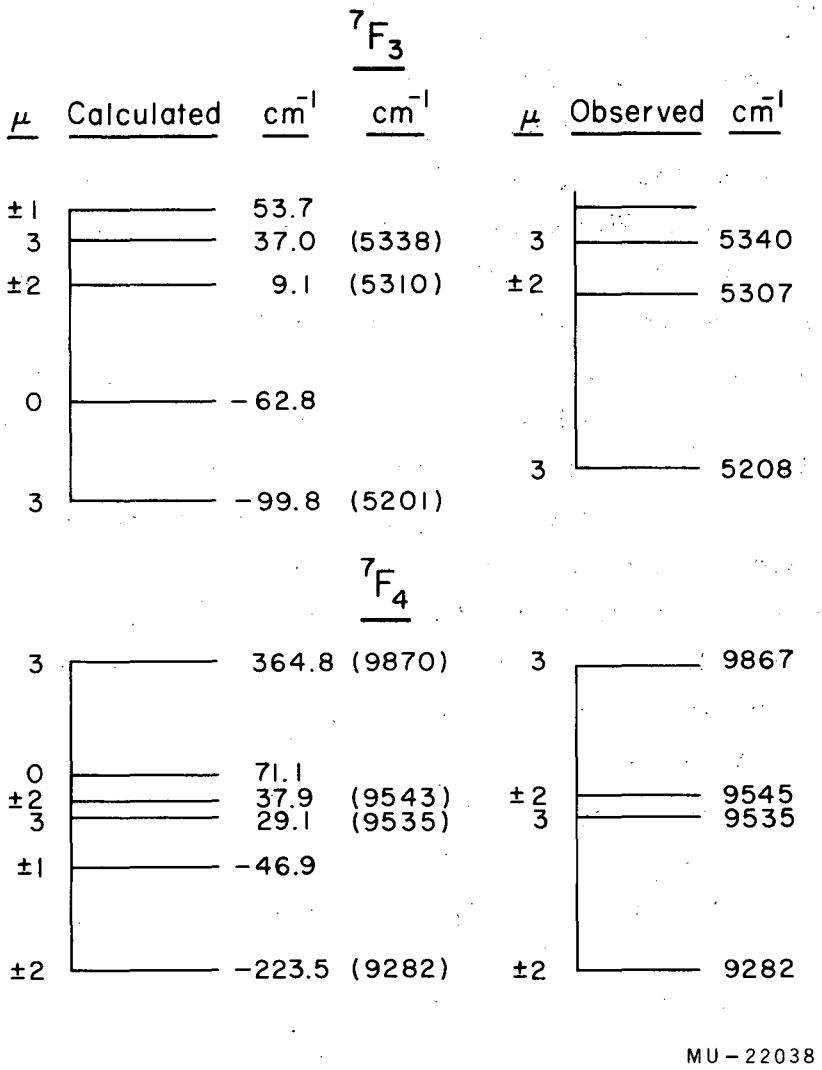

Fig. 25. The ^7F levels of AmIV in $LaCl_3$. The theoretical values are given on the left; the observed energy-level scheme, based on the absorption-spectrum data reported in this paper, is given on the right. Here μ is the crystal quantum number. Energy is expressed in wave numbers.

1. The $^7F_5$ and $^7F_6$ J - levels

Since more absorption lines are observed in the 8100A grouping than correspond to transitions to a single level, we may conclude that two J-levels, the $^7F_5$ and $^7F_6$, are separated by only several hundred wave numbers. While there is a possibility that some of the observed lines are vibrational satellites, the eight absorption lines selected were in most cases reasonably sharp and isolated. Three absorption lines, 8144 π, 8123 σ, and 8060 σ, are rather broad, but clearly polarized; we may attribute the band-like structure to unresolved vibrational satellites to the red of the electronic transitions.

In the crystal-field-splitting calculations presented so far, the states are assumed to be eigenstates of L, S, and J. However, there are several important effects which may cause deviations from this simple model. We have mentioned one of these effects as the breakdown of Russell-Saunders coupling in which levels with the same J will admix. Various components of the crystal field will admix certain states with the same S. However, a far more serious effect in the AmIV ground term, is the interaction between the crystal-field components of the $^7F_5$ and $^7F_6$. Since the proximity of the two levels can perturb the crystalfield components by many tens of wave numbers, we need to calculate the the matrix elements,

$$(J+k,\ J_z + m \mid V_n^m \mid J\ ,\ J_z)\ , \qquad (107)$$

where $k = 1$, $(J+k = 5+1 = 6)$, and V_n^m refers to the particular spherical harmonic which transforms like T_q^k. We may apply the general theory presented by B.R. Judd in the following way.[45]

To find

$$(J+k,\ J_z - m \mid V_n^m \mid J, J_z)\ , \qquad (108)$$

we first evaluate

$$(J+k,\ m - J_z \mid V_n^m \mid J,\ J_z) \qquad (109)$$

and multiply Eq. (109) by $(-1)^{m+k}$. Since many of the matrix elements have similar forms, Judd has found it convenient to define $\phi^{0}_{n,k}(J, J_z)$, $\phi^{3}_{n,k}(J, J_z)$ and $\phi^{6}_{6,k}(J, J_z)$ through,

$$(J+k, J_z \mid V^{0}_{n} \mid J, J_z) = \langle r^n \rangle \langle J+k \,||\theta_n||\, J \rangle$$

$$\phi^{0}_{n,k}(J, J_z) \left[\frac{(J+J_z+k)!\ (J-J_z+k)!}{(J+J_z)!\ (J-J_z)!}\right]^{1/2}, \tag{110}$$

and

$$(J+k,\ J_z+m \mid V^{m}_{n} \mid J, J_z) = \langle r^n \rangle \langle J+k \,||\, \theta_n \,||\, J \rangle$$

$$\phi^{m}_{n,k}(J, J_z) \left[\frac{(J+J_z+k+m)!\ (J-J_z)!}{(J-J_z+k-m)!\ (J+J_z)!}\right]^{1/2}. \tag{111}$$

Analytical expressions for $\phi^{0}_{n,k}(J, J_z)$ are given in Table 4 of Judd's paper.[45] For our calculations we need the following functions:

$$\phi^{0}_{2,1}(5, J_z) = J_z$$

$$\phi^{0}_{4,1}(5, J_z) = J_z (7J_z^2 - 103)$$

$$\phi^{0}_{6,1}(5, J_z) = J_z (33 J_z^4 - 975 J_z^2 + 5262)$$

$$\phi^{6}_{6,1}(5, J_z) = -\frac{1}{14}.$$

Since we are considering the crystal-field interaction between $^7F_5$ and $^7F_6$, J will be equal to 5 and J+k will be equal to 6. Matrix elements other than those between $\Delta J_z = 0, \pm 6$ will be zero in this case. The reduced matrix elements $\langle 6 \,||\, \theta_n \,||\, 5 \rangle$ associated with $^7F_5$ and $^7F_6$ have been evaluated by Elliott and Stevens for TbIV, $4f^8$.[12] The AmIV reduced matrix elements between the $^7F_5$ and $^7F_6$ will be the same except for a change in sign because of the orthonormality of the states. (That is, the AmIV f shell is less than half filled, while the TbIV shell is more than half filled.) The reduced matrix elements for AmIV are $\langle 6 \,||\, \theta_2 \,||\, 5 \rangle = -\frac{1}{15\sqrt{11}}$, $\langle J' = 6 \,||\, \theta_4 \,||\, J = 5 \rangle = \frac{1}{3 \cdot 99\sqrt{11}}$, and $\langle 6 \,||\, \theta_6 \,||\, 5 \rangle = -\frac{1}{99 \cdot 9 \cdot 13\sqrt{11}}$, where $J' = J+1 = 6$. From Eqs. (110) and (111) we can evaluate the following matrix elements:

$$C' = (^7F_6, 5 \,|\, V_n^0 \,|\, ^7F_5, 5) = 5\sqrt{11}\, A_2^0 \langle r^2 \rangle \langle 6 \,||\, \theta_2 \,||\, 5 \rangle + 360\sqrt{11}\, A_4^0 \langle r^4 \rangle \langle 6 \,||\, \theta_4 \,||\, 5 \rangle + 7560\sqrt{11}\, A_6^0 \langle r^6 \rangle \langle 6 \,||\, \theta_6 \,||\, 5 \rangle .$$

$$D' = (^7F_6, 4 \,|\, V_n^0 \,|\, ^7F_5, 4) = 4\sqrt{20}\, A_2^0 \langle r^2 \rangle \langle 6 \,||\, \theta_2 \,||\, 5 \rangle + 36\sqrt{20}\, A_4^0 \langle r^4 \rangle \langle 6 \,||\, \theta_4 \,||\, 5 \rangle - 7560\sqrt{20}\, A_6^0 \langle r^6 \rangle \langle 6 \,||\, \theta_6 \,||\, 5 \rangle .$$

$$E' = (^7F_6, 3 \,|\, V_n^0 \,|\, ^7F_5, 3) = 3\sqrt{27}\, A_2^0 \langle r^2 \rangle \langle 6 \,||\, \theta_2 \,||\, 5 \rangle - 210\sqrt{27}\, A_4^0 \langle r^4 \rangle \langle 6 \,||\, \theta_4 \,||\, 5 \rangle - 2529\sqrt{27}\, A_6^0 \langle r^6 \rangle \langle 6 \,||\, \theta_6 \,||\, 5 \rangle .$$

$$F' = ({}^7F_6,\ 2 \mid V_n^0 \mid {}^7F_5,\ 2) = 2\sqrt{32}\, A_2^0 \langle r^2 \rangle \langle 6 \mid\mid \theta_2 \mid\mid 5 \rangle - 150\sqrt{32} A_4^0 \langle r^4 \rangle$$

$$\langle 6 \mid\mid \theta_4 \mid\mid 5 \rangle + 3780\sqrt{32} A_6^0 \langle r^6 \rangle \langle 6 \mid\mid \theta_6 \mid\mid 5 \rangle .$$

$$G' = ({}^7F_6, 1 \mid\mid V_n^0 \mid {}^7F_5,\ 1) = \sqrt{35} A_2^0 \langle r^2 \rangle \langle 6 \mid\mid \theta_2 \mid\mid 5 \rangle - 96\sqrt{35} A_4^0 \langle r^4 \rangle$$

$$\langle 6 \mid\mid \theta_4 \mid\mid 5 \rangle + 4320\sqrt{35} A_6^0 \langle r^6 \rangle \langle 6 \mid\mid \theta_6 \mid\mid 5 \rangle$$

$$H' = ({}^7F_6,\ 0 \mid V_n^0 \mid {}^7F_5,\ 0) = 0.$$

Here the parameters $A_n^0 \langle r^n \rangle$ have the same value as reported for the other ^7F levels. Also $({}^7F_6,\ -J_z \mid V_n^0 \mid {}^7F_5,\ -J_z)$ equals $({}^7F_6,\ J_z \mid V_n^0 \mid {}^7F_5,\ J_z)$, since the phase factor $(-1)^{m+k} = -1$ is cancelled by the negative sign of $\phi^0_{n,1}(5, -J_z)$. Additional off-diagonal matrix elements are:

$$m = ({}^7F_6, 1 \mid V_6^6 \mid {}^7F_5,\ -5) = -\frac{1}{14}\,[42 \cdot (10)!\,]^{1/2} \langle 6 \mid\mid \theta_6 \mid\mid 5 \rangle\, A_6^6 \langle r^6 \rangle$$

$$n = ({}^7F_6, 2 \mid V_6^6 \mid {}^7F_5,\ -4) = -\frac{1}{14}\,[1680 \cdot (9)!\,]^{1/2} \langle 6 \mid\mid \theta_6 \mid\mid 5 \rangle A_6^6 \langle r^6 \rangle$$

$$p = ({}^7F_6, 3 \mid V_6^6 \mid {}^7F_5,\ -3) = -\frac{1}{14}\,[3360 \cdot (8)!\,]^{1/2} \langle 6 \mid\mid \theta_6 \mid\mid 5 \rangle A_6^6 \langle r^6 \rangle$$

$$q = ({}^7F_6, 4 \mid V_6^6 \mid {}^7F_5,\ -2) = -\frac{1}{14}\,[420 \cdot (10)!\,]^{1/2} \langle 6 \mid\mid \theta_6 \mid\mid 5 \rangle A_6^6 \langle r^6 \rangle$$

$$r = ({}^7F_6, 5 \mid V_6^6 \mid {}^7F_5,\ -1) = -\frac{1}{14}\,[30 \cdot (11)!\,]^{1/2} \langle 6 \mid\mid \theta_6 \mid\mid 5 \rangle\, A_6^6 \langle r^6 \rangle$$

$$s = ({}^7F_6\ ,\ 6\,|V_6^6|\ {}^7F_5\ ,\ 0) = -\frac{1}{14}\ [(12)!\,]^{1/2}\left\langle 6\,||\theta_6||\,5\right\rangle A_6^6\ \left\langle r^6\right\rangle .$$

To evaluate $({}^7F_6\ ,\ -1\,|\,V_6^6\,|\ {}^7F_5\ ,\ 5\,)$ for example, we need only multiply $({}^7F_6\ ,\ 1\ |V_6^6|\ {}^7F_5\ ,\ -5\,)$ by the phase factor $(-1)^{m+k} = -1$. Since we have already evaluated matrix elements for crystal-field components $\Delta J = 0$ in Section II C, we may write our complete 24-by-24 matrix as in Table XXII.

Table XXII. The $^7F_5$ and $^7F_6$ crystal-field splitting matrix.

The capital and small letters refer to matrix elements evaluated on pages 137, 138, 139, 140, and 141. The unprimed J_z quantum numbers are associated with the $^7F_6$ level, while the J'_z quantum numbers are associated with the $^7F_5$. It should be remembered that the separation of the two J-levels by some 200 cm^{-1}, ΔE, is included in this matrix essentially as an additional parameter. Blank spaces refer to matrix elements that are zero.

Upper portion of Table XXII. The $^7F_5$ and $^7F_6$ crystal-field splitting matrix.

J_z	-6	-5	-4	-3	-2	-1	0	1	2	3	4	5	6	5'	4'	3'	2'	1'	0'	-1'	-2'	-3'	-4'	-5'
-6	V						g												-s					
-5		W						h										-r						C'
-4			X						k								-q						D'	
-3				Y						ℓ						-p						E'		
-2					Z						k				-n						F'			
-1						A'						h		-m						G'				
0	g						B'						g						H'					
1		h						A'										G'						m
2			k						Z								F'						n	
3				ℓ						Y						E'						p		
4					k						X				D'						q			
5						h						W		C'						r				
6							g						V						s					

Lower portion of Table XXII. The $^7F_5$ and $^7F_6$ crystal-field splitting matrix.

J_z	-6	-5	-4	-3	-2	-1	0	1	2	3	4	5	6	5'	4'	3'	2'	1'	0'	-1'	-2'	-3'	-4'	-5'
5'						-m						C'		P						d				
4'					-n						D'				Q						é			
3'				-p						E'						R						f		
2'			-q						F'								S						e	
1'		-r						G'										T						d
0'	-s						H'						s						U					
-1'						G'						r		d						T				
-2'					F'						q				e						S			
-3'				E'						p						f						R		
-4'			D'						n								e						Q	
-5'		C'						m										d						P

By a simple interchange of rows and columns, we may reduce the 24-by-24 matrix to six-4-by-4 matrices. When the secular determinent is formed, we find two pairs of 4-by-4's that are similar. In other words, four of our 4-by-4's give us only eight unique eigenvalues instead of 16. This is because of eight doubly degenerate energy levels, (four ± 2, and four ± 1 crystal-field components). The remaining two 4-by-4 matrices give eight unique eigenvalues (four eigenvalues for $\mu = 3$, and four for $\mu = 0$).

The eigenvalues as well as the energy-level scheme are given in Fig. 26. On the left-hand side we give the splitting according to first order perturbation (that is crystal-field splitting in which the nearby J level is ignored; $\Delta J = 0$). Then, to the right we give the results of our present calculation in which we considered the crystal-field components of one level interacting with those of the $J \pm 1$ level only 200 cm^{-1} away. In many cases the components are pushed either to the ultraviolet or infrared of their first-order position by as much as 80 cm^{-1}.

That we have been able to fit all of the observed data (which indicate transitions to 60% of all the crystal-field components for C_{3h} symmetry) seems to be reasonable evidence that the crystal-field-splitting perturbation on the general Hamiltonian is much smaller than the spin-orbit interaction. From our unreported fluorescence data of AmIV we hope to confirm this analysis and the remaining 40% of the components not observed in the absorption spectrum because of selection rules.

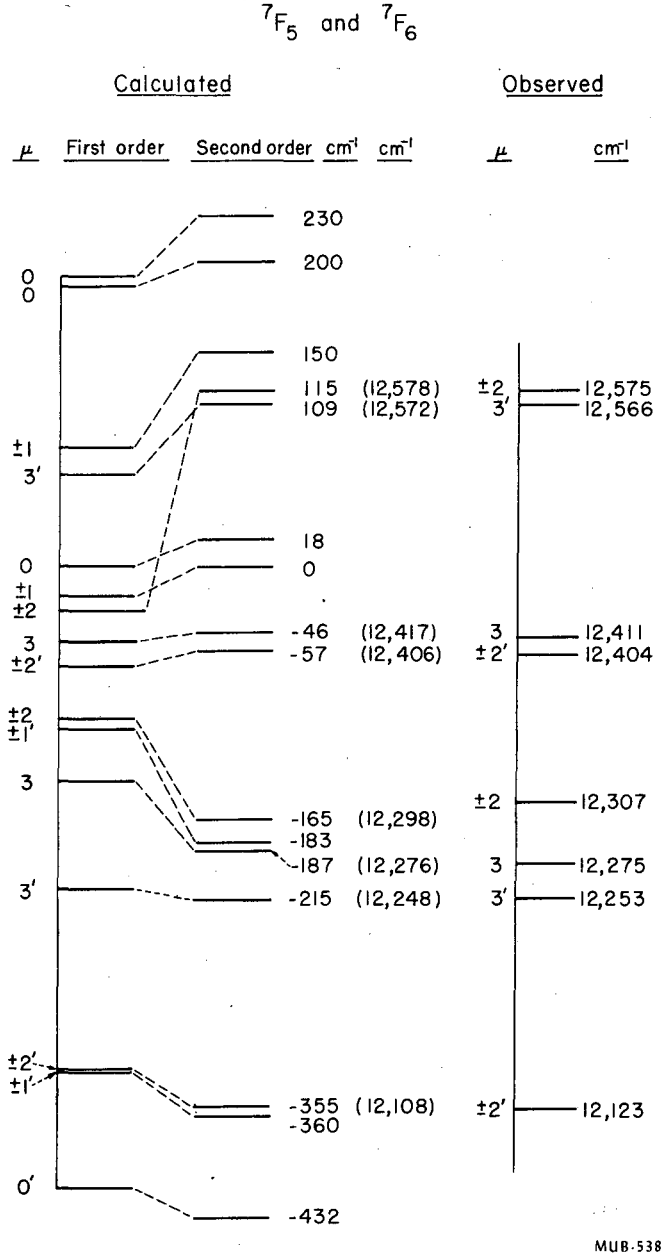

Fig. 26. The $^7F_5$ and $^7F_6$ levels. On the left (first-order perturbation) the calculated splitting is given in which similar crystal-field components of the nearby level are ignored. To the right (second-order perturbation) the crystal-field components of the neighboring level are considered. The field-free levels were assumed to be separated by several hundred wave numbers. On the far right we have tubulated the observed energy-level scheme. Here μ' refers to the crystal-field components of the $^7F_5$ level, while μ refers to the components of $^7F_6$.

V. CONCLUSIONS

Because the six equivalent $\underline{f}$ electrons of AmIV are further from L-S coupling than the rare earth analog, EuIV, it is somewhat difficult to give an estimate of $\zeta_{5\underline{f}}$ for AmIV. However, spectroscopic and magnetic experiments on actinide ions of simple configurations together with results reported here do provide us with a means of estimating a $\zeta_{5\underline{f}}$ for AmIV.

Klinkenberg and Lang, and Racah have reported a value $\zeta_{5\underline{f}}(Th^{+3}) = 1235\ cm^{-1}$ and $\zeta_{5\underline{f}}(Th^{+2}) = 1035\ cm^{-1}$.[46,47] Also Hutchison and Weinstock have obtained $\zeta_{5\underline{f}}(Np^{+6}) = 2450\ cm^{-1}$ from their work on NpF_6, and Conway has suggested $\zeta_{5\underline{f}}(U^{+4}) = 1870\ cm^{-1}$.[48,49] In a recent study of Pa^{+4} in Cs_2ZrCl_6, Axe has found $\zeta_{5\underline{f}} = 1490\ cm^{-1}$ and has fitted all the ζ mentioned in this paragraph to an empirical equation,[50]

$$\zeta_{5\underline{f}} = 200\,(Z' - 87)\ cm^{-1}.$$

Here we have $Z' = Z + Z_i$, where Z is the nuclear charge and Z_i the degree of ionization of the ion. Such an equation will give for AmIV a value of $\zeta_{5\underline{f}}(Am^{+3}) = 2200\ cm^{-1}$. From an analysis of the AmIV data, we obtain a value of $\zeta_{5\underline{f}} = 2450 \pm 200\ cm^{-1}$.

Probably of important interest is the fact that the simple crystal field theory mentioned in Section IIE has served so well to explain the observed infrared optical spectrum of a rather complicated $5\underline{f}$ system. Since several papers have discussed the application of theory to the simplest $5\underline{f}$ systems, we have listed in Table XXIII several of these parameters. It is difficult to make any comparisons, since the cations have different ionic charges and are situated in different crystal environments.

However, it is intersting to compare the AmIV parameters with those of rare ions of the same charge and situated in similar cation sites. Although the AmIV parameters are roughly two to three

Table XXIII. Crystal field parameters for certain actinide and rare earth ions

Ion	Crystal matrix	$A_2^0 \langle r^2 \rangle$ (cm^{-1})	$A_4^0 \langle r^4 \rangle$ (cm^{-1})	$A_6^0 \langle r^6 \rangle$ (cm^{-1})	$A_6^6 \langle r^6 \rangle$ (cm^{-1})	Reference
Np VI	NpF_6[a]	–	5738[b]	540.5[b]	–	51
Pa V	Pa^{+4} in $Cs_2 ZrCl_6$[a]	–	888	41.9	–	50
Am IV	Am^{+3} in $LaCl_3$[c]	206	-94.1	-93.8	1100	—
Eu IV	$Eu(C_2H_5SO_4)_3 \cdot 9H_2O$[c]	80	-63.1	-38.6	510	15
Pr IV	Pr^{+3} in $LaCl_3$[c]	49.5	-37.7	-39.2	396.7	30

[a] The cation lies at the center of an octahedron which has six anions at its vertices.

[b] These values were calculated from the parameters given in Ref. 51.

[c] The cation is situated in a C_{3h} or D_{3h} site in a hexagonal crystal structure.

times larger, ζ_{5f} also is larger than the corresponding ζ_{4f}. We may conclude that, at least in this crystal environment, the crystal-field splitting is much smaller than spin-orbit splitting.

ACKNOWLEDGMENTS

It is a pleasure to acknowledge the help of Professor Burris B. Cunningham who has provided so many thoughful and penetrating suggestions during the course of this research. Also, the discussions with Professor Glenn T. Seaborg have been of great help and encouragement. The author is deeply grateful to Dr. Brian R. Judd who has given such excellent theoretical guidance, and to Mr. John G. Conway who has helped the author to acquire knowledge of experimental spectroscopy. Other experts who have aided this research are Dr. James Wallmann, Dr. Sherman Fried, Mr. Ralph McLaughlin, Mr. George Shalimoff, and Miss Lilly Goda.

Lastly, but most assuredly not least, a word of thanks to Miss Judith A. Higer who typed many sections of this thesis.

This work was done under the auspices of the U.S. Atomic Energy Commission.

REFERENCES

1. G. Racah, Phys. Rev. 61, 186 (1942).
2. G. Racah, Phys. Rev. 62, 438 (1942).
3. G. Racah, Phys. Rev. 63, 367 (1943).
4. G. Racah, Phys. Rev. 76, 1352 (1949).
5. B.R. Judd and R. Loudon, Proc. Roy. Soc. (London) A 251, 127 (1959).
6. E. Reilly, Phys. Rev. 91, 876 (1953).
7. J.P. Elliott, B.R. Judd, and W.A. Runciman, Proc. Roy. Soc. (London) A 240, 509 (1957).
8. B.G. Wybourne, Johns Hopkins University, Baltimore, Maryland, private communication, 1960.
9. J.B. Gruber and J.G. Conway, J. Chem. Phys. 33, (1961).
10. H.A. Bethe, Ann. Physik 3, 133 (1929).
11. K.W.H. Stevens, Proc. Phys. Soc. (London) A 65, 209 (1952).
12. R.J. Elliott and K.W.H. Stevens, Proc. Roy. Soc. (London) A 219, 387 (1953).
13. B.R. Judd, Proc. Phys. Soc. (London) A 74, 330 (1959).
14. W. Low, Paramagnetic Resonance in Solids, (Academic Press, New York, 1960) p. 9.
15. B.R. Judd, lectures given at the University of California in Berkeley, 1960.
16. M. Tinkham, lectures given at the University of California in Berkeley, 1959.
17. E.U. Condon and G.H. Shortley, The Theory of Atomic Spectra, (Cambridge University Press, Cambridge, 1957).
18. M. Tinkham, Advanced Quantum Mechanics of Atoms, Molecules, and Solids,(A.S.U.C. University of California, Berkeley, 1958), p. 174.
19. P.M. Morse, L.A. Young, and E.S. Haurwitz, Phys. Rev. 48, 948 (1935).
20. M. Duncanson and C. Coulson, Proc, Roy. Soc. Edinburgh A 62, 37 (1944).

21. A. Tubis, Phys. Rev. 102, 1049 (1956).
22. J.B. Gruber and J.G. Conway, J. Chem. Phys. 32, 1178 (1960).
23. E.C. Ridley, Proc. Cam. Phil. Soc. 56, 41 (1960).
24. C.K. Jorgensen, Energy Levels of Complexes and Gaseous Ions, (Jul. Gjellerups Forlag) Copenhogen, Denmark, 1957) p. 19.
25. U. Johnsen, Z. Physik 152, 454 (1958).
26. B.G. Wybourne, J. Chem. Phys. 32, 639 (1960).
27. S. Cohen, Relativistic Self-Consistent Calculation for the Normal Uranium Atom, UCRL-8633, February 1959.
28. R. Marrus, W. Nierenberg, and J. Winocur, Hyperfine Structure of Americium-241, UCRL-9207, May 1960.
29. F.H. Spedding, Phys. Rev. 58, 255 (1940).
30. B.R. Judd, Proc. Roy. Soc. (London) A 241, 414 (1957).
31. J.B. Gruber and J.G. Conway, J. Chem. Phys. 32, 1531 (1960).
32. B.R. Judd, Mol. Phys. 2, 407 (1959).
33. A. Edmonds, Angular Momentum in Quantum Mechanics (Princeton University Press, Princeton, 1960) p. 68.
34. R.J. Elliott and K.W.H. Stevens, Proc. Roy. Soc. (London) A 218, 553 (1953).
35. J. Ketelaar, Physica (Haag) 4, 619 (1937).
36. D.R. Fitzwater and R.E. Rundle, Z. Krist. 112, 362 (1959).
37. H. Eyring, J. Walter, and G. Kimball, Quantum Chemistry, (John Wiley and Sons Co., New York, 1944), p. 376.
38. K.H. Hellwege, Ann. Physik 4, 95 (1948).
39. E. Sayre and S. Freed, J. Chem, Phys. 24, 1211 (1956).
40. D.M. Gruen, J.G. Conway, R.D. McLaughlin, and B.B. Cunningham, J. Chem. Phys. 24, 1115 (1956).
41. E. Wong and I. Richman, University of California at Los Angeles, private communication.
42. W.A. Runciman and B.G. Wybourne, J. Chem. Phys. 31, 1149 (1959).
43. H.A. Bethe and F.H. Spedding, Phys. Rev. 52, 454 (1937).
44. K.H. Hellwege and H.G. Kahle, Z. Physik 129, 62 (1951).

45. B. R. Judd, Proc. Roy. Soc. (London) A 227, 552 (1955).
46. P. Klinkenberg and R. Lang, Physica 15, 774 (1949).
47. G. Racah, Physica 16, 651 (1950).
48. C. Hutchison and B. Weinstock, J. Chem. Phys. 32, 56 (1960).
49. J. Conway, J. Chem. Phys. 31, 1002 (1959).
50. J. D. Axe, The Electronic Structure of Octahedrally Coordinated Protactinium (IV) (Thesis), UCRL-9293, July 1960.
51. J. C. Eisenstein and M. H. L. Pryce, Proc. Roy. Soc. (London) A 255, 181 (1960).